nagra.

Arbeitsbericht NAB 16-58

Opalinus Clay in the shallow decompaction zone: Geochemical investigations on drill core samples from borehole Lausen KB

October 2017

M. Mazurek, P. Wersin & J. Hadi

With contributions by
B. Baeyens, R. Dohrmann, J.M. Grenèche,
M. Marques, T. Oyama, D. Rufer & H. N. Waber

National Cooperative
for the Disposal of
Radioactive Waste

Hardstrasse 73
P.O. Box 280
5430 Wettingen
Switzerland
Tel. +41 56 437 11 11

www.nagra.ch

nagra.

Arbeitsbericht NAB 16-58

Opalinus Clay in the shallow decompaction zone: Geochemical investigations on drill core samples from borehole Lausen KB

October 2017

M. Mazurek[1], P. Wersin[1] & J. Hadi[1]

With contributions by
B. Baeyens[2], R. Dohrmann[3], J.M. Grenèche[4], M. Marques[2], T. Oyama[5], D. Rufer[1] & H. N. Waber[1]

[1)] 1Institute of Geological Sciences, University of Bern, Switzerland
[2)] Paul Scherrer Institute, Villigen, Switzerland
[3)] BGR, Hannover, Germany
[4)] Faculté des Sciences et Techniques, Université du Maine, France
[5)] Nuclear Fuel Cycle Backend Research Center, CRIEPI, Abiko-shi, Chiba-ken, Japan

KEYWORDS

Opalinus Clay, Lausen, decompaction zone, geochemistry, porewater, porosity, mineralogy, rock oxidation

National Cooperative
for the Disposal of
Radioactive Waste

Hardstrasse 73
P.O. Box 280
5430 Wettingen
Switzerland
Tel. +41 56 437 11 11

www.nagra.ch

Nagra Arbeitsberichte ("Working Reports") present the results of work in progress that have not necessarily been subject to a comprehensive review. They are intended to provide rapid dissemination of current information.
This report was prepared on behalf of Nagra. The viewpoints presented and conclusions reached are those of the author(s) and do not necessarily represent those of Nagra.

Table of Conents

List of Tables

List of Figures

1 Introduction

Borehole Lausen KB (coord. 2'624'157/1'257'719/345) was drilled in October 2015 to a depth of 146.53 m and yielded a high-quality core with a diameter of 102 mm. The chronology of all field activities, together with a documentation of the technical data, is provided in Vogt et al. (2016). Fig. 1-1 illustrates the position of the borehole in a profile. It is located in a topographic low (Ergolz valley) where Opalinus Clay crops out on the surface.

The main objectives of the study included the characterisation of Opalinus Clay in a surficial position regarding rock/water interactions (such as oxidation), pore-water composition and the effects of decompaction (such as rock deformation, changes of permeability and matrix porosity).

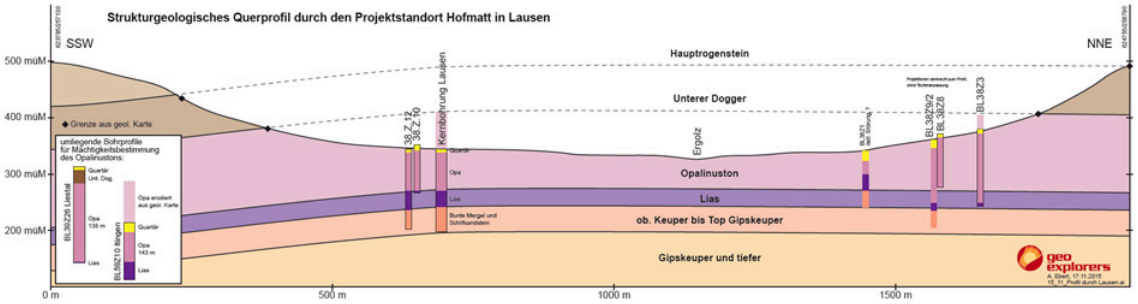

Fig. 1-1: Geological profile across the Ergolz valley, also showing the position of borehole KB Lausen (from Vogt et al. 2016).

2 Geological and hydrogeological setting

2.1 Stratigraphy

The stratigraphic profile of borehole Lausen KB is shown in Fig. 2-1. Below 6.22 m Quaternary sediments, the lower part of the Opalinus Clay, the Staffelegg Fm. (Lias) and parts of the Klettgau Fm. (Keuper) were drilled. The Opalinus Clay is clay-rich in the upper part, whereas the interval 31 – 62 m contains abundant quartz-rich lenses. The lowermost interval 62 – 71.34 m is again clay-rich. This sequence can be hypothetically correlated with the profile observed at Mont Terri, best represented by the BDB-1 borehole (Hostettler et al. 2017). The interval 31 – 62 m may correspond to the lower "sandy facies" at Mont Terri (173.7 – 186.35 m in the BDB-1 borehole), embedded by the upper and lower "shaly facies". The "carbonate-rich sandy facies" that underlies the lower "sandy facies" at Mont Terri cannot be identified at Lausen.

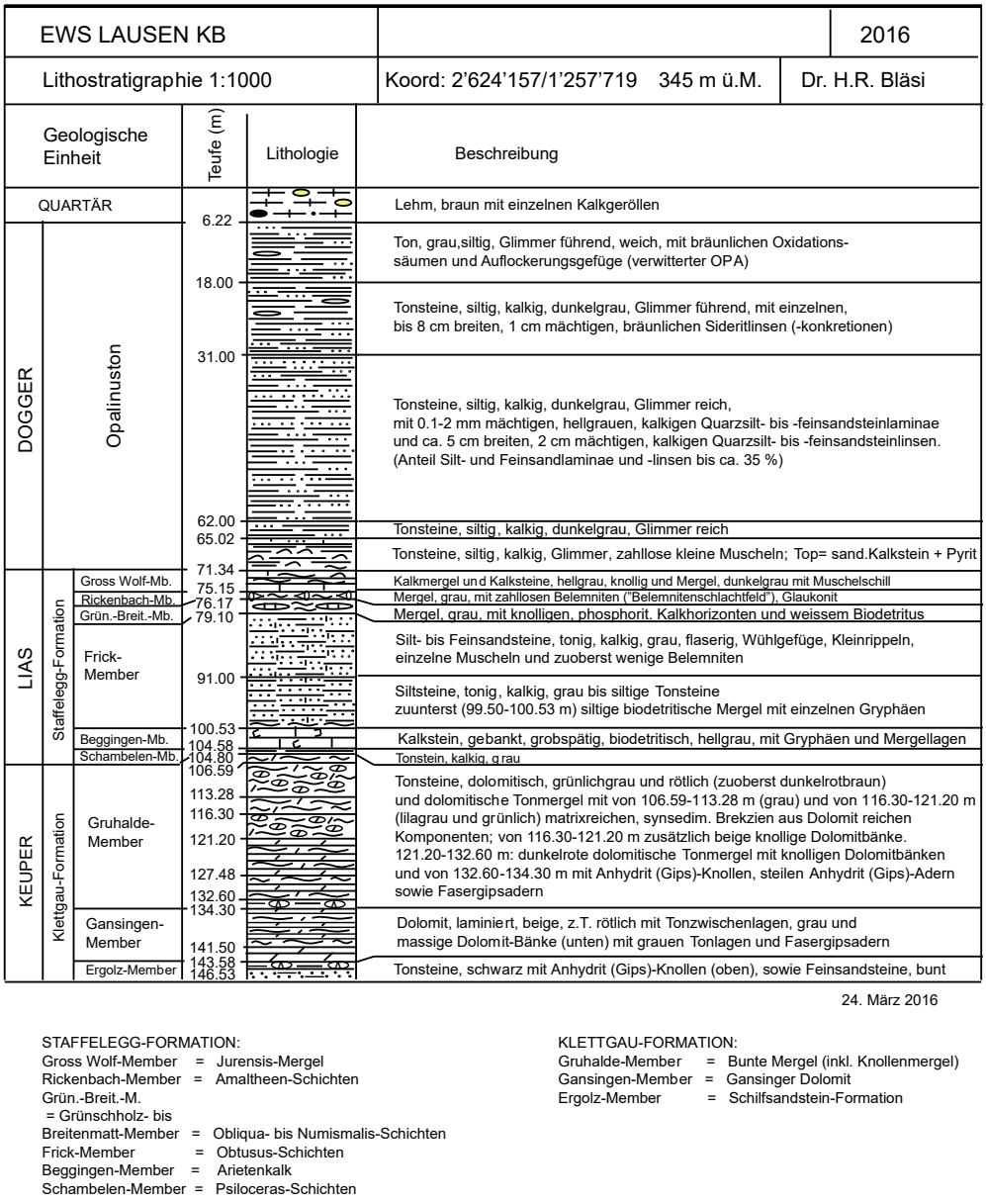

Fig. 2-1: Stratigraphic profile of the KB Lausen borehole (from Vogt et al. 2016).

2.2 Weathering and decompaction

Macroscopically, effects of weathering and decompaction can be identified in the uppermost about 24 m of the core profile, and this part is termed here "weathered zone". Fig. 2-2 summarises the petrographic-structural features of the weathered zone. While this Figure defines sharp boundaries between sub-units, in reality these are smooth transitions.

Down to 12 m depth, the Opalinus Clay is soft, more a clay than a claystone. Nevertheless, the degree of brittle deformation is substantial, and the colour is brownish. Below this depth until 15.4 m, the material becomes somewhat harder, and the brownish colour becomes darker. The degree of deformation is still high. Between 15.4 and 16.4 m, the core is grey, and brownish staining is limited to the vicinity of fractures. Below 16.4 m, brownish oxidation phenomena are no longer seen, but there are still open fractures down to 18.7 m. In the interval 18.7 – 23.7 m, the rock is still fractured, but the structures are mostly closed and do not result in broken core. The core is essentially intact, i.e. with only few core breaks. Below 24 m, Opalinus Clay can no longer be distinguished from its normal occurrence at deeper levels on the basis of macroscopic core inspection. This finding is supported by structural core logging of Vogt et al. (2016), where the degree of fracturing decreases substantially around 24 m. Nevertheless, the effects of weathering and decompaction do not end abruptly at this depth. Vogt et al. (2016) identified some fracturing at deeper levels, even though less pronounced (see Section 5.1). Also, water contents are slightly increased even below 24 m when compared to the largely constant values below 40 m (see Section 4.7).

Depth, from [m]	Depth, to [m]	Unit	Lithology	Colour	Structures and localised alteration	Core quality
0.00	6.22	Quaternary sediments	Soft mud	light brown		Variable: Perfectly cylindrical to dough
6.22	7.60	Strongly altered Opalinus Clay	Less soft mud	light brown		Variable: Perfectly cylindrical to dough
7.60	8.77		Harder mud	brown-grey		Intact core, some horizontal discontinuities
8.77	9.90		Soft, fragmented mud, breccious	brown-grey		Breccia
9.90	10.60		Soft clay	darker brown-grey		Intact core, some horizontal discontinuities
10.60	11.88		Soft rock, homogeneous	dark brown-grey	11.79: Horizontal fracture with bright brown coating	Intact core, some horizontal discontinuities
11.88	12.03		Soft clay, evt. deformed	dark brown-grey		Weak, with horizontal discontinuities
12.03	12.23	Altered Opalinus Clay	Soft rock, homogeneous	dark brown-grey		Intact
12.23	12.45		Less soft rock, homogeneous	very dark brown-grey		Several horizontal fractures
12.45	13.00		Soft rock, homogeneous	dark brown-grey	Potential deformation (horizontal; natural vs artif.?) at 12.65-12.80 and 12.95-13.00	Intact core, some horizontal discontinuities
13.00	13.97		PHOTO MISSING			
13.97	14.07		Soft rock, friable/ deformed	grey-brown		Friable
14.07	15.39		"Rock-like" core, rough surface with flaser texture (dark grey matrix with lighter grey/brownish spots)	dark grey with grey/brownish flaser texture	Many discontinuities (within intact core) with variable orientations and mm-thick oxidation features	Intact
15.39	15.88		Rubble, lithologically similar to above. Deformation at least partially natural	dark grey	Brown fracture coatings	Breccia
15.88	16.31		Intact shale	dark grey	45° steep fractures, closed, oxidised, at 15.88, 16.22, 16.31	Intact
16.31	16.37		Rubble, lithologically similar to above. Deformation at least partially natural	dark grey	Brown fracture coatings	Breccia
16.37	18.71	Decompacted Opalinus Clay with open fractures	Intact shale with flaser-like brighter-grey spots	dark grey	3 cm thick fault, closed, at 17.39, 45°, all grey. 18.08: 60° steep shear plane	Weakly fractured
18.71	18.73		Dito, fractured (natural vs artif.?)	dark grey		strongly fractured
18.73	20.50	Decompacted Opalinus Clay with predominantly closed fractures	Intact shale with few bright grey flasers		Closed, all grey shear planes: 18.94 60° 19.40 20° 19.68 70° 20.28 45° 20.35 45°	Intact
20.50	20.67		Dito	dark grey	2 conjugate fracture systems, all closed	Intact
20.67	23.65		Intact shale with few bright grey flasers	dark grey	Concordant, open: 21.30, 21.48, 21.58	Intact with some open concordant fractures

Fig. 2-2: Lithological and structural characterisation of the weathered zone of Opalinus Clay based on core photographs.

2.3 Hydrogeology

A number of packer tests were conducted in the Opalinus Clay and are documented in Vogt et al. (2016). As shown in Fig. 2.3-1, hydraulic conductivity is 5.2E-13 m/s or less below 28.5 m, which is at the upper limit of typical values for Opalinus Clay at depths of several hundreds of metres (Nagra 2014). At levels above 27.6 m, much higher values are found. Hydraulic potentials are 2.4 m below surface in the shallowest test but become progressively sub-hydrostatic with depth (60 m below surface for the deepest test).

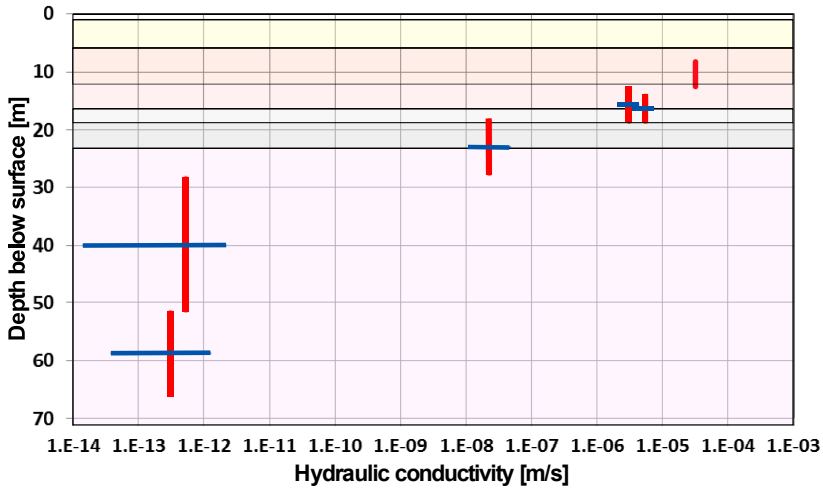

Fig. 2.3-1: Hydraulic conductivity of Opalinus Clay based on packer testing.

Blue bars indicate uncertainty ranges. Colours correspond to those defined in Fig. 2-2. Adapted from Vogt et al. (2016) and Hekel & Brod (2016).

2.4 Ground-water composition

Ground-water samples were obtained from test intervals within the weathered zone and are documented in Huxol et al. (2017). Tab. 2-1 provides a summary of the results. Waters from the Quaternary sediments and the strongly altered Opalinus Clay are only weakly contaminated by drilling fluid and so do not require any correction. The sample from the interval 13 – 18.43 m (LAU-i2) was weakly contaminated, and a correction was performed on the basis of nitrate concentrations[1]. Water from the deepest interval 18.4 – 27.6 m (LAU-i3) was strongly contaminated, and corrections based on uranine and tritium yield different results. The composition of this water is uncertain with the exception of conservative species.

The water type[2] evolves from Ca-Mg-HCO_3 in test LAU-i1 to Ca-Mg-(Na)-HCO_3-(SO_4) in LAU-i2 and Na-Ca-Mg-HCO_3-SO_4 in LAU-i3. Salinity increases from 0.65 g/L in the Quaternary water to 1 – 1.15 g/L in the deepest sample LAU-i3. These salinities are much lower than that of pore water in Opalinus Clay at deeper levels.

Tab. 2-1: Ground-water compositions in the Quaternary sediments and in the weathered zone of Opalinus Clay (data from Huxol et al. 2017).

Test ID	Mean depth [m]	Top interval [m]	Base interval [m]	Correction	Na [mg/L]	K [mg/L]	Ca [mg/L]	Mg [mg/L]	F [mg/L]	Cl [mg/L]	NO3 [mg/L]	SO4 [mg/L]	δ2H [‰V-SMOW]	δ18O [‰V-SMOW]
LAU-Q	6.00			uncorrected	14.0	3.8	125.0	15.7	0.2	10.1	<0.2	17.7	-61.1	-8.85
LAU-i1	10.39	8.32	12.45	uncorrected	12.0	3.4	127.0	19.8	0.1	23.7	<0.2	23.5	-62.8	-8.78
LAU-i2	15.72	13.00	18.43	corrected 1.4% nitrate	42.0	6.0	110.0	27.0	0.2	22.0		76.0	-61.1	-8.64
LAU-i3	23.00	18.40	27.60	corrected 20% uranine	136.0	8.0	89.0	39.0	0.2	26.0	<0.1	209.0	-59.8	-8.72
LAU-i3	23.00	18.40	27.60	corrected 42% tritium	160.0	2.4	90.0	46.0	0.1	20.0	<0.1	243.0	-57.8	-8.46

[1] Contamination according to uranine 0.2 %, according to nitrate 1.4 %.

[2] Including HCO_3^- estimated from charge balance.

3 Sampling and methodology

As the main objective of the investigations was to explore the effects of surface weathering and decompaction, a dense sampling was performed in the uppermost part of Opalinus Clay, with only a few samples from larger depth. In total, 12 standard samples were taken, 10 of which are from Opalinus Clay and 2 from the underlying units. In addition, another 12 samples were taken in the frame of a Master's thesis at the University of Bern (N. Prinpreecha). While these samples were analysed outside the Nagra project, the results are reported here as well. Integration of these samples doubles the number of data points to 24. The laboratory programme is summarised in Tab. 3-1.

Field sampling and laboratory methods are documented at length in Wersin et al. (2013) for the Schlattingen-1 campaign, which serves as a reference for the procedures at Lausen.

Tab. 3-1: Programme for geological and geochemical laboratory investigations.

Method	**Number of samples (Nagra project)**	**Number of samples (MSc thesis N. Prinpreecha)**	**Total number of samples**
Bulk mineralogical composition	12	12	24
Clay mineralogy	6	0	6
Chemical composition of rock	8	0	8
Bulk and grain density	12	12	24
Gravimetric water content	33	12	45
Pore-water squeezing (incl. post-squeezing aq. extraction and analysis of major ions and water isotopes)	12	0	12
Aqueous extraction	12	12	24
Stable water isotopes by diffusive exchange	12	12	24
Cation exchange properties: Ni-en method	7	0	7
Cation exchange properties: Cu-trien and Co-hex methods method	6	0	6
Cation exchange properties: Cs method (PSI)	6	0	6
Cation exchange properties: Cu-trien method (BGR)	6	0	6
Detailed studies on rock oxidation (SEM, Mössbauer spectroscopy, XRD)	6-8	0	6 – 8

4 Results

4.1 Mineralogical composition

4.1.1 Bulk mineralogy

Results of mineralogical analyses listed in Tab. 4-1 and plotted against depth in Fig. 4-1. For the section within Opalinus Clay, the following trends are identified:

- Calcite contents are markedly lower in the uppermost section down to 15.28 m and then increase to values typical of the unaltered clay-rich sub-unit of Opalinus Clay. The increase approximately coincides with the base of the altered Opalinus Clay as defined in Fig. 2-2. The low values in the altered zone are likely due to calcite dissolution.
- Dolomite/ankerite contents are also low in the altered zone, but the effect is less clearly expressed than for calcite. Whether dolomite was partially dissolved needs to be verified by microscopic or SEM studies.
- Siderite is almost quantitatively dissolved within the strongly altered zone (according to the definition in Fig. 2-2) but shows concentrations expected for unaltered Opalinus Clay throughout the rest of the profile.
- Quartz contents are constant and close to the expected values throughout the weathered zone, suggesting that it was unaffected by surface effects. Values in the sub-unit containing abundant silty lenses (31 – 62 m) are higher. Similar findings apply to feldspars.
- Clay-mineral contents are high within the altered zone of Opalinus Clay, corresponding to the zone depleted in carbonates. Contents reach up to 70 wt.-%, which is unusually high even for the clay-rich sub-unit of Opalinus Clay. It is likely that clays are passively enriched due to the dissolution of carbonates.
- Pyrite contents are variable, which reflects the primary heterogeneity of Opalinus Clay. Only in the uppermost part of the altered zone, down to 8.58 m, contents are significantly lower, probably reflecting pyrite dissolution. A similar conclusion also applies to organic carbon.

In summary, carbonates are depleted in the altered Opalinus Clay but have contents typical of unaltered Opalinus Clay in the lower, decompacted part of the weathered zone and below. The dissolution of carbonates is the likely reason for the relative enrichment of clay minerals in the altered zone. Pyrite and organic carbon are depleted only in the upper half of the strongly altered zone, i.e. these effects reach less deep into the formation than carbonate dissolution.

Tab. 4-1: Mineralogical composition of Opalinus Clay.

		CNS analyser				Mineralogy (XRD + CNS)												
Depth [m]	Geological unit	C(org) [wt.%]	C(inorg) [wt.%]	S [wt.%]	N [wt.%]	Calcite [wt.%]	Dolomite / Ankerite [wt.%]	Siderite [wt.%]	Quartz [wt.%]	Albite [wt.%]	K-feldspar [wt.%]	Pyrite [wt.%]	C(org) [wt.%]	Total clay minerals [wt.%]	Illite [wt.%]	Ill/Sm mixed layers [wt.%]	Chlorite [wt.%]	Kaolinite [wt.%]
7.83	Opalinus Clay	0.69	0.47	0.06	0.08	4	b.d.	b.d.	21	0.5	3.0	0.1	0.7	71	21	17	7	27
8.23	Opalinus Clay	0.84	0.53	0.10	0.09	4	0.6	0.1	24	0.4	2.7	0.2	0.8	68				
8.58	Opalinus Clay	0.88	0.45	0.01	0.09	3	b.d.	b.d.	22	0.5	2.0	b.d.	0.9	71	23	19	8	22
10.73	Opalinus Clay	1.00	0.55	0.24	0.08	4	0.2	b.d.	24	0.5	2.0	0.5	1.0	68	18	15	7	27
11.30	Opalinus Clay	0.92	0.79	0.58	0.10	6	0.5	0.2	25	0.3	1.6	1.1	0.9	65				
12.10	Opalinus Clay	1.04	0.71	0.15	0.09	5	0.8	b.d.	22	0.5	1.0	0.3	1.0	70	19	15	7	29
15.28	Opalinus Clay	0.97	0.94	0.21	0.09	5	0.9	2.5	23	0.5	2.0	0.4	1.0	65	17	14	7	27
15.94	Opalinus Clay	0.95	1.20	0.27	0.10	7	1.7	1.4	25	0.7	2.8	0.5	1.0	60				
16.75	Opalinus Clay	0.92	1.31	0.42	0.10	9	1.1	1.3	28	0.4	3.0	0.8	0.9	56				
19.62	Opalinus Clay	0.89	1.64	0.86	0.08	9	0.4	4.6	23	0.5	2.0	1.6	0.9	58				
20.09	Opalinus Clay	1.00	1.10	0.31	0.10	7	1.3	1.2	26	0.4	2.9	0.6	1.0	60				
24.52	Opalinus Clay	0.96	1.41	1.42	0.09	8	0.3	3.5	22	1.0	2.0	2.7	1.0	59	20	16	10	14
29.02	Opalinus Clay	0.92	1.42	0.58	0.09	9	1.7	1.0	28	0.4	3.8	1.1	0.9	54				
33.65	Opalinus Clay	0.78	1.56	0.14	0.07	8	b.d.	5.7	30	1.5	2.5	0.3	0.8	51				
42.88	Opalinus Clay	0.67	1.14	0.19	0.08	8	1.2	0.6	40	1.0	5.0	0.3	0.7	44				
47.58	Opalinus Clay	0.65	1.33	0.31	0.08	9	1.4	1.0	37	0.2	3.0	0.6	0.7	47				
50.13	Opalinus Clay	0.83	1.26	0.40	0.07	7	b.d.	3.7	35	1.5	2.5	0.7	0.8	49				
54.98	Opalinus Clay	0.56	1.82	0.01	0.05	12	1.6	1.3	42	0.7	3.3	b.d.	0.6	39				
60.78	Opalinus Clay	0.90	0.92	0.29	0.08	6	0.3	1.0	31	1.5	2.0	0.5	0.9	56				
77.81	Staffelegg-Fm	0.41	7.40	0.56	0.03	55	5.9	0.1	11	0.1	0.4	1.0	0.4	26				
82.87	Staffelegg-Fm	0.56	1.86	0.78	0.05	13	2.3	b.d.	38	1.0	2.0	1.5	0.6	42				
96.98	Staffelegg-Fm	0.74	1.98	0.24	0.05	15	1.4	b.d.	37	0.8	3.2	0.4	0.7	41				
113.55	Klettgau-Fm	0.10	6.41	0.00	0.05	b.d.	49.3	b.d.	6	0.5	1.0	b.d.	0.1	43				
132.12	Klettgau-Fm	0.05	4.41	0.00	0.03	0	33.6	b.d.	17	0.9	5.6	b.d.	0.1	42				

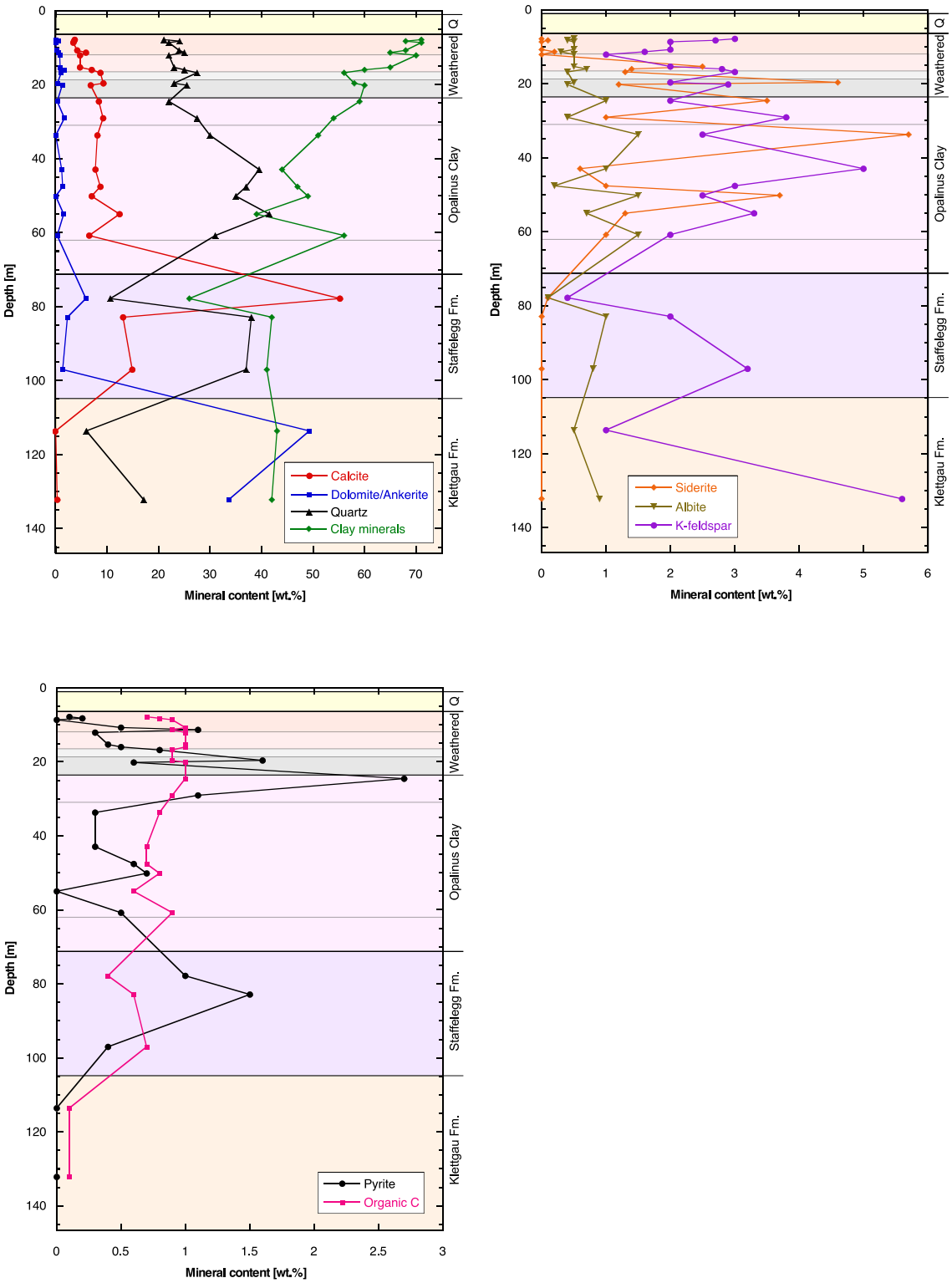

Fig. 4-1: Mineralogical composition as a function of depth.

4.1.2 Clay mineralogy – standard procedure

Five samples from the weathered zone were analysed, plus one from the underlying formation. Data are listed in Tab. 4-1. Note that with the standard procedure, the distinction of kaolinite and chlorite is difficult and somewhat uncertain because of peak overlaps. Overall, there are no major systematic depth trends in the relative contents of clay minerals. Illite and illite-rich illite/smectite mixed layers are the most common clay species, followed by kaolinite and minor chlorite.

The two uppermost samples (7.83 and 8.58 m) show the following distinctive features:

- The peaks kaol 001/chl 002, kaol 002/chl 004 and kaol 003/chl 006 are clearly seen (even though at a greatly reduced intensity) in the XRD patterns of the heated sub-samples, in contrast to all underlying samples where these peaks are absent. Because kaolinite becomes amorphous to X-rays after heating to 550 °C for 1 h, these peaks must represent chlorite. The absence of these peaks in the deeper samples indicates that the nature of chlorite evolves with depth. According to Martin (1954), Fe-rich chlorite are more readily destroyed by heating when compared to Mg-rich chlorite.
- The chl 001 peak disappears in the heated samples, whereas it is present (with a peak height similar to that in the unheated sub-samples) in the underlying samples, where it is simply shifted to slightly lower d values (a known feature due to the dehydroxylation of the hydroxide sheet of chlorite).
- The peak-height ratio chl 001/chl 003 is in the range 3 – 5 in the lower samples but 8 – 10 in the uppermost samples. According to experimental work of Borggaard et al. (1982), oxidised chlorites have a higher ratio than reduced chlorites.
- The chl 001 peak shifts to slightly lower d values upon glycolation (i.e. in comparison with the air-dried sample), indicative of expansion and therefore a smectitic component (likely a chlorite/smectite mixed-layer phase). This effect is seen in the uppermost two samples (7.83 and 8.58 m) and, to a lesser degree, in samples 10.73 and 12.10 m but disappears in the lower samples.

These observations indicate that the nature of the chlorite is different in the uppermost two samples (e.g. oxidised, some smectitic interlayers), probably due to the effects of surface weathering.

Further, the uppermost 4 samples (7.83, 8.58, 10.73, 12.10) show a broad, small peak at d = 4.18 Å (21.25°), which could represent goethite. In the XRD patterns used for bulk mineralogical analysis (no grain-size separation), no goethite peak at all is seen. Given the brown colour of the shallowest samples, a substantial amount of goethite would be expected. Note that in an Fe-oolite sample from the Schlattingen core, a sharp goethite peak was observed, corresponding to a content of 8 wt.-% (Wersin et al. 2013). The fact that the goethite peak in the shallow samples from Lausen is small, broad and only seen after grain-size separation is likely due to its bad crystallinity. There may be badly crystallised or amorphous Fe-hydroxides in the Lausen core that cannot be quantified by X-ray diffraction.

4.1.3 Clay mineralogy – detailed study

Domed XRD

In order to prevent possible redox reactions during data acquisition, a set of analyses were performed in a polycarbonate container under dry anaerobic conditions (domed XRD). The powdered original samples (i.e. not the treated < 2 µm fraction as used for the standard procedure) were front-loaded on the sample holder in the chamber, and the surface was flattened with a glass slide. This means that the mineral grains were only weakly oriented, again unlike in the standard procedure where oriented samples were used. The samples were analysed with a PANalytical X'Pert PRO X-ray diffractometer, with Cu Kα radiation with a wave length of 1.54 Å at 40 mA and 40 kV. They were scanned from 5 to 60 °2θ angle using a step size of 0.0167 °2θ and a very long acquisition time of 1600 s per step, with automated divergence slits. The long acquisition time improves counting statistics, resulting in a better resolution. The samples were rotated during measurement at a rate of one revolution every 8 seconds.

The XRD patterns were evaluated with the PANalytical Highscore® software (phase identification and background correction), using the same functions and same parameters for the background correction for each series of samples (different for domed and normal samples). Automatic background correction was used for domed samples. The background was manually determined for undomed samples in order to further refine the quantification of the patterns.

The resulting diffraction patterns are shown in Fig. 4-2 and Fig. 4-3. The broad peak in the range 16 – 19 °2θ is due to the dome and does not represent a characteristic of the sample. In the detailed representations of Fig. 4-3, the following features are observed:

- Clay 1 (region of chl 001): The peaks of the two uppermost samples (7.83 and 8.58 m) are asymmetric, with a shoulder towards higher d spacings (effect of smectite interlayers?). There is a weak shift of the peak position towards smaller d spacings with depth.
- Clay 3 (region of chl 002 and kaol 001): The higher peak of kaolinite can be distinguished from the smaller chlorite peak.
- Clay 6 (region of chl 004 and kaol 002): Kaolinite and chlorite are even better distinguished. As for chl 002, the chl 004 peak height tends to increase with depth.

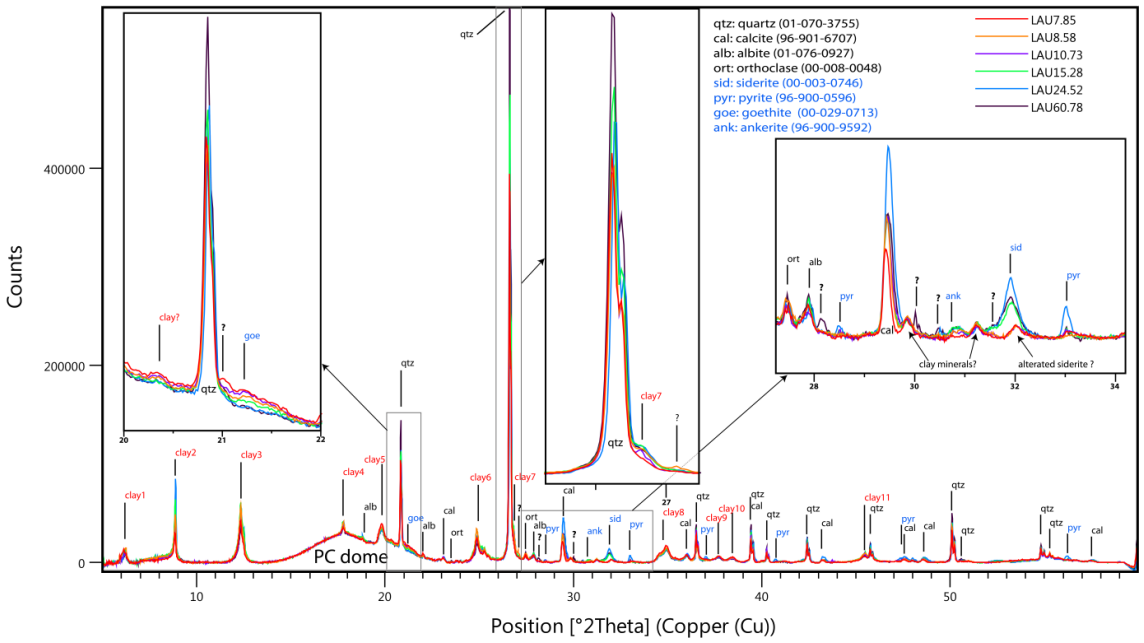

Fig. 4-2: Diffraction patterns obtained by domed XRD.

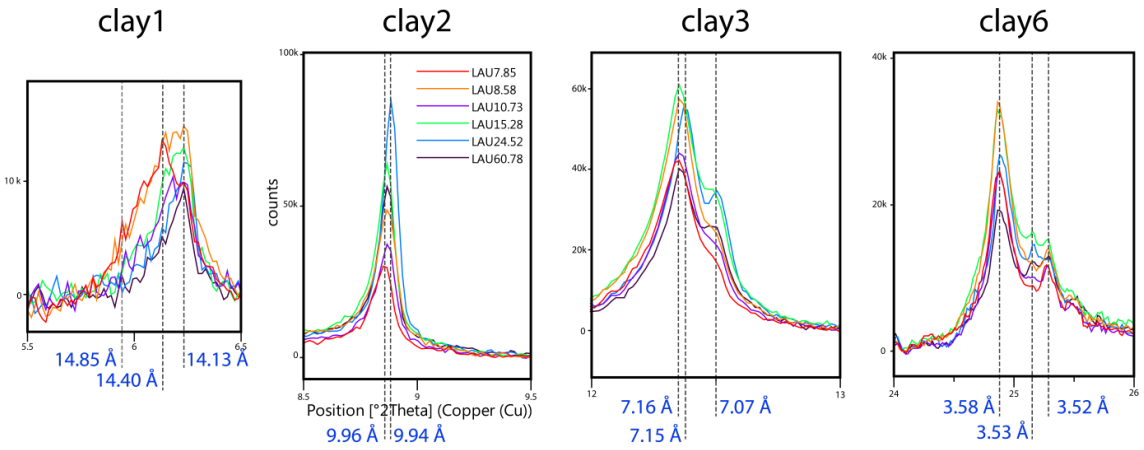

Fig. 4-3: Details of domed XRD patterns.
See Fig. 4-2 for legend to colours.

Normal (undomed) XRD

Undomed XRD patterns were obtained using the same protocol as for the domed samples, except for the absence of the dome that protects the sample from the atmosphere. The patterns are indistinguishable from the domed patterns, except for a lower background, the absence of the broad peak of the dome, and slightly higher peak intensities. This indicates that redox reactions do not play a role over the short time scales of air exposure (about 1 week).

In order to identify relative changes of the composition of the clay fraction with depth, the areas below the clay peaks were quantified in the range 5 – 27 °2θ after manual background stripping, and the areas of individual peaks were normalised to the total area of all clay-mineral peaks in the studied angular range. The results are shown in Fig. 4-4. Note that the relative peak areas serve exclusively to detect depth trends of the same clay species but do not yield information about the absolute contents. While the same set of clay minerals is observed in all samples, the relative fraction of kaolinite tends to decrease slightly with depth, with the opposite tendency for chlorite and illite.

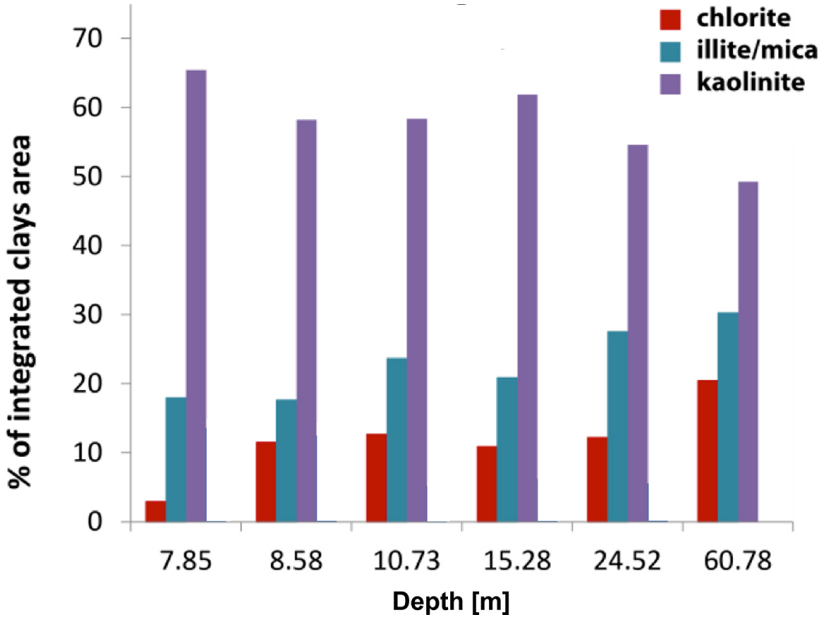

Fig. 4-4: Peak areas of individual clay minerals, normalised to the total area below all clay-related peaks.

4.2 Chemical composition of the rock

Results are listed in Tab. 4-2 (major elements) and Tab. 4-3 (trace elements). The depth trends are illustrated in Fig. 4-5 and Fig. 4-6. For the major elements, the following observations can be made:

- SiO_2 contents are slightly higher in the lowermost two samples, which are located in the silty (i.e. quartz-rich) facies.
- Al_2O_3 contents are higher in the weathered zone, consistent with the observed high content of clay minerals.

- Total Fe_2O_3 does not show any significant distinction between weathered zone and unweathered rock.
- MgO is slightly depleted in the upper part of the weathered zone where the rock matrix is brownish (i.e. down to 15.4 m), probably a consequence of dolomite dissolution.
- In the same zone, CaO is depleted, which is due to major dissolution of calcite.
- A slight depletion of Na_2O could be due to some degree of albite dissolution in the weathered zone, even though the trend is weak.
- The slight enrichment of K_2O in the weathered zone reflects the higher clay-mineral contents in this zone.

The majority of trace elements do not show systematic depth trends, with the following exceptions:

- As CaO and MgO, Sr is depleted in the upper part of the weathered zone, consistent with carbonate dissolution.
- Li, V, Cr, Cu and U are slighlty enriched in the weathered zone.
- B, Co, Ni, As, Sb and Pb are slightly enriched in the uppermost 1 – 2 samples (i.e. in the strongly altered zone).
- All other trace elements show no systematic trends with depth.

In summary, the most significant features are low concentrations of CaO, MgO and Sr in the uppermost 15.4 m where the rock matrix is brownish. In agreement with mineralogical data, carbonate minerals were partially dissolved in this zone. In contrast, total Fe_2O_3 shows no clear depth trend, even though the relative proportions of Fe^{2+} and Fe^{3+} have changed due to oxidation.

Tab. 4-2: Chemical composition of the rock: Major elements.

Analysed by X-ray fluorescence (XRF).

Depth [m]	Geological unit	SiO2 [wt.%]	TiO2 [wt.%]	Al2O3 [wt.%]	Fe2O3 tot [wt.%]	MnO [wt.%]	MgO [wt.%]	CaO [wt.%]	Na2O [wt.%]	K2O [wt.%]	P2O5 [wt.%]	Loss on ignition to 450 °C [wt.%]	Loss on ignition to 1000 °C [wt.%]	Sum [wt.%]
7.83	Opalinus Clay	53.2	1.01	20.7	6.82	0.07	1.5	3.1	0.2	2.85	0.29	4.28	10.10	99.84
8.58	Opalinus Clay	54.5	1.04	21.5	5.62	0.05	1.6	2.8	0.2	2.97	0.19	3.97	9.88	100.35
10.73	Opalinus Clay	54.0	1.00	19.9	6.83	0.09	1.6	3.5	0.2	2.80	0.29	3.68	10.00	100.21
12.10	Opalinus Clay	53.3	1.01	20.3	5.95	0.07	1.8	3.9	0.2	2.86	0.20	3.28	10.60	100.19
15.28	Opalinus Clay	54.6	1.01	20.2	5.65	0.08	1.9	3.6	0.2	2.84	0.19	4.21	10.30	100.57
24.52	Opalinus Clay	50.5	0.90	18.1	6.90	0.12	2.0	5.8	0.3	2.61	0.49	4.86	11.80	99.52
33.65	Opalinus Clay	55.3	0.86	15.8	6.32	0.11	1.9	5.5	0.4	2.47	0.30	4.86	10.80	99.76
60.78	Opalinus Clay	58.0	0.94	17.5	4.90	0.08	1.9	4.2	0.4	2.75	0.22	3.69	9.41	100.3

Tab. 4-3: Chemical composition of the rock: Trace elements.

Analysed by ICP-MS (Ce, Er, Gd, La, Nd, Sm, Th, U, Yb, Dy, Eu, Ho, Lu, Pr, Tb, Tm, Y) and ICP-AES (Ag, As, B, Ba, Be, Bi, Ce, Cd, Co, Cr, Cu, La, Li, Mo, Nb, Ni, Pb, Sb, Sn, Sr, V, W, Y, Zn, Zr).

Depth [m]	Geological unit	Li [ppm]	Be [ppm]	B [ppm]	V [ppm]	Cr [ppm]	Co [ppm]	Ni [ppm]	Cu [ppm]	Zn [ppm]	As [ppm]	Sr [ppm]	Y 1 [ppm]	Y 2 [ppm]	Zr [ppm]	Nb [ppm]	Mo [ppm]	Ag [ppm]	Cd [ppm]	Sn [ppm]	Sb [ppm]	Ba [ppm]
7.83	Opalinus Clay	195	3	232	159	148	33	74	26	129	65	176	31	30.9	210	20	<5	<0.2	<2	17	11	331
8.58	Opalinus Clay	195	3	213	158	148	25	60	22	128	43	188	28	27.9	209	20	<5	<0.2	<2	16	<10	345
10.73	Opalinus Clay	163	3	194	148	139	24	58	19	137	52	180	32	32.1	218	<20	<5	<0.2	<2	15	<10	317
12.10	Opalinus Clay	160	3	188	144	135	25	58	19	123	45	197	28	27.4	204	21	<5	<0.2	<2	15	<10	308
15.28	Opalinus Clay	166	3	190	144	140	24	57	21	121	44	217	29	29.3	211	<20	<5	<0.2	<2	15	<10	303
24.52	Opalinus Clay	137	3	189	133	129	26	60	18	150	50	284	37	36.2	186	<20	<5	<0.2	<2	14	<10	281
33.65	Opalinus Clay	96	2	167	122	126	22	47	14	111	47	236	30	29.1	254	<20	<5	<0.2	<2	14	<10	308
60.78	Opalinus Clay	128	2	175	122	127	21	47	16	114	45	245	29	28.3	248	<20	<5	<0.2	<2	15	<10	324

Depth [m]	Geological unit	La 1 [ppm]	La 2 [ppm]	Ce 1 [ppm]	Ce2 [ppm]	Pr [ppm]	Nd [ppm]	Sm [ppm]	Eu [ppm]	Gd [ppm]	Tb [ppm]	Dy [ppm]	Ho [ppm]	Er [ppm]	Tm [ppm]	Yb [ppm]	Lu [ppm]	W [ppm]	Pb [ppm]	Bi [ppm]	Th [ppm]	U [ppm]
7.83	Opalinus Clay	48	51.0	102.0	99	11.8	44.0	8.11	1.73	6.88	1.11	6.12	1.19	3.37	0.48	3.22	0.48	17	36	<10	13.0	2.73
8.58	Opalinus Clay	47	51.1	97.7	91	11.0	38.4	6.84	1.43	5.73	0.95	5.39	1.08	3.14	0.48	3.15	0.48	15	19	<10	18.0	2.67
10.73	Opalinus Clay	47	51.5	104.0	94	12.2	45.1	8.54	1.81	7.16	1.17	6.32	1.23	3.49	0.50	3.31	0.49	12	14	<10	14.8	2.75
12.10	Opalinus Clay	45	48.6	93.7	86	10.7	37.7	6.68	1.39	5.56	0.94	5.32	1.05	3.10	0.45	3.08	0.46	13	14	<10	14.8	2.54
15.28	Opalinus Clay	45	50.6	99.9	88	11.4	40.5	7.22	1.52	5.98	0.99	5.71	1.15	3.31	0.49	3.25	0.48	10	13	<10	10.8	2.72
24.52	Opalinus Clay	48	51.0	111.0	102	13.8	55.3	11.00	2.44	9.45	1.45	7.62	1.38	3.66	0.51	3.24	0.48	10	16	<10	14.4	2.57
33.65	Opalinus Clay	42	44.1	89.6	84	10.8	40.7	7.72	1.62	6.47	1.05	5.71	1.11	3.09	0.44	2.96	0.44	12	11	<10	13.2	2.34
60.78	Opalinus Clay	42	44.7	89.9	85	10.5	38.1	6.97	1.47	5.87	0.97	5.47	1.06	3.11	0.46	3.07	0.45	16	12	<10	12.8	2.42

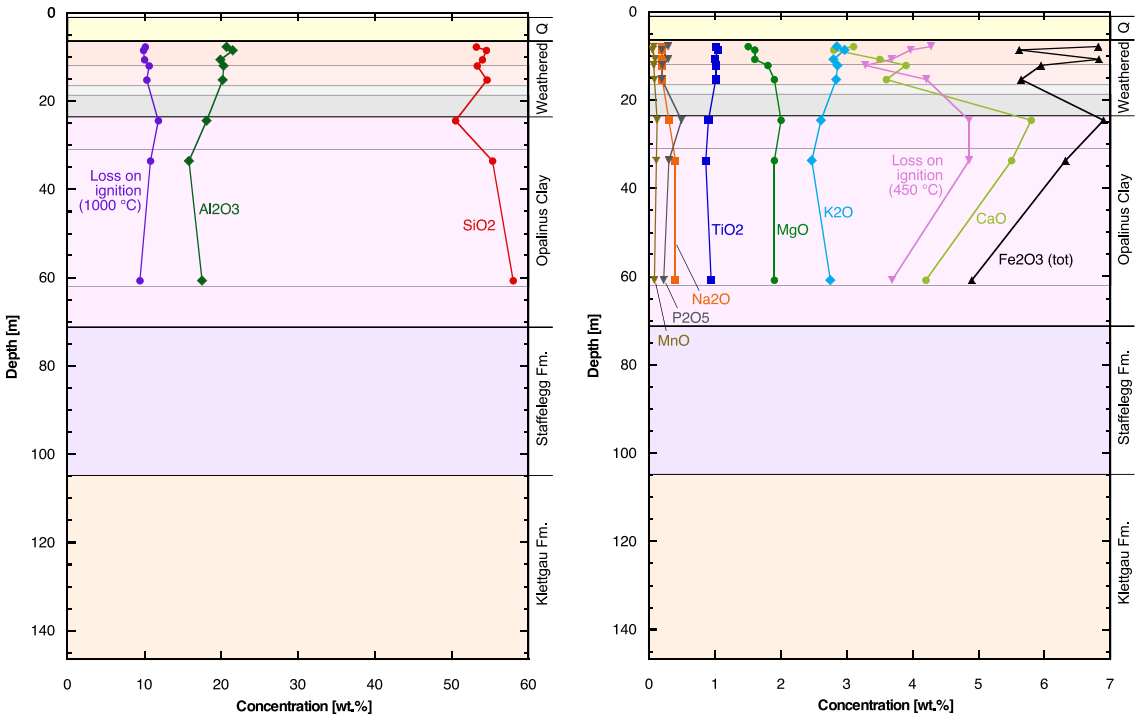

Fig. 4-5: Major-element rock composition as a function of depth.

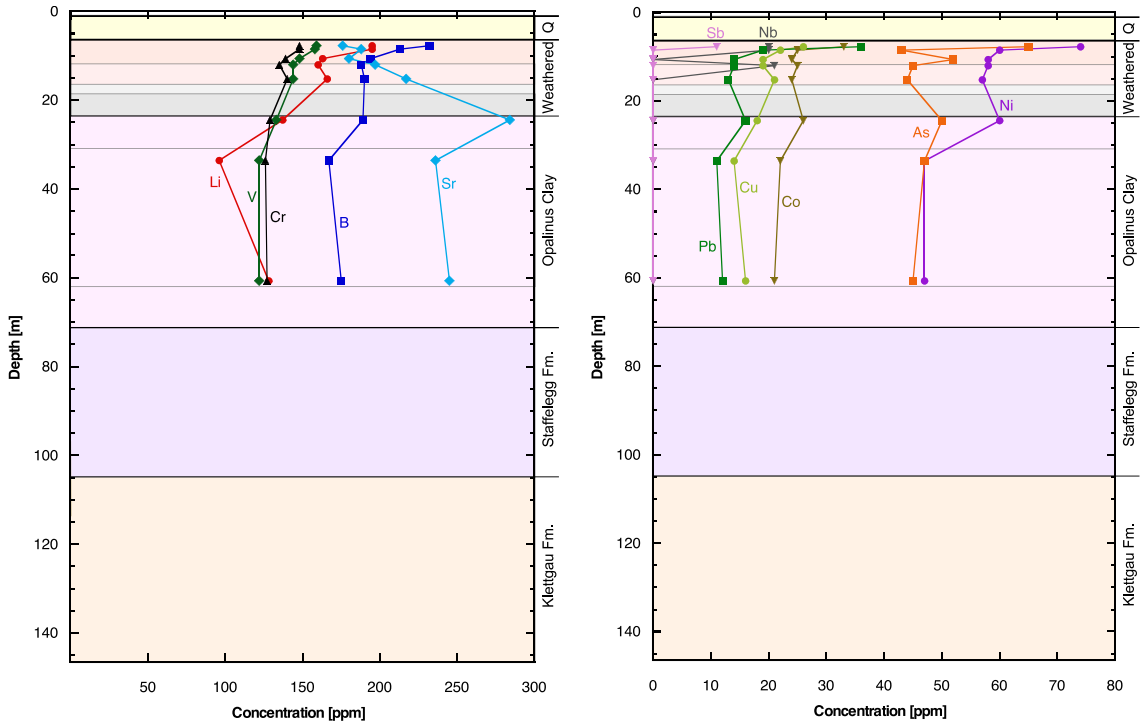

Fig. 4-6: Concentrations of selected trace elements in the rock as a function of depth.

4.3 Fe-bearing minerals

One of the objectives of the Lausen campaign was to characterise the geochemical effects of surface weathering on Opalinus Clay. Therefore, the distribution and oxidation state of Fe as a function of depth are of concern.

In Tab. 4-4, the total Fe obtained from the chemical rock analysis (Tab. 4-2) and the contents of Fe-bearing minerals determined by XRD (Tab. 4-1) are used to calculate the fractions of total Fe residing in pyrite, siderite and dolomite/ankerite. Pyrite and siderite are assumed to have stoichiometric Fe contents. For dolomite/ankerite, a Fe/Mg atomic ratio of 0.5 has been assumed, based on the microprobe data of Lerouge et al. (2014) performed on samples of Opalinus Clay from the Benken borehole. Note that, according to the same source, siderite may be non-stoichiometric and contain some Mg and Ca. On the other hand, calcite is not considered here but may contain a minor component of Fe. Under these assumptions, Tab. 4-4 suggests that in the strongly altered Opalinus Clay (i.e. to a depth of about 12 m), most of the Fe is present in minerals other than pyrite and siderite, most likely in Fe-hydroxides and clay minerals. At larger depths, pyrite and siderite become major carriers of Fe, even though there is still a substantial Fe fraction originating from other minerals.

Note that in the XRD patterns of the clay fraction, a broad peak is identified at d = 4.18 Å (21.25°) in the 4 uppermost samples (7.83, 8.58, 10.73, 12.10) and could represent goethite (Section 4.1.2). This peak is not seen in the clay patterns of deeper samples.

Further data on the nature of Fe minerals have been obtained from Mössbauer spectroscopy (Section 4.5).

Tab. 4-4: Distribution of Fe in different minerals based on X-ray diffraction.

Values "less than" (<) refer to the detection limit of mineral identification by X-ray diffraction.

Depth [m]	**Fe_{tot} in rock** [g/kg]	**Fe_{tot} in rock** [mol/kg]	**Fe in pyrite (FeS_2)** [% of Fe_{tot}]	**Fe in siderite ($FeCO_3$)** [% of Fe_{tot}]	**Fe in dolomite/ ankerite ($CaMg_{0.5}Fe_{0.5}(CO_3)_2$)** [% of Fe_{tot}]	**Rest** [% of Fe_{tot}]
7.83	47.70	0.854	1.2	< 5.0	< 1.5	> 92.3
8.58	39.31	0.704	0.3	< 6.1	< 1.8	> 91.8
10.73	47.77	0.855	4.5	< 5.0	0.7	> 89.8
12.10	41.62	0.745	3.1	< 5.8	2.7	> 88.4
15.28	39.52	0.708	4.7	30.3	3.3	61.8
24.52	48.26	0.864	25.6	35.1	0.9	38.4
33.65	44.20	0.792	2.7	62.0	< 1.6	> 33.7
60.78	34.27	0.614	7.5	13.7	1.3	77.5

4.4 SEM investigations

Two samples (8.23 m and 16.17 m) were studied with scanning electron microscopy (SEM) combined with energy dispersive X-ray spectrometry (EDX). The scope was to obtain information on the elemental distribution at high resolution in oxidation zones around fractures. The drill core samples (Fig. 4-7) were cut and embedded in degassed epoxy resin using the freeze drying and vacuum technique of Hadi et al. (2017). They were subsequently cut with a disc saw and polished with petroleum.

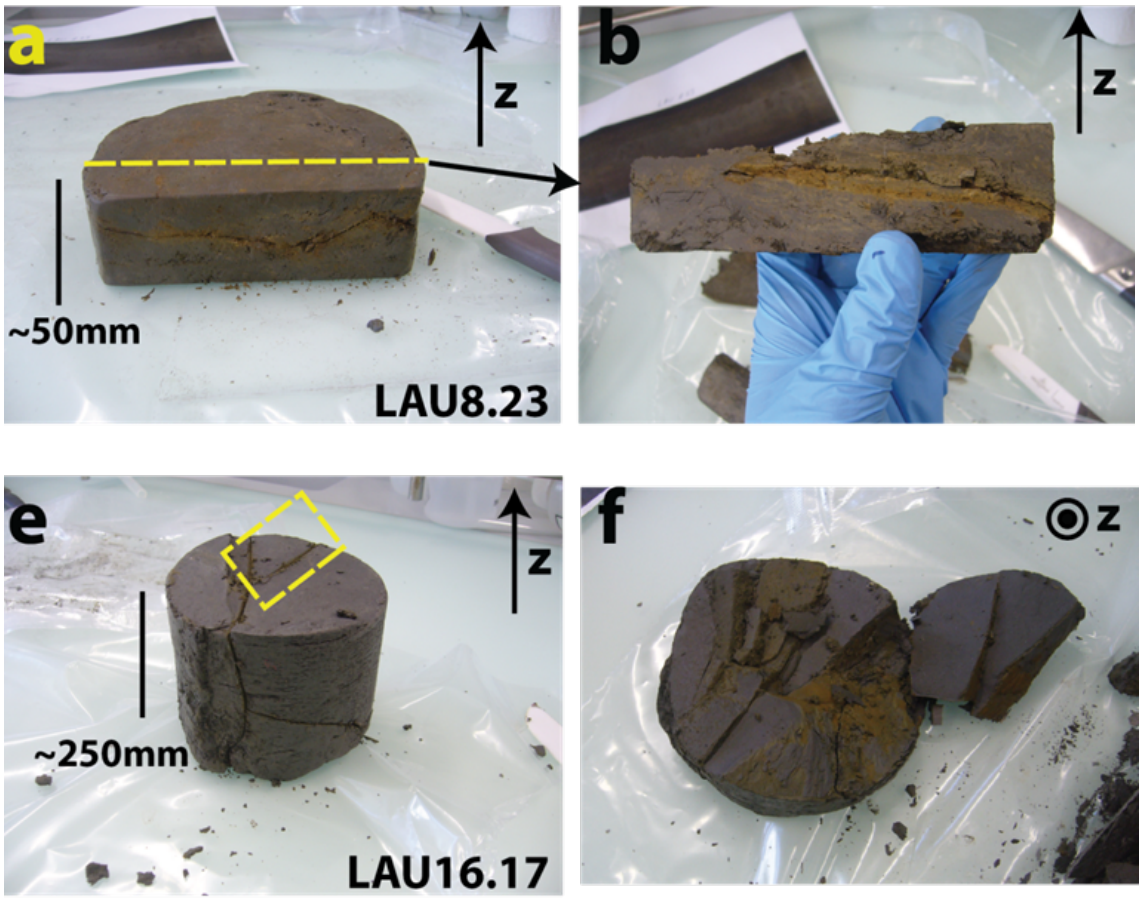

Fig. 4-7: Samples prepared for SEM analysis.
a, b: sample 8.23 m; e, f: sample 16.17 m

4.4.1 Sample 16.17

The sample originates from the zone where the rock matrix is grey and brown staining is limited to rims around fractures (see Fig. 2-2), of which sample 16.17 is an example. Chemical profiles perpendicular to the vertical fracture with a visible thin orange-brown rim at two different magnifications (100 and 1000 times) were acquired, as sketched in Fig. 4-8. Low-resolution elemental maps covering a surface of 10 x 50 mm^2 are shown for Si, Al, Fe and Mg in Fig. 4-9 and for K, Na, Ca and S in Fig. 4-10. The carbon map of Fig. 4-8 primarily reflects the epoxy resin that entered cracks and pores during impregnation. Besides the main vertical fracture, fairly thin (< 100 µm) and long cracks parallel to bedding are observed. Furthermore, an array of thin fractures (< 10 µm) adjacent and fairly parallel to the main fracture can be visualised. These are connected to the main fracture by a series a small cracks (< 5 µm wide). The observed features can be assumed to have existed before sampling, but were enlarged due to sample shrinkage upon freeze-drying.

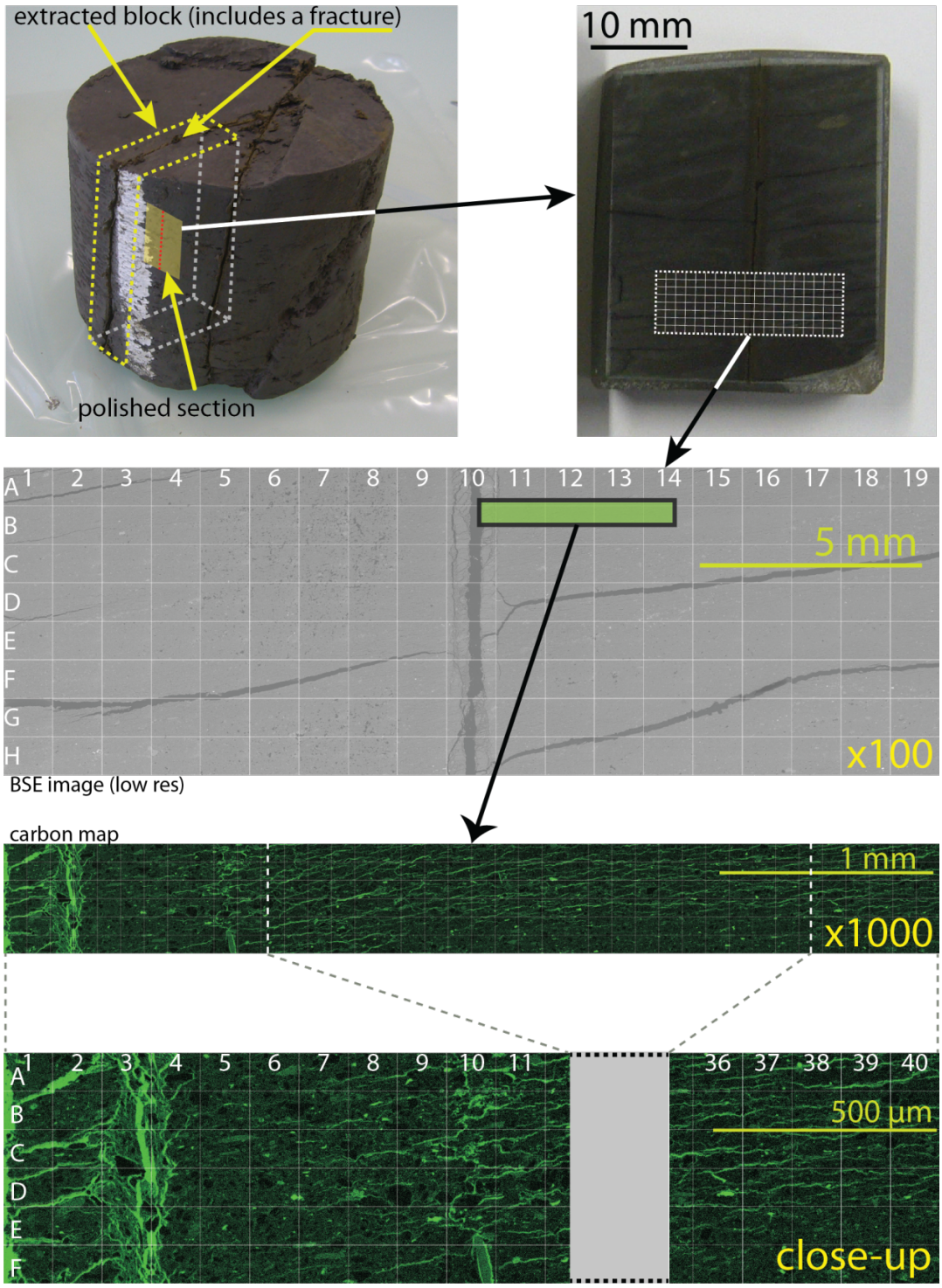

Fig. 4-8: SEM investigations of sample 16.17.

Upper half: Sample localisation and polished thick section showing the backscatter electron (BSE) image and the grid used for analyses at low resolution (100x). *Lower half:* Carbon maps generated at high magnification (1'000x) displaying small-scale fracture patterns adjacent to the macroscopic fracture, which is located along the left side of the illustration. As the sample was impregnated in epoxy resin, the carbon map highlights the pore space. Elemental maps were generated perpendicular to main vertical fracture

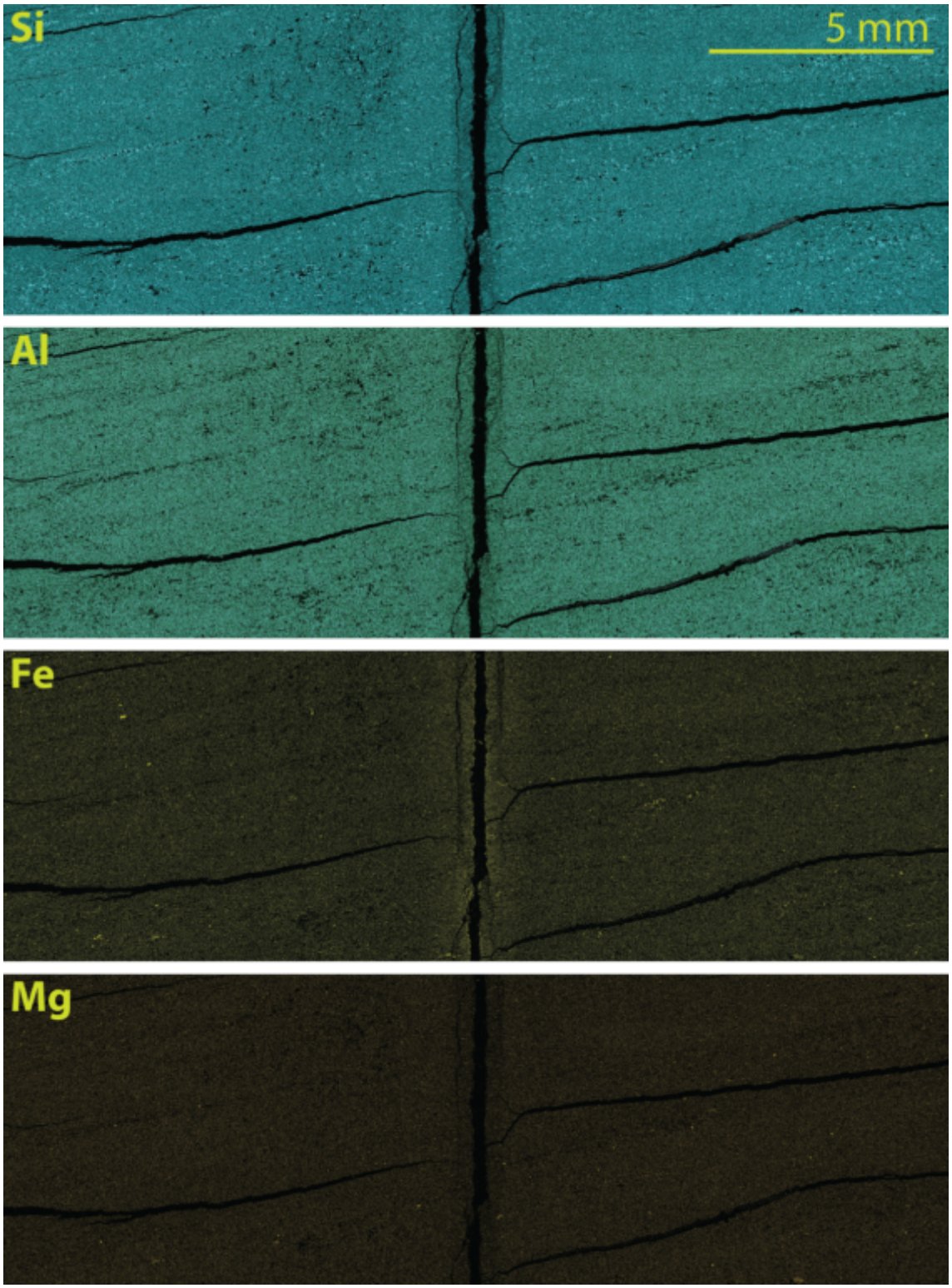

Fig. 4-9: Si, Al, Fe and Mg maps for sample 16.17 based on SEM-EDX at a magnification of 100x.

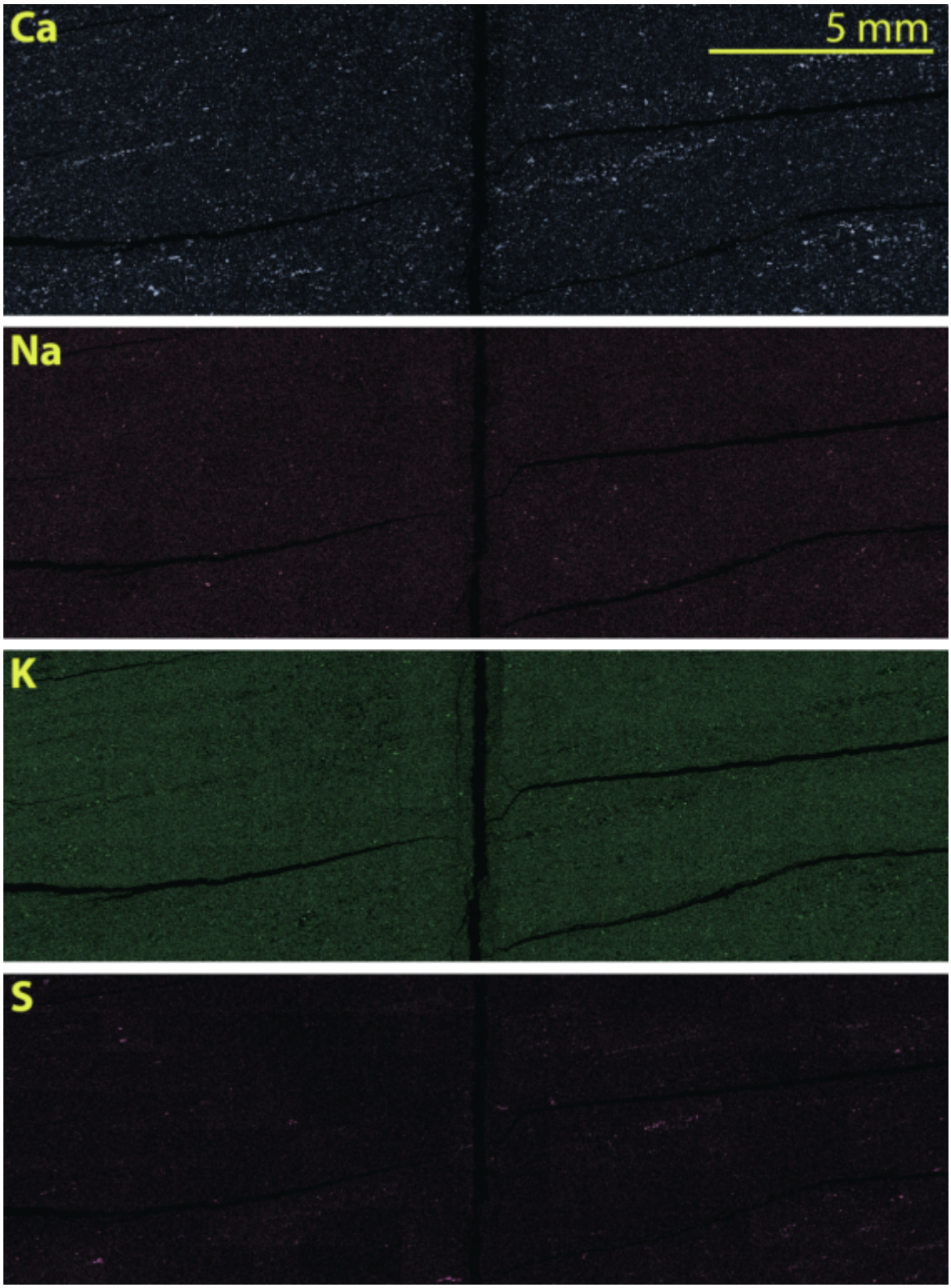

Fig. 4-10: Ca, Na, K and S maps for sample 16.17 based on SEM-EDX at a magnification of 100x.

The Si map exhibits a uniform distribution, the brighter spots representing quartz grains. This is supported by the Al map, in which Al mainly resides in clays and feldspars but shows no signal where the bright Si spots are located. Mg is also distributed homogeneously throughout the sample, except for some bright spots which are likely due to the presence of dolomite grains. The Ca map shows numerous bright spots, which are presumably calcite grains (up to ~ 10 μm large). These are often found to be concentrated along subhorizontal features. The visible discrete Na and K spots probably reflect feldspar grains. Fe is enriched in the vicinity of the fracture and even more so at the fracture surface. Otherwise it is distributed fairly homogeneously throughout the sample (reflecting the structural Fe in the clay), but is enriched in randomly located bright spots. Most of these can be attributed to pyrite by overlay with the S map, but some of them are S free and probably reflect siderite or ankerite.

Semi-quantitative information can be obtained from elemental profiles normalised against Al, which is the least mobile main element (Wersin et al. 2015). The Al-normalised profiles of Si, Ca, Fe, S, K and Na for the low magnification are shown in Fig. 4-11. A sharp symmetrical increase of the Fe/Al ratio close to the fracture (~ 0.2 mm from the interface) can be identified. Away from the fracture surface, there is a small gradual increase until 5 mm. The Si/Al and K/Al ratios exhibit no change except a slight decrease immediately adjacent to the fracture. The Ca/Al and, to a lesser degree, the Mg/Al ratio display a decrease towards the fracture, starting about 10 mm from the surface and probably reflecting dissolution of carbonate minerals. The zone of Ca and Mg depletion is larger than that of Fe enrichment. The Na/Al profile indicates no clear trends.

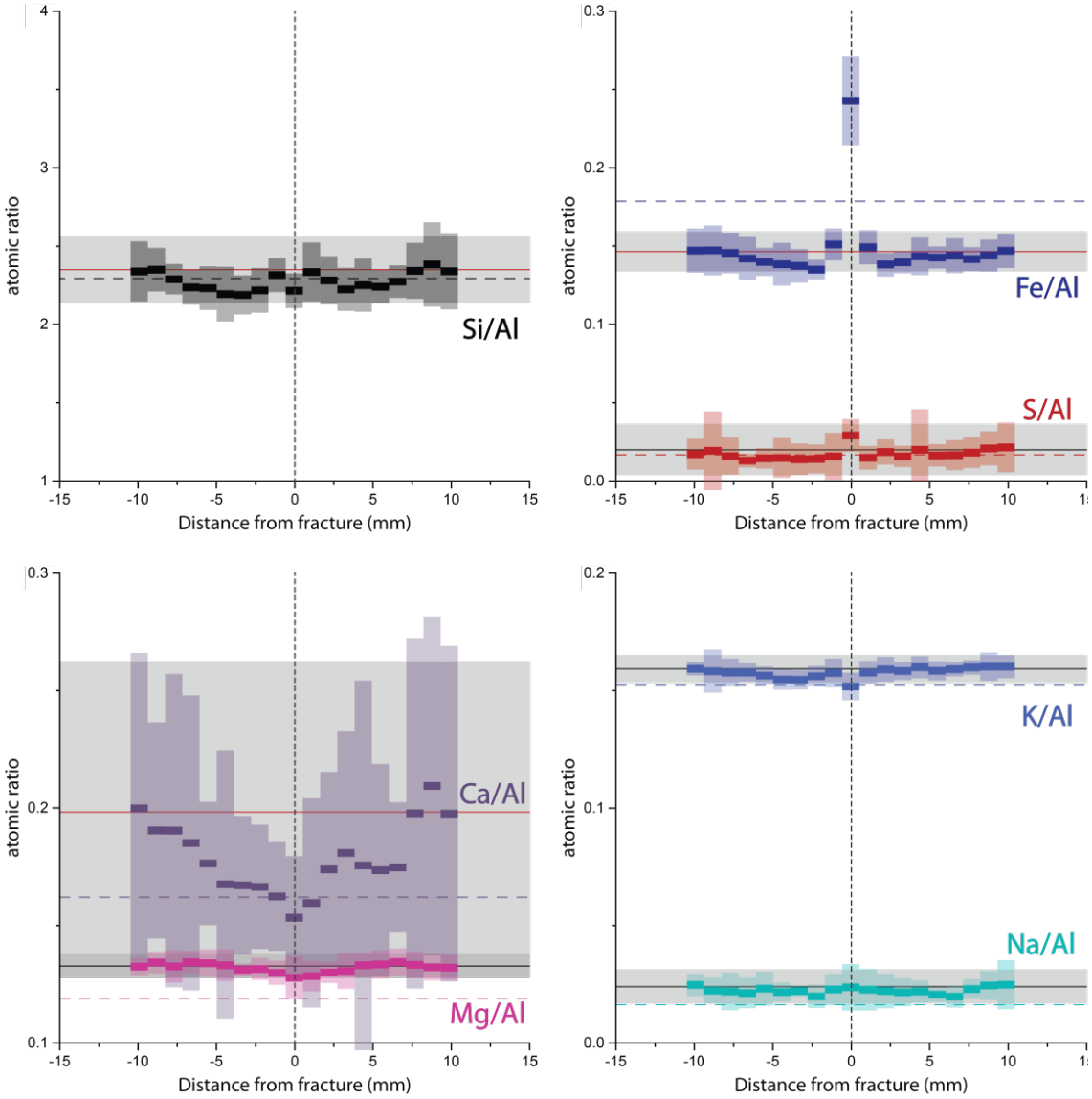

Fig. 4-11: Elemental profiles for sample 16.17 acquired at magnification of 100x.

For a given element X, coloured bars represent the average X/Al ratio in each column of the mapped grid (rectangle of same colour represents ± 2σ). Broken horizontal lines of same colour represent average reference value in powdered samples from similar depth (XRF analysis). Solid horizontal lines represent average EDX value in the bulk of the sample (i.e. far from the fracture, at distance > 7.5 mm), and light grey areas represent ± 2σ.

4.4.2 Sample 8.23

Mesoscopically, a subhorizontal fracture with a large irregular orange-yellow oxidation zone (5 – 15 mm thick) can be identified (Fig. 4-12, top left). The oxidation zone has a breccious aspect, possibly related to a collapse movement following partial dissolution within the weathered zone. The backscatter image (Fig. 4-12, top right) shows the highly heterogeneous nature of the clay structure in this zone, with the brighter aggregates (ranging from tens of µm to a few mm in size) surrounded by a darker clayey matrix. Numerous microfractures occur at the aggregate-matrix

boundaries and also cross-cut the aggregates. The fracturing is generally fairly parallel to the orientation of the perturbed area and thus to bedding, resulting in a layered structure.

Elemental maps are depicted in Fig. 4-13 and Fig. 4-14. In general, a fairly even distribution and similar patterns for Si, Al, Mg and K as for the lower sample 16.17 are observed. Quartz and calcite are present in elongated zones in the perturbed area, but occur also randomly in the clay matrix. The S content is very low, except in a few spots, which presumably reflect pyrite because Fe is concentrated there as well. The Fe map accentuates the large aggregates in the disturbed area, evidencing the enrichment of this element therein. In the surrounding matrix Fe is more evenly distributed.

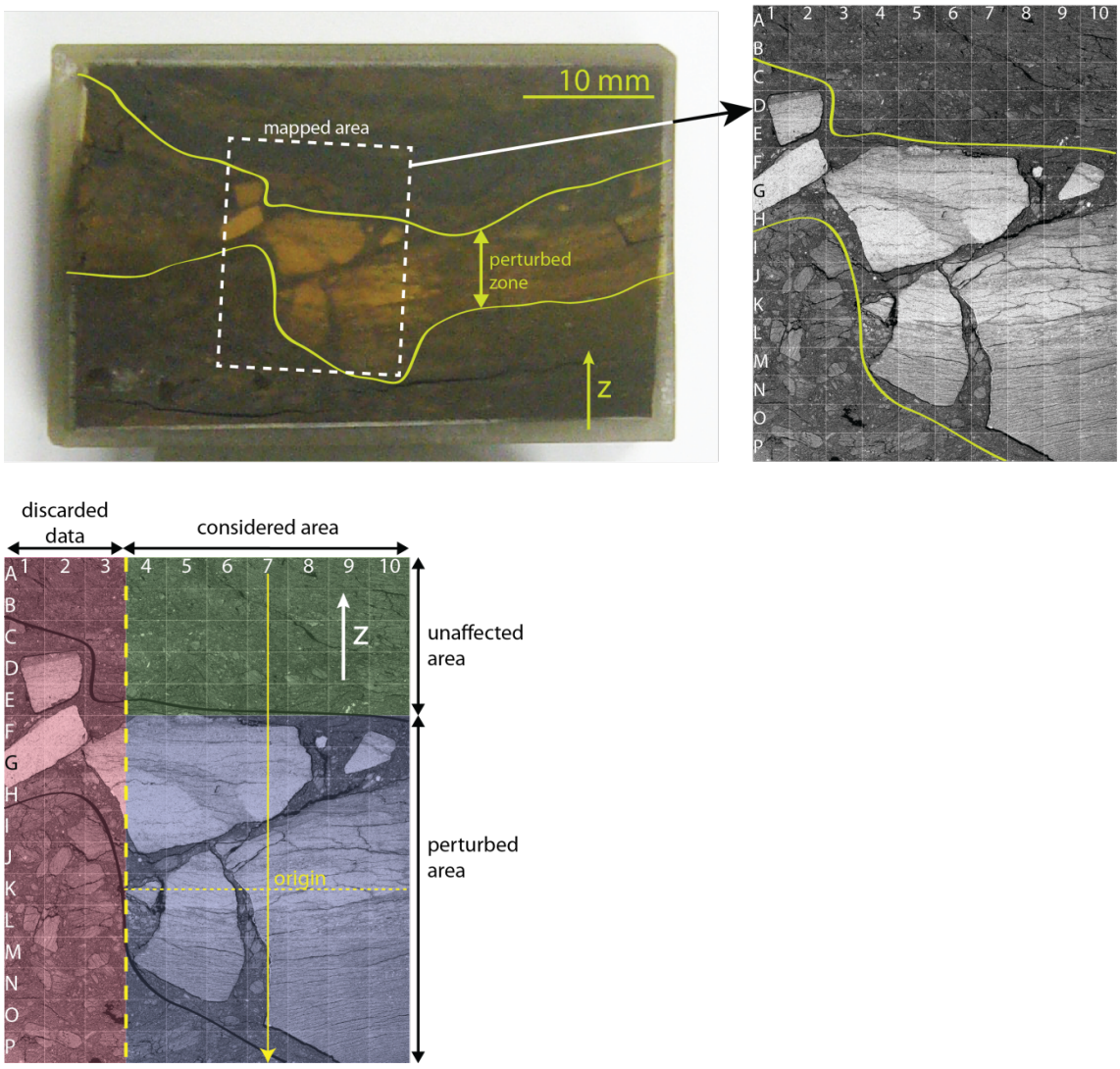

Fig. 4-12: Mesoscopic aspect of sample 8.23 used for SEM investigations.

Top left: Polished thick section. The yellow lines delimit the perturbed area, visually observed as a brown/orange halo contrasting with the darker clay matrix. *Top right:* Low-resolution (80x) BE image and analysis grid *Bottom:* Image showing grid and direction of elemental profiles. Colours reflect the zones considered for establishing the chemicals profiles (red = discarded area). Two further areas were distinguished: an area unaffected by Fe enrichment (olive green) and a perturbed area (blue)

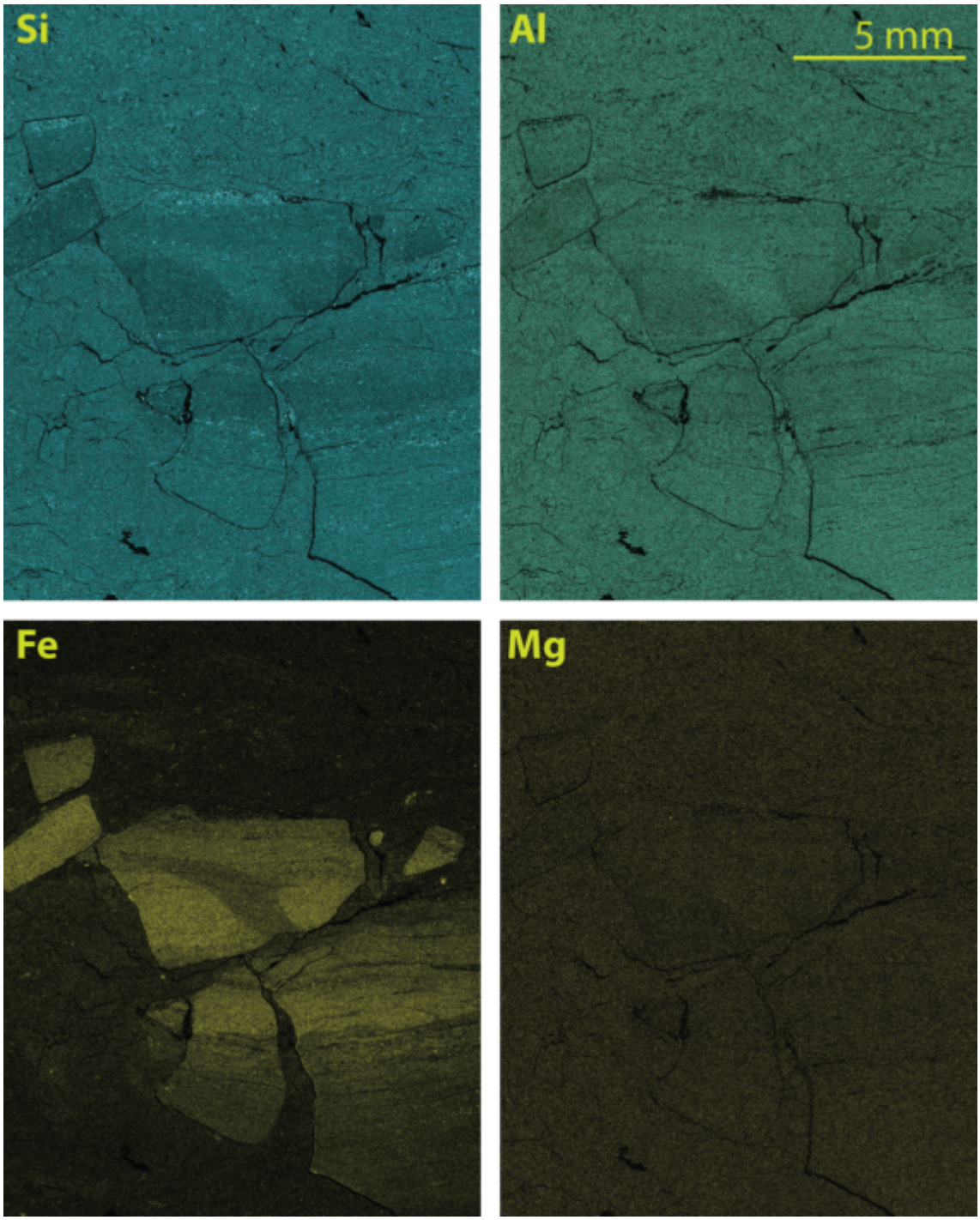

Fig. 4-13: Si, Al, Fe and Mg maps for sample 8.23 based on SEM-EDX at a magnification of 100x.

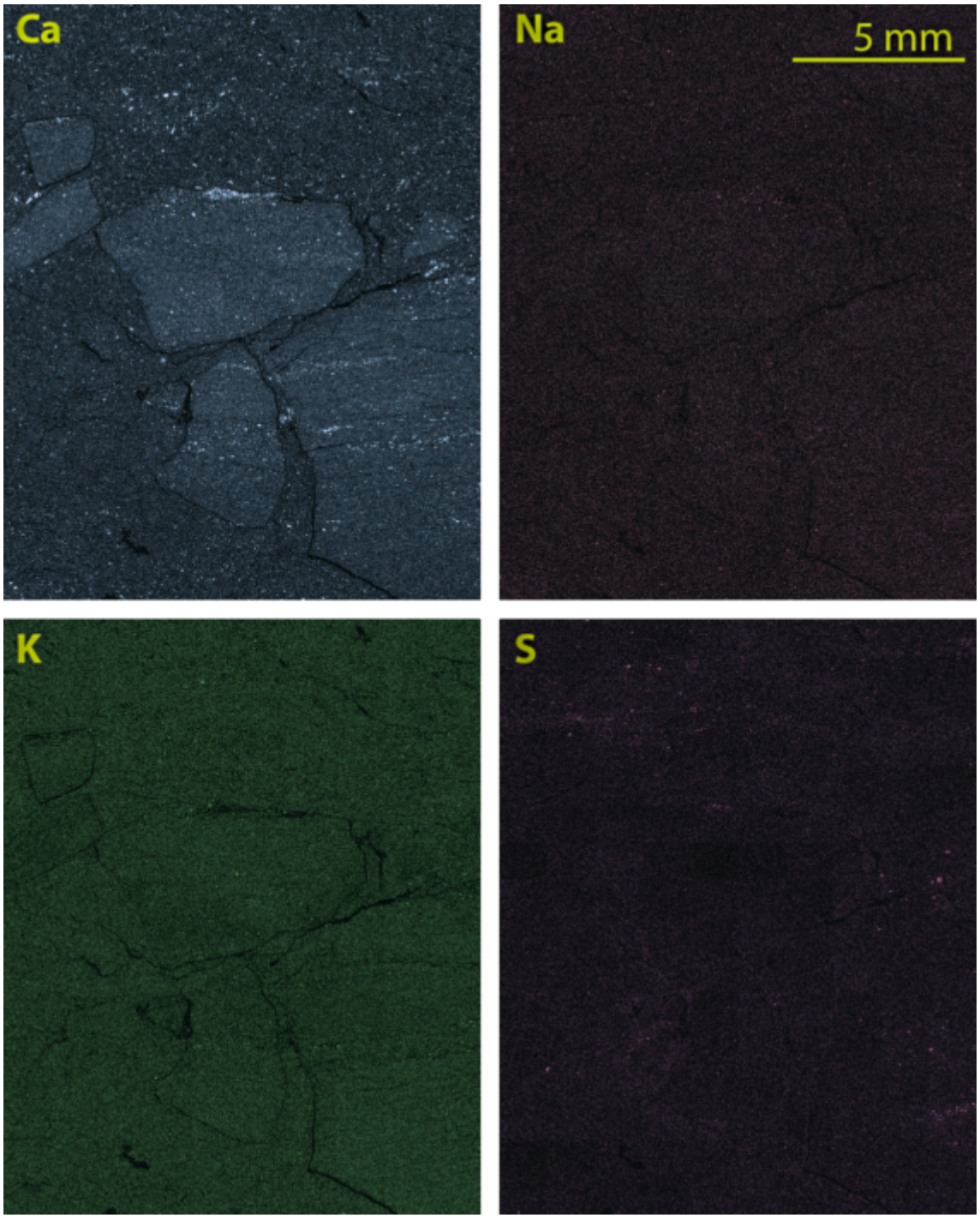

Fig. 4-14: Ca, Na, K and S maps for sample 8.23 based on SEM-EDX at a magnification of 100x.

In view of the complex geometry of the Fe-enriched area, the Al-normalised elemental profiles were acquired in two steps. In the first step, a two-dimensional chemical grid of the major element ratios in the investigated area was generated. For each grid element, a colour scale relative to the unperturbed bulk value was defined. The chemical grids are shown in Fig. 4-15 and Fig. 4-16.

The grids for Si and K suggest that the perturbed area is slightly depleted in these elements. The distribution of Na and S is more heterogeneous. Both Ca and Fe display a strong enrichment in the perturbed area. In the case of Fe, this increase reaches up to 700 % of the bulk level.

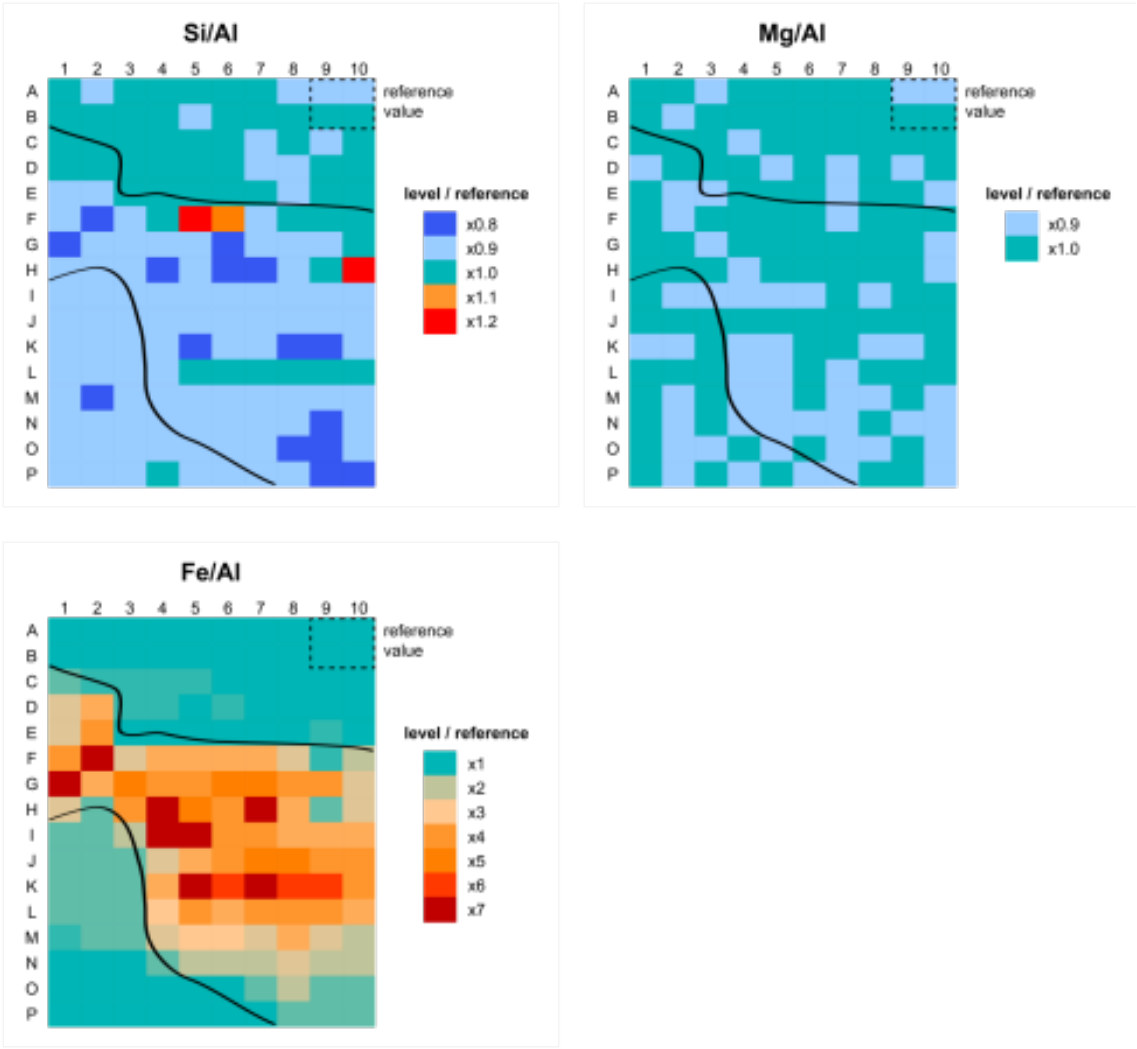

Fig. 4-15: Al-normalised chemical grids of major elements Si, Mg and Fe in the area of sample from 8.23 at magnification of 80x.

For a given element, the colour scale is defined relative to the average value in sectors A-B/9-10 (Fig. 4-12), assumed to be far enough from the perturbed zone and thus representative of the average value in the bulk of the sample. The dark curves delineate the perturbed zone as observed by eye.

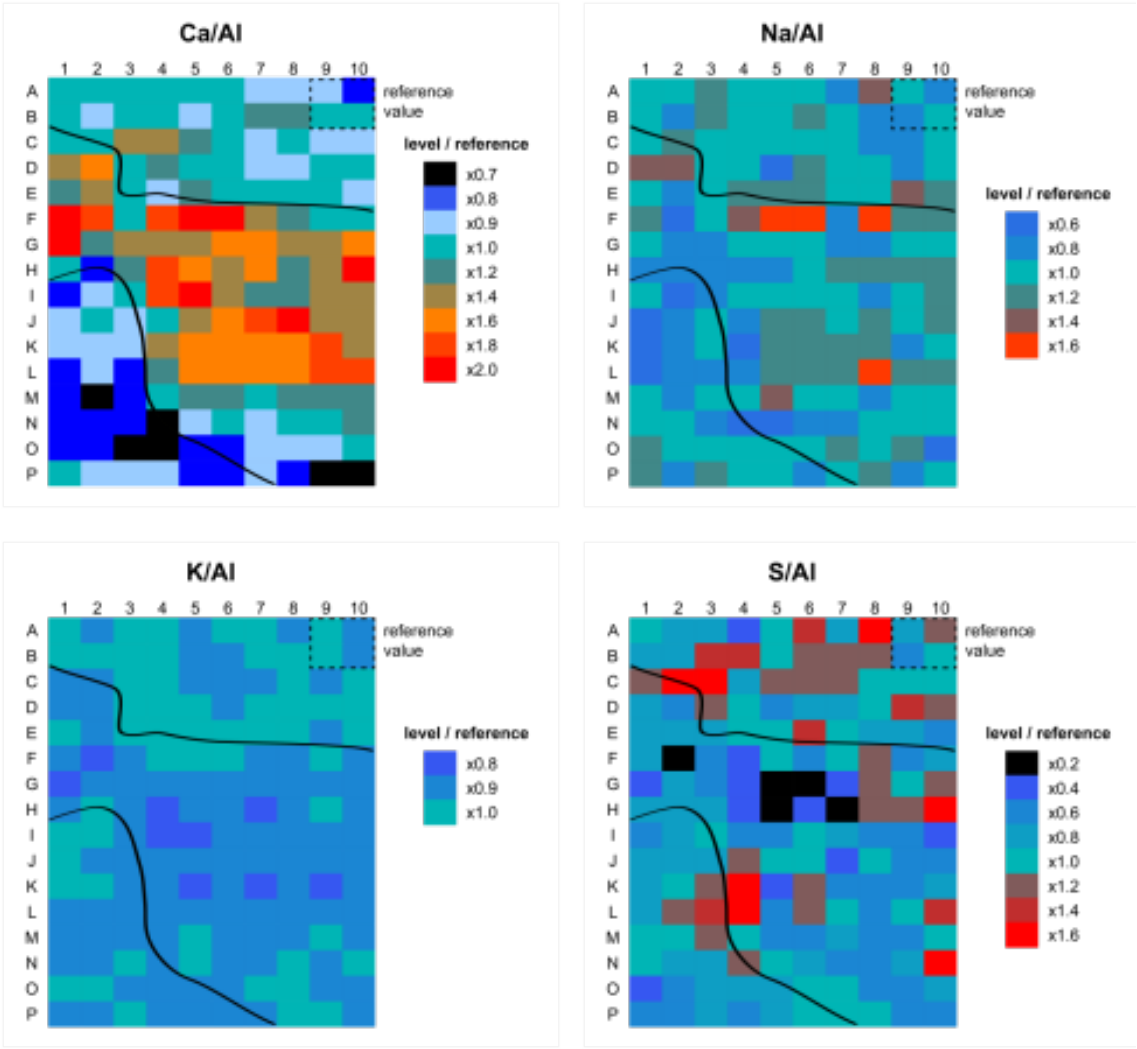

Fig. 4-16: Al-normalised chemical grids of minor elements Ca, Na, K and S in the area of sample 8.23 mapped at magnification of 80x.

For a given element, the color scale is defined relative to the average value in sectors A-B/9-10 (Fig. 4-12), assumed to be far enough from the perturbed zone and thus representative of the average value in the bulk of the sample. The dark curves delineate the perturbed zone as observed by eye

In a second step, chemical profiles along the yellow arrow in Fig. 4-12 (bottom) were generated by pooling the information from each row. The three first columns were not used for the pooling (red zone in Fig. 4-12, bottom) because the perturbed area is narrower and shifted upward compared to the rest of the mapped area. In the selected area, the upper boundary of the perturbed zone is fairly horizontal. The lower boundary is somewhat oblique to the applied grid, resulting in a somewhat blurred definition in the profiles. The resulting profiles are shown in Fig. 4-17. The most conspicuous feature is the strong increase (4 – 6 times) of Fe/Al.

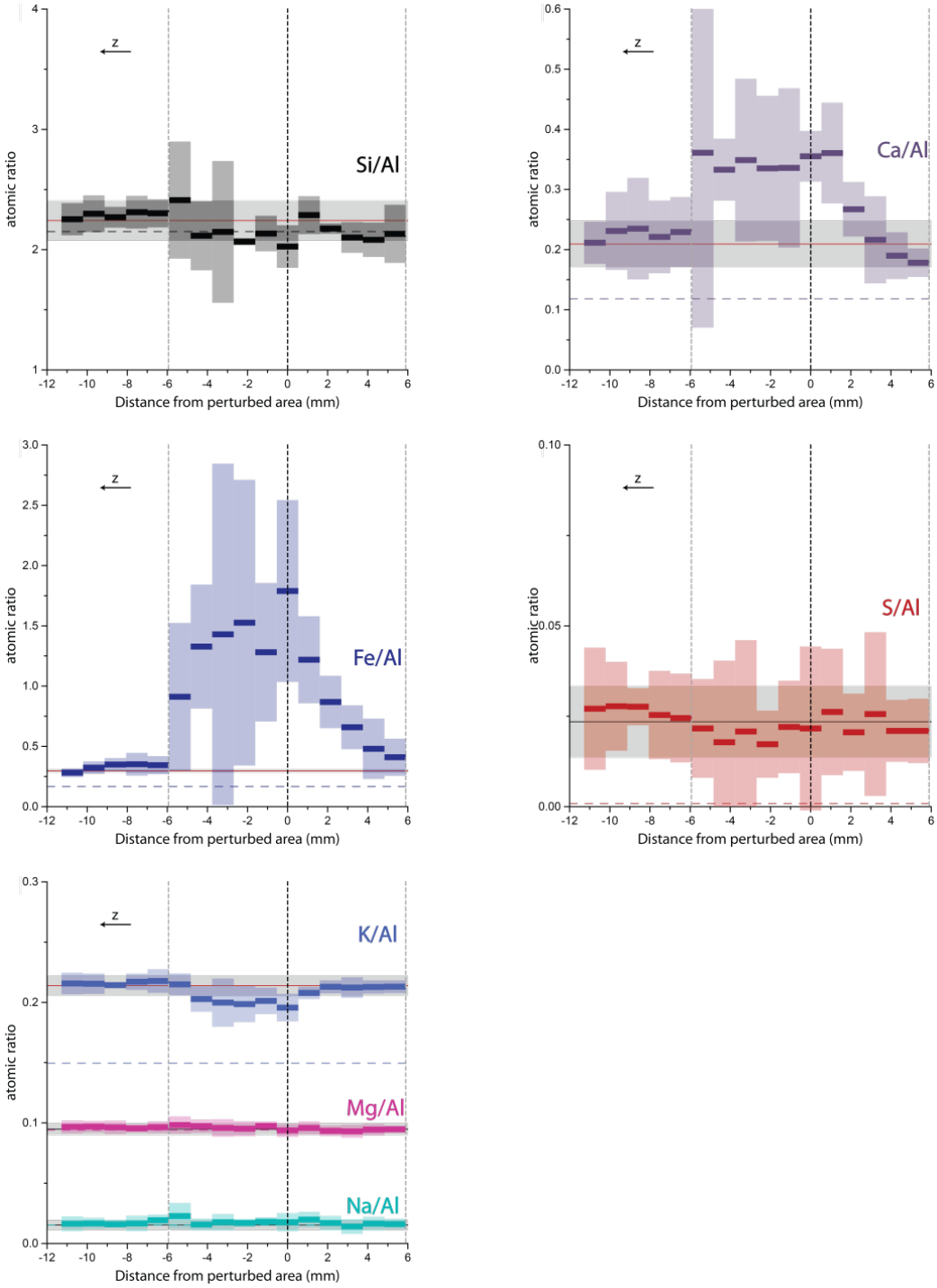

Fig. 4-17: Elemental profiles for sample 8.23 perpendicular to to the perturbed area acquired at a magnification of 80x.

The perturbed area corresponds to the range -6 to +6 mm on the x axis (blue area in Fig. 4-12, bottom), and the unaffected area to the range -12 to -6 mm (olive-green area in Fig. 4-12). For a given element X, coloured bars represent the average X/Al ratio in each column of the mapped grid (rectangle of the same colour represents ± 2σ). Broken horizontal lines of same colour represent average reference value in powdered samples from similar depth (XRF analysis). Solid horizontal lines represent average EDX values in the bulk of the sample (i.e. far from the fracture, sectors A-B/9-10 in Fig. 4-12), and light grey areas represent ± 2σ.

4.5 Mössbauer spectroscopy and phenanthroline method

4.5.1 Methodology

^{57}Fe Mössbauer spectroscopy is a useful tool for analysing iron species in rocks. In combination with other methods (e.g. XRD, XRF), the fitting of Mössbauer spectra, the estimation of Fe^{2+}/Fe^{3+} ratios and the quantification of Fe minerals is greatly facilitated.

In Opalinus Clay, paramagnetic high-spin (HS) octahedral Fe^{2+} species include structural Fe^{2+} in clay minerals (mainly chlorite, illite, smectite) and carbonates (siderite, ankerite). High-spin octahedral Fe^{3+} includes structural Fe^{3+} in clay minerals (smectite, illite) and goethite. A further paramagnetic (low-spin) species is pyrite, whose spectra overlap with HS-paramagnetic Fe^{3+}. Goethite may also be present as a supermagnetic HS species, which is detectable at low temperature (77 K). The Mössbauer spectra were recorded at room temperature (RT, 295 K) and at 77 K using a constant acceleration spectrometer and a ^{57}Co source diffused into an Rhodium matrix. Velocity calibrations were carried out using an Fe foil at RT. The values of the hyperfine parameters were refined using a least-squared fitting procedure with a discrete number of independent quadrupolar doublets and magnetic sextets composed of Lorentzian lines. The values of isomer shift are reported relative to that of the Fe spectrum obtained at RT. The proportions of each Fe species were established from the relative spectral area, assuming thus the same values of the f-Lamb-Mössbauer factors characteristic of each phase. The studied claystone matrix involves various $Fe^{2+/3+}$ bearing species (with various crystal-size distributions), which can result in very similar or overlapping signatures. Interpretation of such spectra is not straightforward and was facilitated by the use of XRF and XRD data as well as the in-house database of Fe bearing compounds. The Mössbauer spectra consist of the superposition of quadrupolar and magnetic features. They were fitted with minimal sets of features consisting in quadrupolar doublets and magnetic sextets, whose potential attributions are detailed in Tab. 4-5.

Tab. 4-5: Set of components used to fit the Mössbauer spectra and their possible attribution.

Component of the spectra		**Possible attribution**	**Remark**
HS-oct-Fe(III)	Doublet	Clay minerals (e.g. Montmorillonite, illite, micas, kaolinite)	
		Small (< 5nm) grains of goethite "nano-goethite"	
		Medium (5 – 25 nm) grains of goethite	Only at 300 K
		Green rust	
		Lepidocrocite, sorbed Fe (III), ferrihydrite	
HS-oct-Fe(II)	Doublet	Clay minerals (mainly illite, chlorite and/or mica, and probably montmorillonite)	
		Siderite/ankerite, sorbed Fe(II), diverse Fe(II) precipitates	
Pyrite	Doublet	Pyrite	
Goethite	Sextet	Medium (5 – 25nm) to large (> 25nm) grains of goethite	Only at 77 K

All observed doublets represent paramagnetic high-spin octahedral Fe (further referred to as "para-oct-Fe"), but can also include super-paramagnetic species at room temperature (e.g. small grains of goethite). The sextets represent magnetic species (at room temperature only), and also include super-paramagnetic species at low temperature. It must be emphasised that the list of possible attributions (Tab. 4-5) is not exhaustive, only the most likely species are listed. Spectra were in most cases measured at two different temperatures, in order to have more detail on the samples (e.g. super-paramagnetism) and to check the validity of the fit (must be consistent between the two temperatures).

The magnetic and super-paramagnetic (i.e. magnetic at low temperature, such as "large enough" goethite or hematite grains; Vandenberghe & De Grave 2013) species can be discriminated from paramagnetic species by analysis at contrasting temperatures (300 K and 77 K in the present case). Indeed, goethite grains tend to exhibit different signatures, depending on their size. "Large" grains (> 25 – 30 nm) are magnetic at both temperatures, "medium" (between 5 – 8 and 20 nm) ones are magnetic only at low temperature, and "small" (< 5 – 8 nm) ones are paramagnetic at both temperatures. It must be emphasised that these size ranges are rough estimates, as such behaviour depends also on distance between grains, crystallinity and interferences with other Fe phases. Similar behaviour can be expected for hematite, but the interpretation is less straightforward because of more significant crystallographic changes induced by temperature variations and higher dependence on grain size. In the present data, the distinction between goethite and hematite is mostly based on their hyperfine magnetic field and the way it is affected by temperature variations (hematite exhibits a higher field).

The presence of pyrite further complicates the interpretation of spectra because this low spin Fe^{2+} compound has a signature that can easily be erroneously interpreted as high spin octahedral Fe^{3+} (e.g. lepidocrocite, clay minerals, hydroxides). In the present approach, the occurrence of pyrite (grain size, distribution and maximum content regarding Fe pool) was first assessed by the comparison with XRD patterns, SEM/EDX (BSE images, chemical maps) and XRF (Fe/S) data. If the probability of presence (content and/or distribution) is high (as in the lowermost samples), its presence is imposed in the fitting but the content is let free to vary (the initial value is set to the maximum predicted value from XRF). On the contrary, if it is low (as for the shallow samples), fitting is tested with or without imposing the presence of pyrite, and its presence is only considered if significant improvement of fitting is achieved. Otherwise it is neglected (i.e. pyrite content < 2 % of total Fe).

Six powdered samples were prepared in a glovebox and conditioned in degassed epoxy resin before analysis. Their spectra at room temperature and at 77 K are presented in Fig. 4-18. From fitting of the Mössbauer spectra and accounting for total Fe obtained from XRF, the proportions of the different Fe pools and the Fe^{2+}/Fe^{3+} ratios were estimated.

Iron speciation was measured chemically using a modified 1,10-phenanthroline method (Amonette & Templeton 1998, Stucki & Anderson, 1981a, b), outside the anaerobic chamber, in a dark room under red light. Dissolution of the sample (and thus of Fe) was only partial in all cases and the result could thus not be used for estimation of total Fe content. Nevertheless, Fe reduction levels were found to be very consistent with Mössbauer results, suggesting that, although dissolution was not complete, the dissolution of Fe^{3+} and Fe^{2+} was fairly congruent.

4.5.2 Results from Mössbauer spectra and chemical analysis

Mössbauer spectra of the 6 samples are displayed in Fig. 4-18. Tab. 4-6 regroups the information relative to the distribution of the Fe pools identified in the various samples inferred from 77 K spectra – except for carbonates, whose contents were inferred from RT spectra. The four main components are displayed in the spectra, i.e. HS-oct-Fe(III), HS-oct-Fe(II), goethite and pyrite. Except for pyrite, these components are often composed of two to three sub-components. The composed spectra of goethite reflect the grain-size distribution. With regard to HS-oct-Fe species, the composed spectra reflect the variable octahedral environment (e.g. different clay sites or different minerals).

Magnetic species are only observed in the 77 K spectra of the four uppermost samples (7.83, 8.58, 10.73 and 15.28). Such features are explained by the presence of super-paramagnetic goethite (i.e. "mid" sized grains of goethite, 5 – 25 nm). Goethite accounts for the main iron pool in the three uppermost samples. The absence of such features in the spectra of samples 24.52 and 60.78 does not completely rule out the presence of goethite. In general, the pool of paramagnetic HS-Fe(III) is fairly small in these two samples (at most 15 %), and likely reflects predominantly structural Fe in clay minerals (e.g. in kaolinite and illite).

In the case of sample 24.52, multiple fits are possible because one of the components attributed to HS-Fe(III) has hyperfine parameters very close to those of pyrite. The deduced amount of pyrite is 16 ± 10 % of total Fe (in case all S is associated to pyrite). Higher values are more likely, as suggested by chemical and mineralogical analyses (see below). The amount of pyrite determined for the other samples is consistent with the chemical and mineralogical data, i.e. negligible in the two uppermost samples, and moderate in samples 10.73, 15.28 and 60.78 (4 – 5 %). This suggests that S is mainly associated to Fe in the four lowermost samples.

Total Fe(II) content (and thus reduction level of Fe) increases as a function of depth. Fe(II) is mainly present as paramagnetic HS-Fe(II) and to a lower extent as pyrite. The lowest amounts of Fe(II) are found in the three uppermost samples (20 – 30 % of total Fe). The highest amounts are found in the two lowermost samples (85 – 95 %), and the reduction level of sample 15.28 is intermediate (56 %).

One or two different components are needed to fit the spectral area attributed to HS-Fe(II), further referred to as Fe(II)-A, Fe(II)-B and Fe(II)-C. In case of the four lowermost samples, the Fe(II)-C component is fairly consistent with that of siderite according to literature (Stevens et al. 2005). One must however emphasise that for siderite hyperfine parameters depend on crystallinity. Moreover, other Fe species may exhibit similar features (e.g. structural or sorbed Fe in clays). Finally, the presence of ankerite in limited amounts can also be suspected (especially in sample 15.28). As a consequence, this component of the spectra (Fe(II)-C) can be considered as a high estimate of the content in ferrous carbonates. The Fe(II)-A component observed in all samples is consistent with structural Fe(II) over a large range of clay minerals. This is also the case for the Fe(II)-B component observed in sample 8.58.

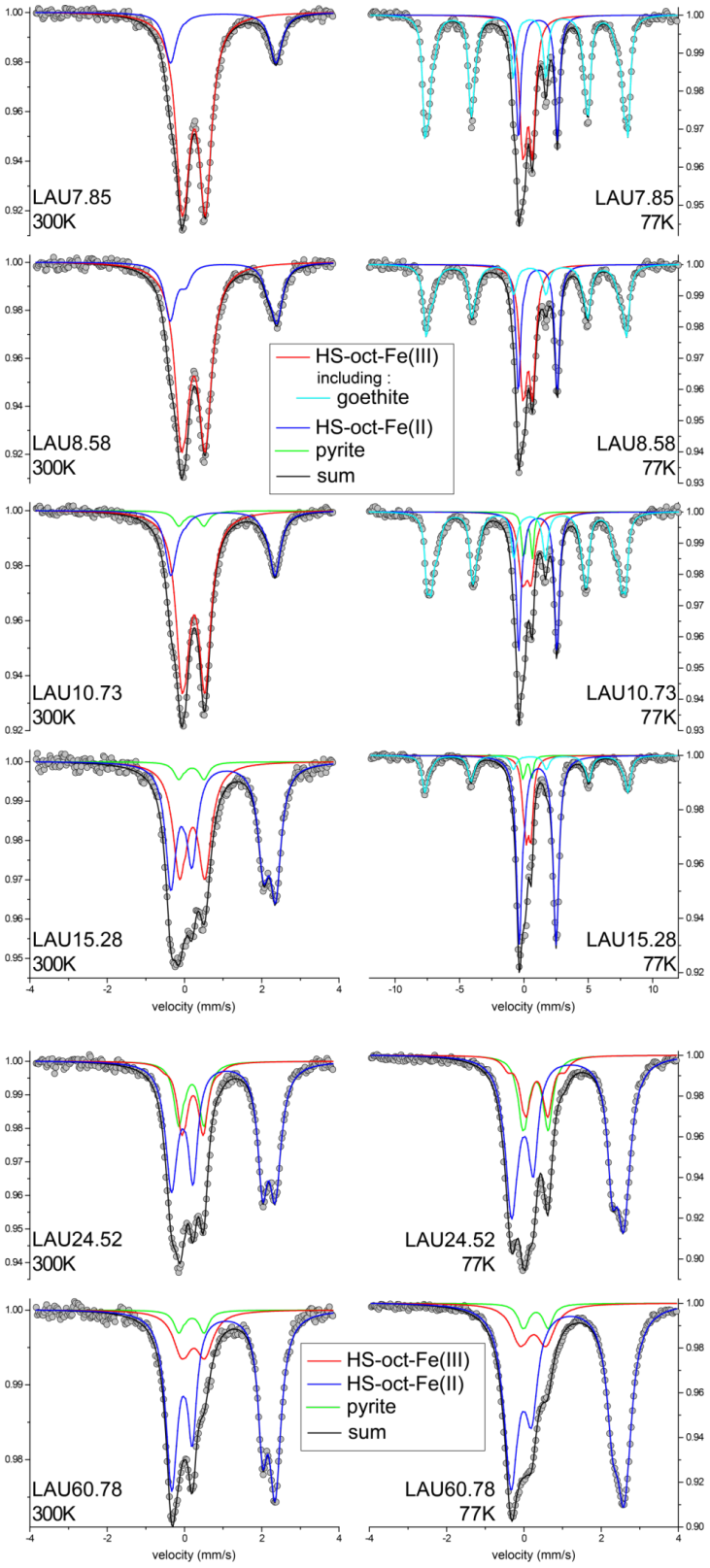

Fig. 4-18: Mössbauer spectra at room temperature and at 77 K.

For the two lowermost spectra a different velocity scale is shown given the lower resolution of these spectra.

Tab. 4-6: Mineralogical data on Fe phases in.ferred from Mössbauer analysis using proportions at 77 K, except for carbonates.

Data from chemical analysis (phenanthroline method) are indicated in italics for comparison.

Sample	**Total Fe(II)**		**HS-Fe(II)** (sum of clay minerals and carbonates)	**Paramag. HS-Fe(III)*** (mainly clay minerals, nano-goethite)	**Goethite** (min.)**	**Pyrite**	**Carbonates (siderite, ankerite)** (max.)
	% of Fe_{tot}						
7.83	*18.9*	< 19	18	25	57	< 1	< 1
8.58	*28.6*	< 25	24	31	45	< 1	< 1
10.73	*35.9*	25	25	16	54	5	2
15.28	*60.9*	59	55	16	25	4	26
24.52	*82.8*	85 ± 10***	69	15 ± 10***	< 1	16 ± 10***	28
60.78	*94.5*	86	81	14	< 1	5	26

* Can include nano-goethite.
** Minimum content (only mid-sized goethite).
*** Values vary with pyrite content.

In Fig. 4-19, the reduction level (Fe^{2+}/Fe_{tot}) based on Mössbauer data is compared with data obtained independently from the phenanthroline method. A good consistency (± 10 %) between both methods is identified. A clear decrease in reduction level from ~ 85 % in the two lowermost samples (in fresh rock below the weathered zone) with decreasing depth is noted, reaching ~ 18 % in shallowest sample.

Fig. 4-20 combines the information form Mössbauer spectroscopy (Fe species) according to the data listed in Tab. 4-6 and XRF (total Fe content, Tab. 4-2). The decrease of reduction level towards the surface is explained mainly by the appearance of Fe(III) oxide (goethite) and the loss of Fe carbonate and pyrite. Mössbauer data evidence the presence of goethite in samples 7.83, 8.58, 10.73 and 15.28. This phase was phase not identified by XRD analysis, most likely due to its bad crystallinity (Section 4.1.2, Tab. 4-3.1).

Tab. 4-6 and Fig. 4-20 indicate that there are HS-Fe(II) and HS-Fe(III) contributions that cannot be easily attributed to specific phases. While this issue is not further detailed here, it is likely that they belong to clay minerals, such as chlorite, to a large part.

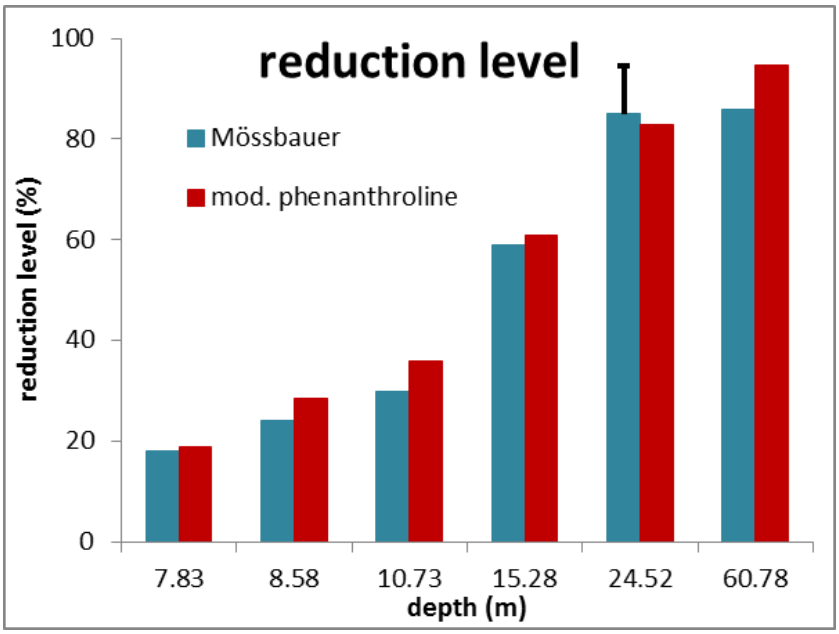

Fig. 4-19: Reduction level (Fe^{2+}/Fe_{tot}) obtained from Mössbauer analysis and the phenanthroline method.

Black bar: Range related to uncertainty in pyrite content in this specific sample.

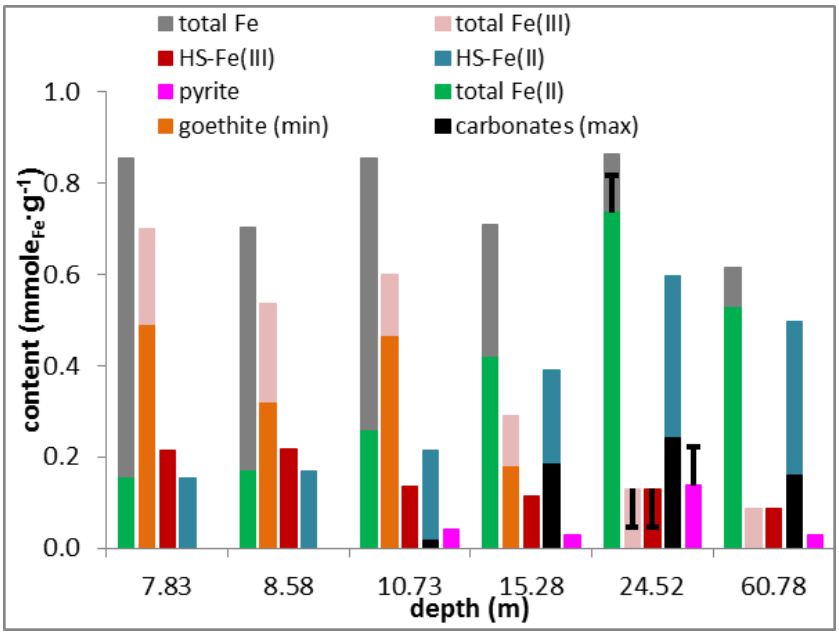

Fig. 4-20: Distribution of Fe species derived from fitting of Mössbauer spectra.

Total Fe derived from XRF data. Black T bar represents the range of probable values for sample 24.52. Unit of y axis is mmol Fe per g rock.

4.5.3 Summary of Mössbauer spectroscopy analysis

Main findings from Mössbauer spectroscopy include:

- There is a clear change in the ratio of Fe^{2+}/Fe^{3+} occurring above sample 24.52, with a decreasing trend towards the surface. The independent phenanthroline method yields very similar results.
- This change is manifested by the lower structural Fe^{2+}/Fe^{3+} ratio in clay minerals observed at 15.28 m depth, followed by the loss of Fe-bearing carbonates and pyrite observed at shallower levels. Concomitantly, goethite contents are increased.
- The distribution of pyrite and siderite determined from XRD and CNS analysis is largely supported by Mössbauer data (Tab. 4-7).
- The difference in reduction level noted by Mössbauer data in the clay fraction is in line with the shift in chlorite composition indicated from XRD.
- The occurrence of goethite in considerable amounts at shallow levels identified by Mössbauer spectroscopy is not confirmed by XRD where no Fe oxide phases were identified in the bulk material. This discrepancy might arise from the low crystallinity of the goethite particles. In samples subjected to grain-size separation for the analysis of clay mineralogy (Section 4.1), a small, wide peak at d = 4.18 Å, which could correspond to weakly crystalline goethite, was identified in the uppermost samples.

Tab. 4-7: Comparison of XRD/CNS and Mössbauer data pertinent to pyrite and siderite

Sample	Pyrite		Siderite	
	CNS	Mössbauer	XRD	Mössbauer (carb = sid + ank)
7.83	0.1	< 0.1	b.d.	< 0.1
8.58	< 0.02	< 0.1	b.d.	< 0.1
10.73	0.5	0.5	b.d.	0.2
15.28	0.4	0.3	2.5	2.1
24.52	2.7	2.1	3.5	2.5
60.78	0.5	0.4	1.0	2.4

b.d. = below detection

4.6 Cation-exchange data

A suite of methods at different institutions were applied to investigate the cation-exchange capacity (CEC) and the composition of the exchanger population. The methods differed substantially in terms of the nature of the index cation, masses of rock and added water, liquid/solid ratios, contact times and atmospheres. The methods are Co-hexamine ($Co(NH_3)_6^{3+}$; Rémy & Orsini 1976, Hadi et al. 2016), Cu-triethylenetetramine (Meier & Kahr 1999, Dohrmann & Kaufhold 2009), $CsNO_3$ (Baeyens & Bradbury 2004) and Ni-ethylenediamine ($Ni(en)_n^{2+}$; Bradbury & Baeyens 1997/1998). Tab. 4-8 provides an overview of the relevant experimental conditions.

Tab. 4-8: Experimental conditions used by different laboratories for cation-exchange studies. Mass of solution includes mass of pore water in case of saturated samples.

Institution	**BGR R. Dohrmann**	**Uni Bern H.N. Waber**	**Uni Bern J. Hadi**	**Uni Bern J. Hadi**	**PSI B. Baeyens**
Responsible method	Cu-trien	Ni-en	Cu-trien	Co-hex	$CsNO_3$
CEC extractions					
Objective	Consumption of index cation & exchanger population				
Initial sample state	Dry	Naturally saturated	Naturally saturated, then freeze-dried		-
Dry rock mass [g]	1-2 – 2.0	25 – 29	0.75 – 0.76	1.84	-
Mass of solution [mL]	30 (solution is calcite-saturated)	32 – 36	14.6 – 15.0	35.9 – 36.5	-
S/L [kg/L]	0.04 – 0.067	0.69 – 0.90	0.05	0.05	-
L/S [L/kg]	15 – 25	1.11 – 1.44	20	20	-
Contact time [h]	2	168	2	1	-
Atmosphere	Air	N_2	N_2	N_2	-
Aqueous extractions					*$CsNO_3$ extractions*
Objective	-	Anions (+cations) from pore water and mineral dissolution	Anions (+cations) from pore water and mineral dissolution		Anions from pore water and mineral dissolution & exchanger population
Initial sample state	-	Naturally saturated	Naturally saturated, then freeze-dried		Air-dried
Dry rock mass [g]	-	24.4 – 28.7	3.58 – 3.63 1.79 – 1.81 0.72 – 0.73		0.79
Mass of solution [mL]	-	31.0 – 34.9	35.8 – 36.6		40
S/L [kg/L]	-	0.70 – 0.91	0.1 0.05 0.02		0.02
L/S [L/kg]	-	1.10 – 1.43	10 20 50		50
Contact time [h]	-	48	1 – 2		72
Atmosphere	-	N_2	N_2		N_2

4.6.1 CEC and cations in CEC solutions

The consumption of the index cation and the concentrations of cations in the extract solutions are listed in Tab. 4-9. Note that the listed raw cation data include contributions from the exchanger, from the pore water and from minerals dissolved during extraction (carbonates, sulphates). Possible contributions of NH_4^+ and H^+ to the exchanger population were not quantified.

- Regarding the consumption of the index cation (CEC) and the sum of cations in solution, there are differences between the different methods (Fig. 4-21). The *Cu-trien BGR Dohrmann* data and the *Co-hex Uni Bern Hadi* data are similar, and the sum of cations is close to the CEC derived from the consumption of the index cation. Note that *BGR Dohrmann* used a calcite-saturated solution for extraction, in order to minimise dissolution of carbonate minerals. The *Cu-trien Uni Bern Hadi* data show an excess of dissolved cations, possibly due to the fact that no measures to prevent calcite dissolution were taken. The *Ni-en Uni Bern Waber* data show a substantial excess of CEC derived from Ni consumption when compared to the sum of dissolved cations.
- CEC data were also produced using the ^{134}Cs dilution method by *PSI Baeyens*. They show a CEC that is substantially below the sum of dissolved cations. This is likely due to the fact that Ca^{2+} in solution, augmented by the inevitable contribution from calcite dissolution, competes with Cs^+ for sorption sites, leading to an underestimation of CEC by the ^{134}Cs dilution method. While this method has been shown to work well for single clay minerals and pure bentonites, it is considered to be unsuitable for carbonate-containing rocks, such as Opalinus Clay. Therefore, even though data were produced for the Lausen samples, they are not presented and discussed here. On the other hand, the $CsNO_3$ extractions, yielding data on Na^+, K^+, Ca^{2+} and Mg^{2+} concentrations in solution, are thought to provide relevant data.
- Both the sum of cations and the consumption of the index cation show a positive correlation with clay-mineral content (Fig. 4-22). Note that the slopes of this correlation do not trend towards the origin – the extrapolated clay-mineral content at CEC = 0 is markedly positive.
- When scaling CEC and the sum of cations to total clay-mineral content, the 2 – 3 shallowest samples yield markedly higher values than all others (Fig. 4-23). This again means that the clay mineralogy in these samples must be different, in agreement with the mineralogical investigations that indicate the presence of oxidised chlorite and/or a chlorite-smectite mixed-layer phase. Further, badly crystallised goethite is present at least in the uppermost samples, which might affect CEC data (interval 7.83 – 12.10 m, see Section 4.1). Further, one may speculate that small contents of other Fe-hydroxides (unidentified by Mössbauer spectroscopy) or traces of Mn-hydroxides may also contribute to the measured CEC.
- The concentrations of Na^+ and K^+ increase with depth, while the opposite trend is identified for Ca^{2+} (Fig. 4-24). This mirrors the fact that pore-water composition evolves from a dilute Ca-dominated water at shallow levels towards a Na-dominated, more saline water at depth (Section 5.2). No clear trend is seen for Mg^{2+}.
- The raw data for Na^+ in solution are remarkably consistent for all methods, whereas major discrepancies are found for all other cations (Fig. 4-24).

Tab. 4-9: Results of cation-exchange data obtained by various techniques and laboratories

Cation concentrations are shown as measured (no corrections). CEC refers to the consumption of the index cation.

Sample ID				Cation in CEC extracts (raw data, no corrections)								CEC
Institution & operator	Method	Depth [m]	Subsample	S:L [kg/L]	L:S [L/kg]	Na+ [meq/kg rock]	K+ [meq/ kg rock]	Ca2+ [meq/ kg rock]	Mg2+ [meq/ kg rock]	Sr2+ [meq/ kg rock]	Sum cations [meq/ kg rock]	CEC [meq/ kg rock]
BGR Dohrmann	Cu-trien	7.83	c	0.0667	14.99	2	6	124	17	0	149	158
		7.83	d	0.0667	14.99	1	4	125	18	0	148	157
		8.58	c	0.0670	14.94	1	5	122	19	0	147	157
		8.58	d	0.0667	14.99	1	4	122	19	0	146	156
		10.73	c	0.0667	15.00	1	5	105	16	1	128	134
		10.73	d	0.0669	14.94	1	5	104	15	1	127	134
		15.28	c	0.0667	14.99	2	7	104	11	0	125	128
		15.28	d	0.0667	14.99	2	7	102	11	0	123	128
		24.52	c	0.0670	14.93	19	8	49	32	0	108	106
		24.52	d	0.0667	14.99	19	8	49	32	0	109	106
		60.78	c	0.0668	14.97	37	8	39	20	0	104	97
		60.78	d	0.0669	14.96	37	8	39	20	0	104	96
BGR Dohrmann	Cu-trien	7.83	a	0.0400	25.00	1	5	132	18	0	157	164
		7.83	b	0.0400	24.98	3	7	132	18	0	159	165
		8.58	a	0.0400	24.98	1	5	130	20	0	156	165
		8.58	b	0.0400	24.98	1	5	130	20	0	156	165
		10.73	a	0.0400	24.99	1	6	108	16	1	132	140
		10.73	b	0.0400	24.98	1	6	108	16	1	132	140
		15.28	a	0.0400	24.98	2	7	98	14	0	122	134
		15.28	b	0.0400	24.99	2	8	105	14	0	129	130
		24.52	a	0.0400	24.98	21	8	51	33	0	113	108
		24.52	b	0.0400	24.98	21	8	50	33	0	112	107
		60.78	a	0.0401	24.95	36	8	40	21	0	105	99
		60.78	b	0.0400	25.00	37	8	40	21	0	106	98
Uni Bern Waber	Ni-en	7.83		0.6947	1.44	0.9	2.0	114.0	16.3	0.4	133.5	197.6
		8.58		0.7185	1.39	0.8	2.2	110.1	15.9	0.3	129.3	184.5
		10.73		0.7495	1.33	0.8	2.1	95.8	15.8	0.3	114.8	169.0
		15.28		0.8130	1.23	2.0	2.9	68.4	28.2	0.6	102.0	149.8
		24.52		0.8926	1.12	20.0	4.6	48.4	36.6	1.5	111.0	136.7
		60.78		0.8991	1.11	33.8	4.4	27.5	25.3	0.5	91.5	114.7
		82.87		0.8851	1.13	31.9	4.0	30.5	25.0	0.4	91.8	106.8
PSI Baeyens	CsNO3	7.83	average	0.0197	50.76	1.2	7.0	164.4	16.4		189.0	
		8.58	average	0.0198	50.51	0.9	6.0	161.5	18.2		186.6	
		10.73	average	0.0198	50.51	1.0	6.2	140.9	13.9		162.0	
		15.28	average	0.0199	50.25	2.3	8.9	119.0	17.2		147.0	
		24.52	average	0.0198	50.51	19.3	8.8	78.2	32.5		138.8	
		60.78	average	0.0199	50.25	36.8	9.0	69.8	25.1		140.7	
Uni Bern Hadi	Co-hex	7.83		0.0500	20.01	1	5.8	152	20	0.4	180	192
		8.58		0.0500	20.01	2	5.2	148	22	0.4	177	185
		10.73		0.0500	20.02	1	5.6	120	17	0.3	144	154
		15.28		0.0499	20.03	2	7.8	121	16	0.7	147	153
		24.52		0.0500	20.02	17	8.1	58	32	1.5	117	130
		60.78		0.0499	20.05	33	8.1	48	23	1.1	113	128
Uni Bern Hadi	Cu-trien	7.83		0.0500	19.99	1	3.8	156	19	0.3	180	164
		8.58		0.0500	19.98	1	3.6	153	20	0.3	178	161
		10.73		0.0500	19.98	1	4.2	141	37	0.3	184	149
		15.28		0.0500	20.01	3	5.9	131	29	0.7	169	139
		24.52		0.0500	20.01	19	7.0	79	19	1.6	125	122
		60.78		0.0502	19.92	35	6.7	66	20	0.7	129	114

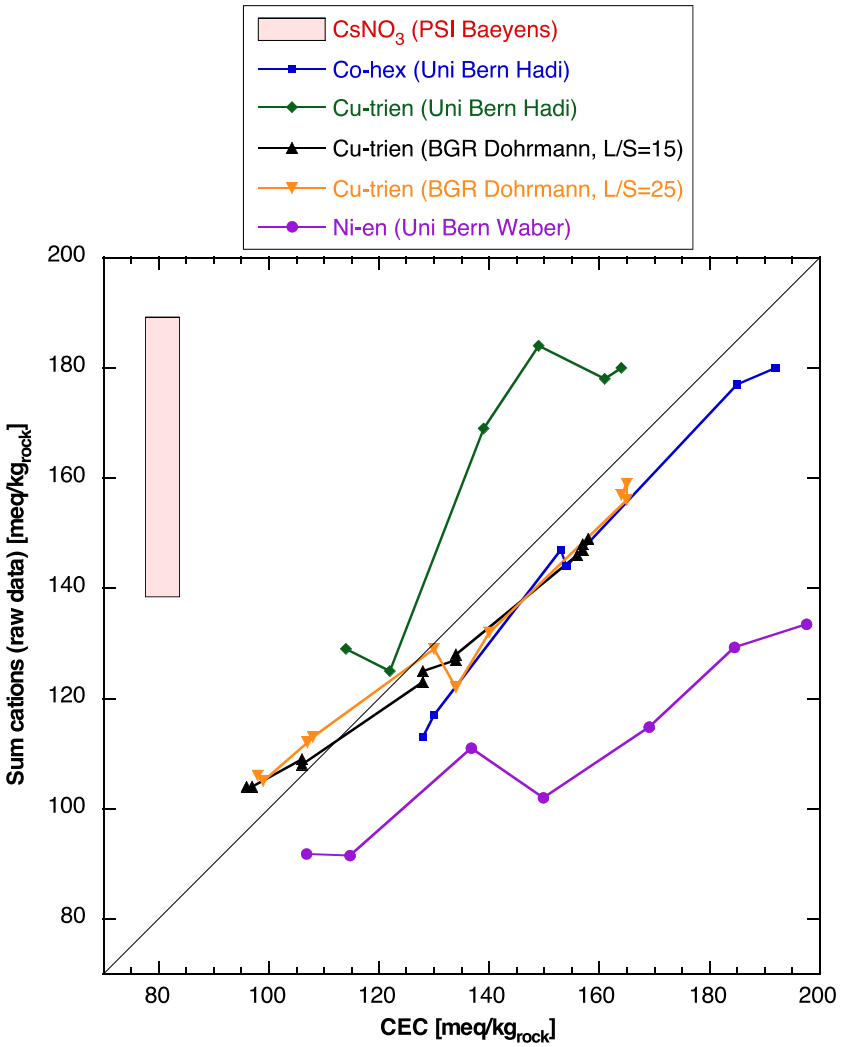

Fig. 4-21: Consumption of the index cation (CEC) vs. sum of cations in solution (uncorrected data).

No CEC data are available for the $CsNO_3$ method, red bar indicates range of the sum of cations.

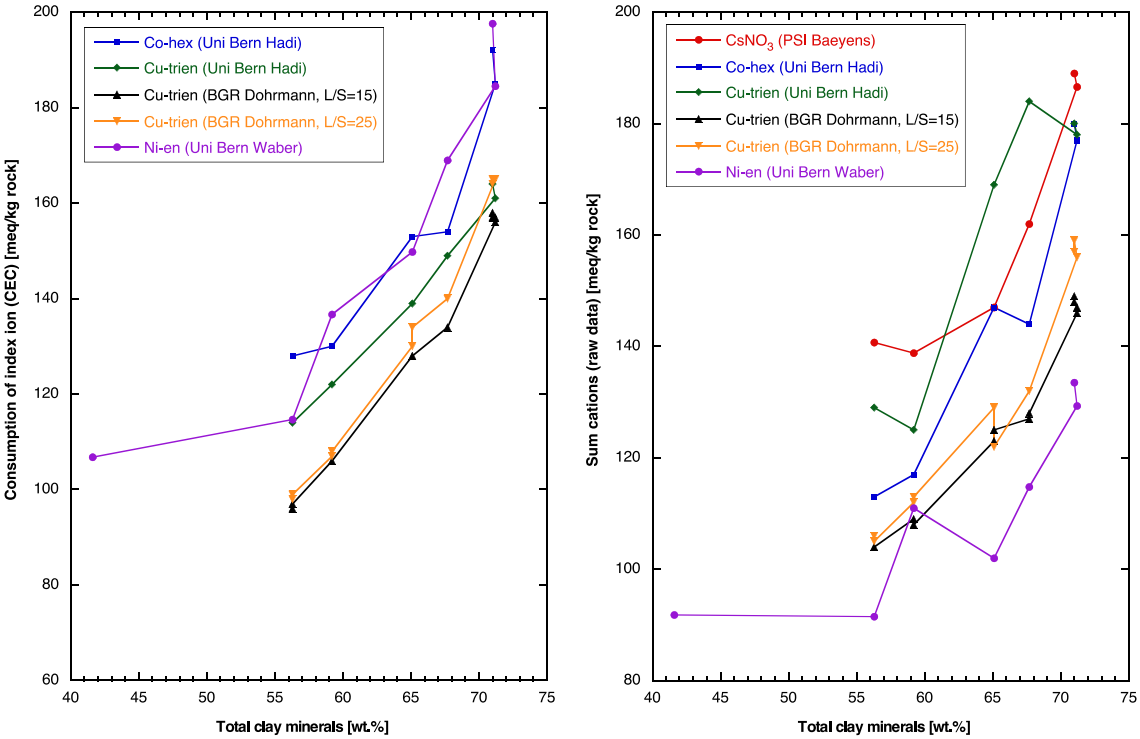

Fig. 4-22: Consumption of the index cation (CEC) and the sum of cations in solution (uncorrected data) as a function of clay-mineral content.

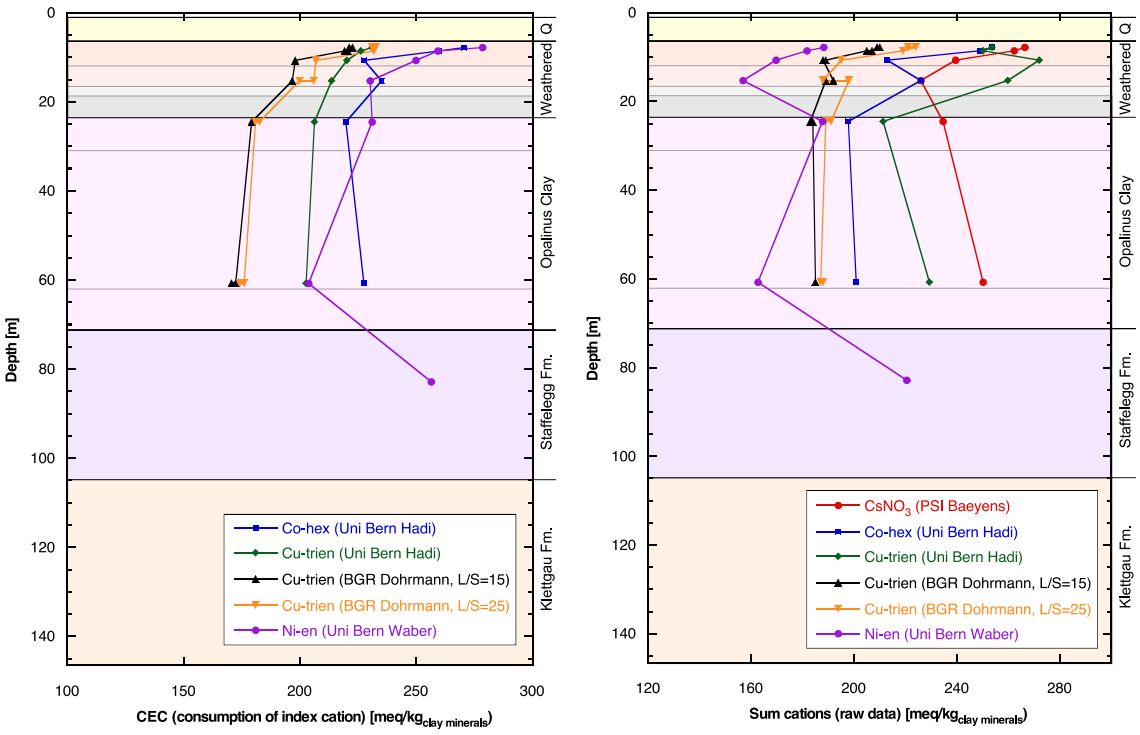

Fig. 4-23: Consumption of the index cation (CEC) and the sum of cations in solution, scaled to pure clay (uncorrected data), as a function of depth.

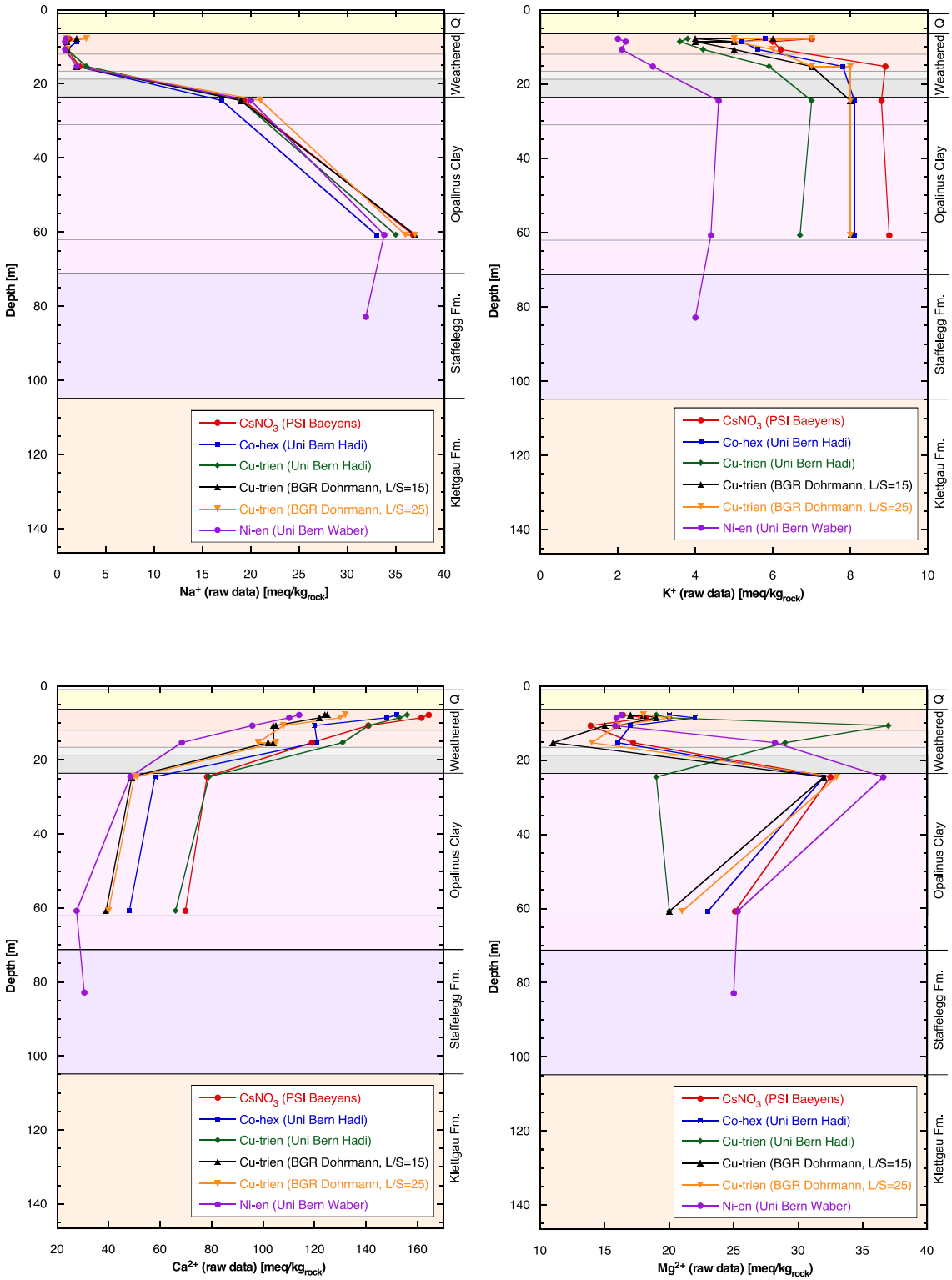

Fig. 4-24: Concentrations of individual cations in solution (raw data) as a function of depth.

4.6.2 Aqueous extraction of samples used for CEC measurements

Aqueous extraction was performed by *Uni Bern Waber* (L/S around 1) and by *Uni Bern Hadi* (L/S of 10, 20 and 50). The data are shown in units of meq/kg_{rock} in Tab. 4-10. The pore-water composition of samples adjacent to those for aqueous extraction and cation exchange was studied by squeezing experiments (Section 4.9). Using the measured water content and assuming that the squeezed waters represent the composition of the anion-accessible porosity fraction (0.58, see Section 4.9.3), the concentrations obtained from squeezing at low pressure were also recalculated to units of meq/kg_{rock} (Tab. 4-11). Note that squeezing data for samples from the weathered zone are uncertain, in particular for the lowest squeezing pressures. Therefore, data obtained at 100 MPa were used, whereas for the deeper samples, the data obtained at the lowest pressure were applied.

The same recalculation procedure was also performed for the available ground-water data (Huxol et al. 2017), and the resulting concentrations are shown in Tab. 4-12. Water samples are only available from the uppermost part of the profile and originate from packer intervals several metres long. The exact depth locations of the inflows are not known, which adds uncertainty to the attribution of the ground-water data to those obtained from rock samples. The chosen attribution is also shown in Tab. 4-12. Also note that the short residence times of the shallow ground waters make the comparison with pore-water data questionable because diffusive equilibration between these water types may not have been complete.

Ion concentrations in aqueous extracts are shown as a function of the liquid/solid ratio (L/S) in Fig. 4-25, together with pore-water data obtained from squeezing, and the following observations can be made:

- Na^+ and K^+ concentrations increase with L/S, which is a consequence of desorption of monovalent cations with increasing dilution (i.e. decreasing salinity).
- Ca^{2+} and Mg^{2+} show more complex patterns. Samples from the Opalinus Clay below the weathered zone show an initial decrease (likely an effect of decreasing salinity and increasing affinity of bivalent cations on the exchanger) followed by a sharp increase (likely an effect of carbonate disolution). Samples from the weathered zone do not show the initial decrease, given the fact that the waters have a low salinity (so the affinity does not change much with further dilution) and the contribution of carbonate dissolution has a higher relative impact.
- Cl^- in samples below the weathered zone shows a slight decrease, whereas the reverse trend is seen within the weathered zone. These trends with L/S are not well understood – if Cl^- behaved conservatively, its concentration should be independent of L/S. While some uncertainty is related to the squeezing data (choice of the anion-accessible porosity fraction, Cl^- concentration in the uppermost samples as discussed in Section 4.9.2), concentrations based on squeezing confirm the trends seen in the aqueous-extraction data.
- In samples below the weathered zone and in the deepest sample of the weathered zone (15.28), SO_4^{2-} concentration in squeezed water is markedly lower than in the extracts, suggesting that a S-bearing mineral was dissolved during extraction. SO_4^{2-} data of *Uni Bern Hadi* show concentrations that are essentially independent of L/S, which could be due to the total dissolution of a sulphate mineral, such as celestite. *Uni Bern Waber*'s data yield slightly higher values (as for Cl^-), for reasons currently not understood.
- In the 3 shallowest samples, SO_4^{2-} in the squeezed water is higher than in the extracts for reasons that are unclear at this stage.
- TIC data show a general trend towards a substantial increase with L/S, which mirrors the growing contribution of carbonate dissolution with increasing L/S.

- Aqueous extraction of sample 15.28 by *Uni Bern Waber* shows data that do not follow the general trend and often form outliers. The reasons are not understood.

PSI Baeyens did not perform aqueous extraction but obtained anion concentrations from extracts in a $CsNO_3$ solution at L/S of 50 (Tab. 4-13). While Cl^- concentrations are comparable to those obtained by *Uni Bern Hadi* on the basis of aqueous extraction, sulphate concentrations obtained by *PSI Baeyens* are substantially higher (Fig. 4-26). The likely source for the additional sulphate is sulphide oxidation, given the fact that the experiments were performed under atmospheric conditions. Total concentrations of inorganic carbon in *PSI Baeyens*'s data set are also substantially higher than those obtained by *Uni Bern Hadi*, suggesting that more calcite was dissolved (Fig. 4-26). Only when subtracting the carbon content of the initial solution, the contents become comparable. It is possible that the additional calcite dissolution was induced by sulphide oxidation (which lowers pH).

Tab. 4-10: Aqueous-extraction data recalculated to units of meq/kg_{rock}

HCO_3^- data of *Uni Bern Waber* are based on measured TIC. In the absence of TIC measurements, *Uni Bern Hadi* calculated HCO_3^- by charge balance.

Institution & operator	Type of extraction	Contact time [h]	Depth [m]	Wet mass [g]	Dry mass [g]	Solution added [g]	S:L [kg/L]	L/S [L/kg]	Na+ [meq/ kg rock]	K+ [meq/ kg rock]	Ca2+ [meq/ kg rock]	Mg2+ [meq/ kg rock]	F- [meq/ kg rock]	Cl- [meq/ kg rock]	SO4 2- [meq/ kg rock]	HCO3- [meq/ kg rock]	Sum dissolved ions [meq/ kg rock]
Uni Bern Waber	Wet rock	48	7.83	29.8	24.4	29.5	0.699	1.432	0.390	0.196	3.439	0.661	0.04	0.06	0.25	4.96	10.00
			8.58	30.6	25.8	29.3	0.758	1.320	0.337	0.196	3.198	0.648	0.03	0.08	0.24	4.60	9.34
			10.73	28.6	24.6	28.9	0.746	1.340	0.377	0.221	3.204	0.659	0.03	0.09	0.47	4.32	9.38
			15.28	29.6	26.6	29.5	0.815	1.227	1.002	0.348	3.331	1.284	0.02	0.06	0.77	5.79	12.60
			24.52	30.2	28.1	28.9	0.906	1.104	6.061	0.244	0.324	0.251	0.11	0.62	4.10	2.16	13.88
			60.78	29.8	28.1	30.0	0.888	1.126	12.75	0.277	0.319	0.257	0.13	2.82	6.72	4.16	27.44
			82.87	30.3	28.7	30.0	0.908	1.101	11.98	0.260	0.298	0.253	0.17	2.71	7.74	1.42	24.83
Uni Bern Hadi	Dry rock	2	7.83		3.584	35.9	0.100	10.0	0.734	0.630	6.416	0.959		0.096	0.221	8.4	17.48
			8.58		3.612	36.2	0.100	10.0	0.618	0.657	6.315	1.029		0.094	0.189	8.3	17.24
			10.73		3.598	36.0	0.100	10.0	0.716	0.953	6.139	0.939		0.123	0.331	8.3	17.50
			15.28		3.634	36.4	0.100	10.0	1.652	1.129	3.414	0.448		0.089	1.772	4.8	13.29
			24.52		3.605	36.1	0.100	10.0	12.81	1.028	0.727	0.409		0.560	3.066	11.3	29.94
			60.78		3.628	36.4	0.100	10.0	23.01	0.700	0.387	0.192		2.459	5.706	16.1	48.59
Uni Bern Hadi	Dry rock	2	7.83		1.795	36.0	0.050	20.0	0.843	1.025	8.463	1.154		0.106	0.258	11.1	22.97
			8.58		1.814	36.4	0.050	20.0	0.711	1.056	8.065	1.220		0.104	0.225	10.7	22.11
			10.73		1.812	36.3	0.050	20.0	0.804	1.533	8.240	1.149		0.122	0.367	11.2	23.45
			15.28		1.810	36.3	0.050	20.1	1.930	2.150	6.400	0.726		0.109	1.865	9.2	22.41
			24.52		1.791	35.9	0.050	20.1	15.18	2.014	1.568	0.800		0.566	3.134	15.9	39.12
			60.78		1.797	36.0	0.050	20.0	28.23	1.655	0.870	0.363		2.484	5.807	22.8	62.23
Uni Bern Hadi	Dry rock	2	7.83		0.716	35.8	0.020	50.0	0.985	1.717	14.54	1.803		0.141	0.257	18.7	38.10
			8.58		0.732	36.6	0.020	50.0	0.830	1.684	14.15	1.963		0.152	0.220	18.3	37.25
			10.73		0.722	36.1	0.020	50.0	0.914	2.327	14.55	1.751		0.156	0.475	18.9	39.09
			15.28		0.727	36.4	0.020	50.0	2.221	3.525	14.57	1.701		0.178	1.840	20.0	44.04
			24.52		0.725	36.3	0.020	50.0	17.28	3.260	5.850	2.516		0.645	3.072	25.2	57.80
			60.78		0.727	36.4	0.020	50.0	32.57	2.766	3.974	1.436		2.497	6.011	32.2	81.48

Tab. 4-11: Composition of waters squeezed at the lowest pressure recalculated to units of meq/kg_{rock}, using the measured water content and assuming an anion-accessible porosity fraction of 0.58.

For squeezed samples 10.88 and 15.05, data for a pressure of 100 MPa are listed, as the lower-pressure data are likely affected by artefacts (see Section 4.9). The attribution of squeezed samples (col. 2) to samples subjected to aqueous extraction (col. 1) is also shown.

ID (aq. ex.)	ID (sq.)		Water squeezed at low pressure, data in mg/L									Water squeezed at low pressure, data in meq/kg rock @ AAPF=0.58							
Sample for aqueous extraction: Depth [m]	Sample for squeezing: Depth [m]	Squeezing pressure [MPa]	Na+ [mg/L]	K+ [mg/L]	Ca2+ [mg/L]	Mg2+ [mg/L]	Sr2+ [mg/L]	Cl- [mg/L]	SO42- [mg/L]	TIC [mg/L]	TOC [mg/L]	Na+ [meq/kg rock]	K+ [meq/kg rock]	Ca2+ [meq/kg rock]	Mg2+ [meq/kg rock]	Sr2+ [meq/kg rock]	Cl- [meq/kg rock]	SO42- [meq/kg rock]	TIC as HCO3- [meq/kg rock]
7.83	10.88	100	41.9	8.33	201.8	39.06	0.84	25.08	521.6	44.69	25.88	0.234	0.027	1.291	0.412	0.002	0.091	1.392	0.477
8.58	10.88	100	41.9	8.33	201.8	39.06	0.84	25.08	521.6	44.69	25.88	0.195	0.023	1.077	0.344	0.002	0.076	1.162	0.398
10.73	10.88	100	41.9	8.33	201.8	39.06	0.84	25.08	521.6	44.69	25.88	0.174	0.020	0.962	0.307	0.002	0.068	1.037	0.356
15.28	15.05	100	60.43	6.64	58.7	19.93	0.88	19.90	92.98	58.62	21.57	0.176	0.011	0.196	0.110	0.001	0.037	0.129	0.326
24.52	24.93	50	1167	37.00	178.5	102.6	6.30	739.1	2270	35.05	82.21	2.191	0.041	0.385	0.364	0.006	0.900	2.041	0.126
60.78	49.75	100	3224	70.85	453.5	242.4	6.25	3180	4387	34.09	62.71	4.835	0.062	0.780	0.688	0.005	3.093	3.149	0.098
82.87	80.47	300	3313	57.45	548	299.4	10.25	3428	5033	31.62	83.80	4.572	0.047	0.867	0.782	0.007	3.068	3.325	0.084

Tab. 4-12: Pore-water compositions obtained from ground-water analyses (Huxol et al. 2017), recalculated to units of meq/kg_{rock}, using the measured water content and assuming an anion-accessible porosity fraction of 0.58.

The attribution of ground-water samples (col. 2) to samples subjected to aqueous extraction (col. 1) is also shown.

ID (aq. ex.)	ID (ground water)			Ground water, data in mg/L						Ground water, data in meq/kg rock @ AAPF = 0.58					
Sample for aqueous extraction: Depth [m]	Ground-water sample: Mean depth [m]	Top [m]	Base [m]	Na+ [mg/L]	K+ [mg/L]	Ca2+ [mg/L]	Mg2+ [mg/L]	Cl- [mg/L]	SO4 2- [mg/L]	Na+ [meq/kg rock]	K+ [meq/kg rock]	Ca2+ [meq/kg rock]	Mg2+ [meq/kg rock]	Cl- [meq/kg rock]	SO4 2- [meq/kg rock]
7.83	10.39	8.32	12.45	12.0	3.4	127.0	19.8	23.7	23.5	0.067	0.011	0.814	0.209	0.086	0.063
8.58	10.39	8.32	12.45	12.0	3.4	127.0	19.8	23.7	23.5	0.056	0.009	0.679	0.174	0.072	0.052
10.73	10.39	8.32	12.45	12.0	3.4	127.0	19.8	23.7	23.5	0.050	0.008	0.606	0.156	0.064	0.047
15.28	15.72	13.00	18.43	42.0	6.0	110.0	27.0	22.0	76.0	0.122	0.010	0.367	0.148	0.041	0.106
24.52	23.00	18.40	27.60	143.0	6.4	89.0	41.0	24.0	220.0	0.268	0.007	0.192	0.146	0.029	0.198

Tab. 4-13: Anion concentrations in $CsNO_3$ extracts of *PSI Baeyens* in units of meq/kg_{rock}.

Institution & operator	Type of extraction	Contact time [h]	Depth [m]	Wet water content [wt.%]	Wet mass [g]	Dry mass [g]	Solution added [g]	S:L [kg/L]	L/S [L/kg]	Cl- [meq/ kg rock]	SO4 2- [meq/ kg rock]	HCO3- [meq/ kg rock]
PSI Baeyens	Air-dried rock	72	7.83	1.76	0.80	0.79	40	0.0197	50.8	<1	<3	12.7
			8.58	1.15				0.0198	50.5	<1	<3	13.3
			10.73	1.20				0.0198	50.5	<1	<3	17.1
			15.28	0.60				0.0199	50.3	<1	6.3	17.5
			24.52	1.27				0.0198	50.5	<1	9.5	17.5
			60.78	0.75				0.0199	50.3	2.86	11.1	25.6

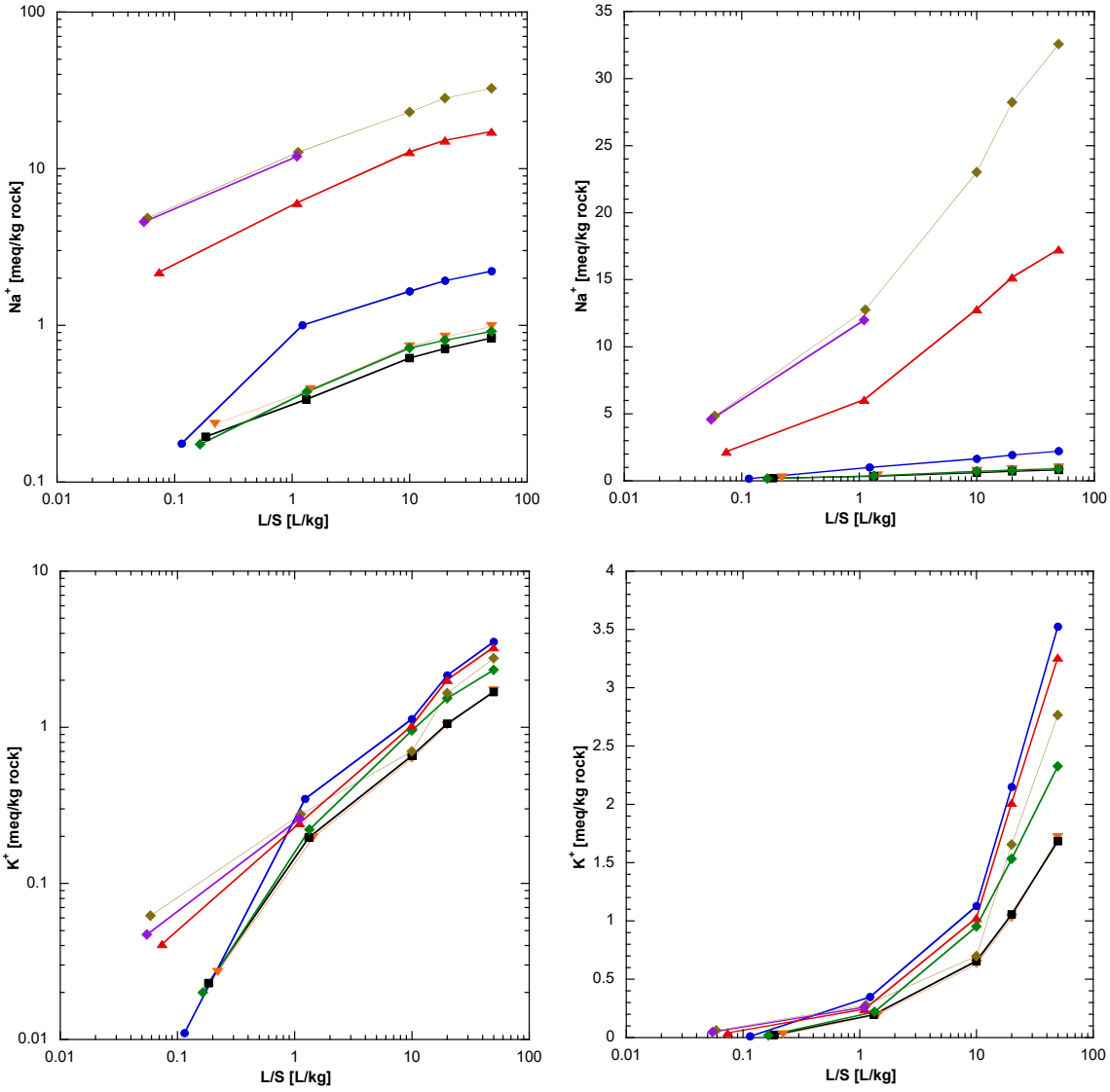

Fig. 4-25: Ion concentrations in aqueous extracts and of waters obtained by squeezing as a function of the liquid/solid (L/S) ratio.

Data for L/S around 0.1: Squeezing; data for L/.S around 1: Extracts of *Uni Bern Waber*; Data for L/S of 10, 20, 50: *Uni Bern Hadi.*

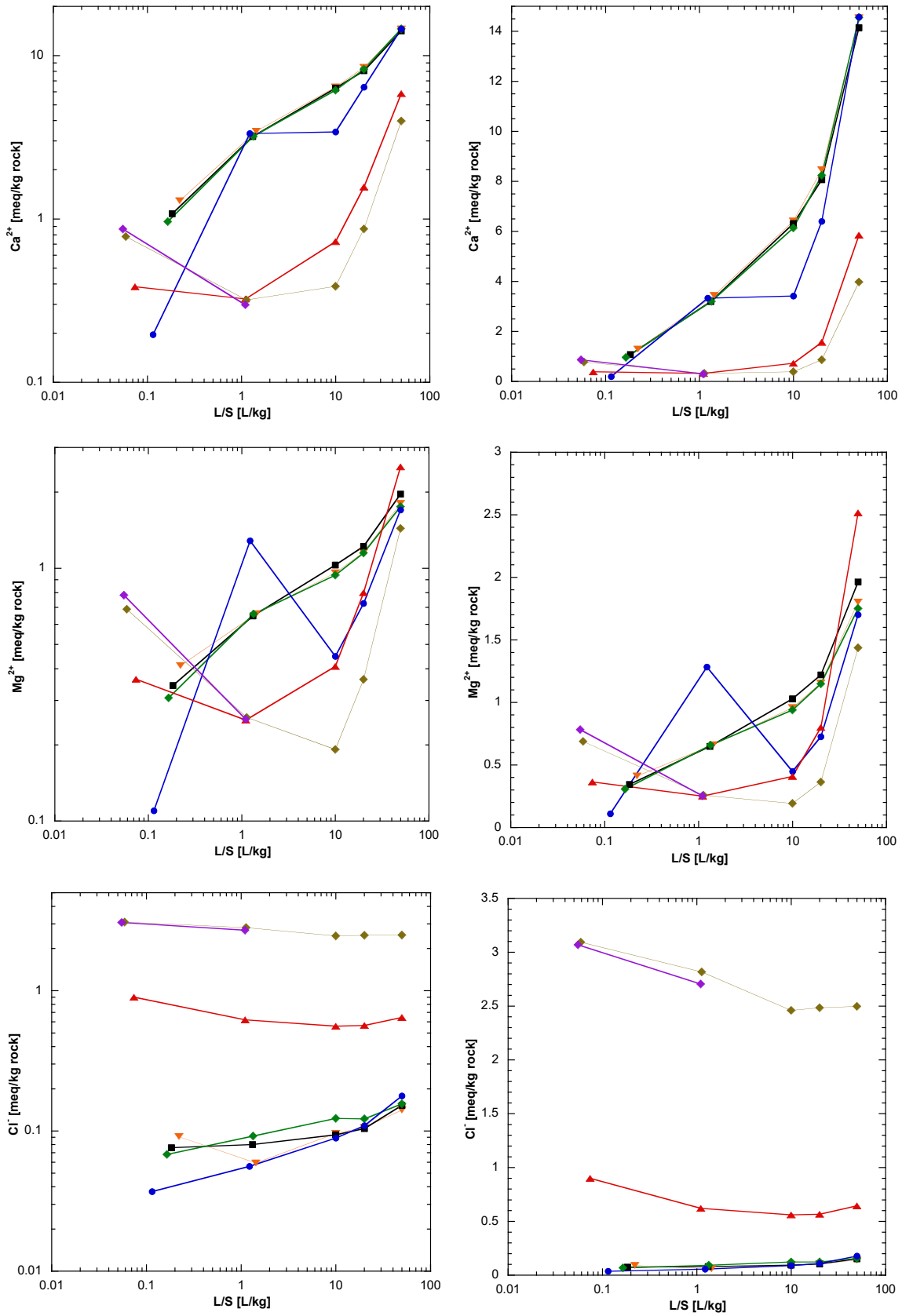
Ca2+ [meq/kg rock]
L/S [L/kg]
Mg2+ [meq/kg rock]
L/S [L/kg]
Cl- [meq/kg rock]
L/S [L/kg]

Fig. 4-25: Cont.

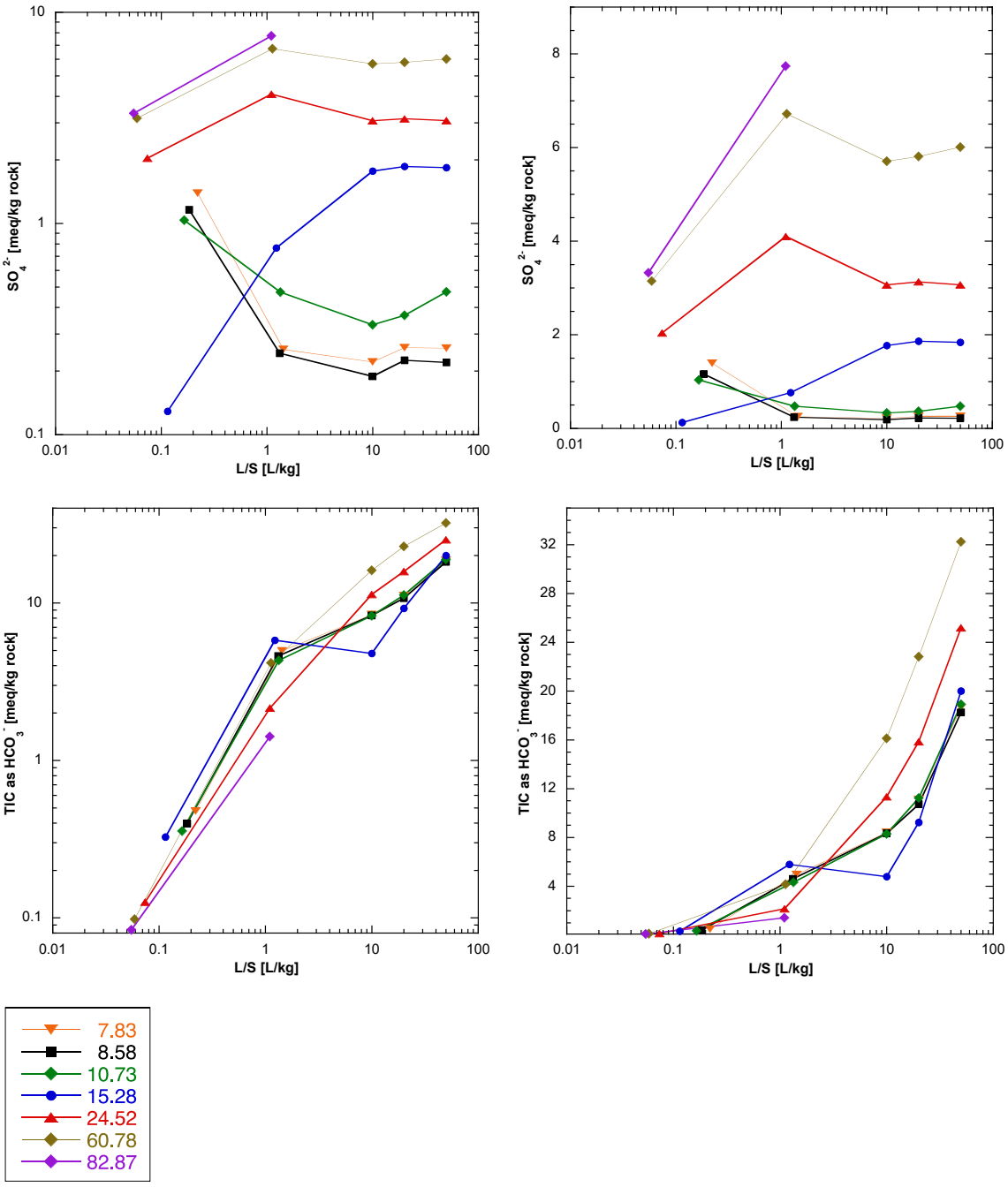
SO4 2- [meq/kg rock]
L/S [L/kg]
TIC as HCO3 - [meq/kg rock]
7.83
8.58
10.73
15.28
24.52
60.78
82.87

Fig. 4-25: Cont.

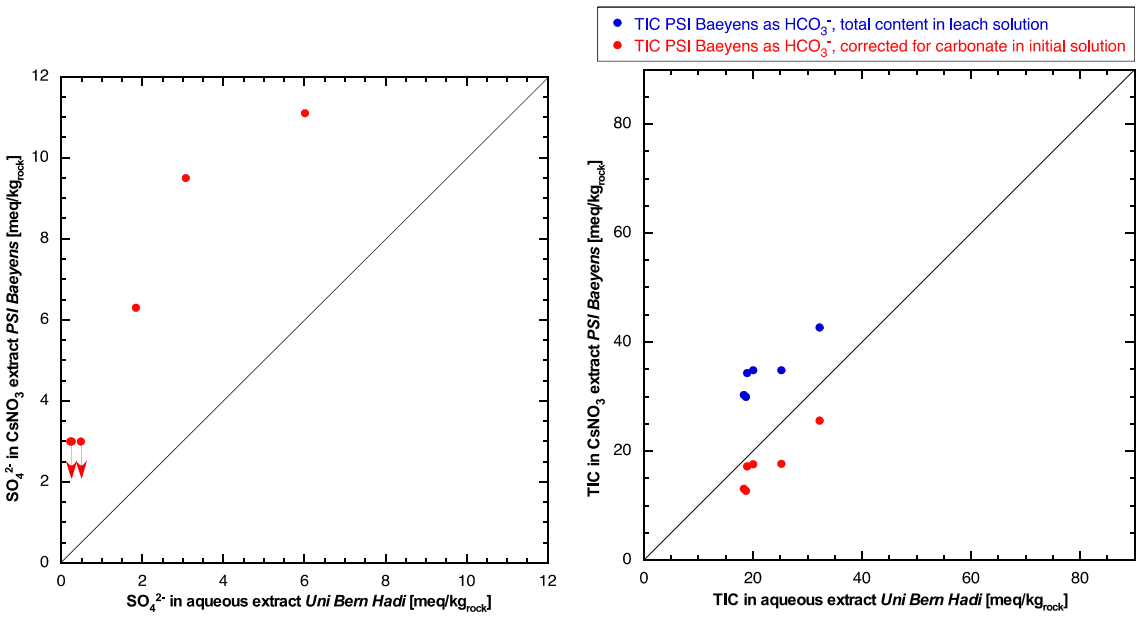

Fig. 4-26: SO_4^{2-} and inorganic carbon concentrations in aqueous extracts of *Uni Bern Hadi* and $CsNO_3$ extracts of *PSI Baeyens* at a L/S = 50 L/kg.

Arrows indicate values below detection.

4.7 Densities, water content and porosity

Water content was quantified by measuring mass loss upon heating at 105 °C or upon freeze drying, as well as by water-isotope mass balance based on the diffusive isotope exchange method. These data were then re-calculated to porosities, together with porosity data obtained from density measurements. All data are listed in Tab. 4-14. The following observations can be made:

- All methods of porosity determination show consistent values, except for freeze drying that slightly underestimates porosity due to incomplete release of water (Tab. 4-14, Fig. 4-27).
- In the uppermost 30 – 40 m, porosity increases substantially towards the surface and reaches almost 0.4 in the shallowest sample. Below that depth, porosity shows no systematic depth trend within Opalinus Clay. It is worth noting that the interval in which porosity is increased reaches well below the weathered zone (Fig. 4-27). However, it is not clear whether the slight increase of porosity in samples 24.52 and 29.02 is due to surficial decompaction or due to the higher clay-mineral content, as these samples are from the shaly facies, in contrast to all underlying samples (see also Fig. 4-28).
- Below the weatehered zone, a fair correlation between porosity and clay-mineral content is identified (Fig. 4-28). The slope of the correlation becomes steeper within the weathered zone.

Tab. 4-14: Summary of density, water-content and porosity measurements.

Errors on densities: 1σ deviation of measurements on 3 subsamples. Errors on gravimetric water content: 1σ deviation of measurements on 2 – 3 subsamples. Errors on water content from isotope exchange: Propagated analytical error.

Sample ID		Densities				Water content and water-content porosity												Porosity			
						Gravimetric water content		Gravimetric water content (samples used for diffusive isotope exchange)		Gravimetric water content upon freeze drying		Water content based of diffusive isotope exchange									
Depth [m]	Geological unit	Grain density [g/cm3]	Error [g/cm3]	Bulk wet density [g/cm3]	Error [g/cm3]	Bulk dry density (calculated) [g/cm3]	Porosity from densities [–]	Wet water content [wt%]	Error [wt%]	Dry water content [wt%]	Error [wt%]	Wet water content [wt%]	Error [wt%]	Dry water content [wt%]	Error [wt%]	Wet water content [wt%]	Error [wt%]	Dry water content [wt%]	Error [wt%]	Porosity from gravimetric water content [–]	Porosity from gravimetric water content (diff. exch. sample) [–]	Porosity from freeze drying [–]	Porosity from diffusive isotope exchange [–]
7.83	Opalinus Clay	2.702	0.003	2.019	0.014	1.654	0.388	18.10	0.19	22.10	0.29	18.11	0.24	22.08	0.36	18.06	0.20	22.04	0.24	18.29	1.11	22.39	1.36	0.374	0.374	0.373	0.377
8.23	Opalinus Clay	2.694	0.002	2.100	0.039	1.772	0.342	15.61	0.02	18.49	0.03									17.42	0.83	21.09	1.01	0.333			0.362
8.58	Opalinus Clay	2.682	0.003	2.042	0.039	1.724	0.357	15.57	0.23	18.45	0.32	15.41	0.49	18.20	0.68	14.64	0.03	17.15	0.03	16.54	0.81	19.82	0.97	0.331	0.328	0.315	0.347
10.73	Opalinus Clay	2.691	0.002	2.083	0.048	1.788	0.335	14.14	0.25	16.47	0.34	13.42	0.39	15.49	0.52	14.12	0.26	16.43	0.31	13.64	0.85	15.79	0.99	0.307	0.294	0.307	0.298
11.30	Opalinus Clay	2.689	0.002	2.063	0.035	1.777	0.339	13.85	0.05	16.07	0.07									14.82	0.69	17.40	0.81	0.302			0.319
12.10	Opalinus Clay	2.680	0.002	2.074	0.020	1.818	0.322	12.34	0.78	14.09	1.02	12.63	0.30	14.46	0.40					13.09	0.55	15.06	0.64	0.274	0.279		0.287
15.28	Opalinus Clay	2.683	0.001	2.258	0.021	2.025	0.245	10.32	0.08	11.51	0.09	10.53	0.17	11.76	0.21	11.02	0.14	12.38	0.16	11.19	0.42	12.60	0.48	0.236	0.240	0.249	0.253
15.94	Opalinus Clay	2.692	0.001	2.315	0.017	2.093	0.222	9.59	0.12	10.60	0.15									9.63	0.39	10.66	0.43	0.222			0.223
16.75	Opalinus Clay	2.702	0.002	2.355	0.009	2.150	0.204	8.71	0.17	9.54	0.20									9.65	0.37	10.68	0.41	0.205			0.224
19.62	Opalinus Clay	2.705	0.001	2.325	0.056	2.147	0.206	7.67	0.58	8.30	0.68	8.55	0.29	9.35	0.35					9.22	0.31	10.15	0.34	0.183	0.202		0.215
20.09	Opalinus Clay	2.689	0.002	2.364	0.014	2.185	0.187	7.60	0.18	8.22	0.21									8.28	0.25	9.03	0.27	0.181			0.195
24.52	Opalinus Clay	2.719	0.001	2.412	0.011	2.245	0.174	6.93	0.16	7.45	0.18	6.81	0.04	7.31	0.04	6.05	0.04	6.44	0.04	7.25	0.20	7.82	0.22	0.168	0.166	0.149	0.175
29.02	Opalinus Clay	2.701	0.002	2.436	0.014	2.284	0.154	6.24	0.17	6.65	0.20	5.89	0.07	6.27	0.08	5.53	0.04	5.85	0.05	6.86	0.19	7.36	0.20	0.152			0.166
33.65	Opalinus Clay	2.715	0.002	2.445	0.003	2.301	0.152	5.90	0.02	6.27	0.02									6.23	0.15	6.64	0.16	0.145	0.145	0.137	0.153
42.88	Opalinus Clay	2.697	0.001	2.484	0.013	2.353	0.128	5.27	0.24	5.56	0.26									5.49	0.13	5.81	0.14	0.130			0.136
47.58	Opalinus Clay	2.710	0.002	2.462	0.007	2.328	0.141	5.45	0.02	5.77	0.02									6.16	0.16	6.56	0.17	0.135			0.151
50.13	Opalinus Clay	2.711	0.001	2.490	0.030	2.354	0.132	5.46	0.03	5.78	0.04	5.36	0.05	5.67	0.05					5.61	0.15	5.94	0.16	0.135	0.133		0.139
54.98	Opalinus Clay	2.726	0.001	2.507	0.028	2.379	0.127	5.10	0.22	5.37	0.24									5.80	0.14	6.15	0.15	0.128			0.144
60.78	Opalinus Clay	2.692	0.002	2.424	0.053	2.288	0.150	5.61	0.08	5.94	0.09	5.70	0.28	6.06	0.32	4.74	0.35	4.98	0.36	5.96	0.14	6.34	0.15	0.138	0.140	0.118	0.146
77.81	Staffelegg-Fm	2.739	0.001	2.551	0.002	2.446	0.107	4.11	0.11	4.29	0.12									3.95	0.10	4.11	0.10	0.105			0.101
82.87	Staffelegg-Fm	2.709	0.001	2.485	0.017	2.356	0.130	5.19	0.12	5.47	0.14	4.98	0.09	5.26	0.10	4.49	0.10	4.70	0.10	5.46	0.16	5.78	0.17	0.129	0.124	0.113	0.135
96.98	Staffelegg-Fm	2.700	0.001	2.497	0.012	2.375	0.120	4.90	0.39	5.15	0.43									5.64	0.15	5.98	0.16	0.122			0.139
113.55	Klettgau-Fm	2.780	0.001	2.527	0.004	2.364	0.149	6.44	0.03	6.88	0.03	6.36	0.02	6.81	0.02	5.79	0.03	6.14	0.03	6.85	0.20	7.35	0.21	0.161	0.159	0.146	0.170
132.12	Klettgau-Fm	2.782	0.001	2.586	0.012	2.470	0.112	4.47	0.06	4.68	0.07									4.49	0.09	4.70	0.09	0.115			0.116

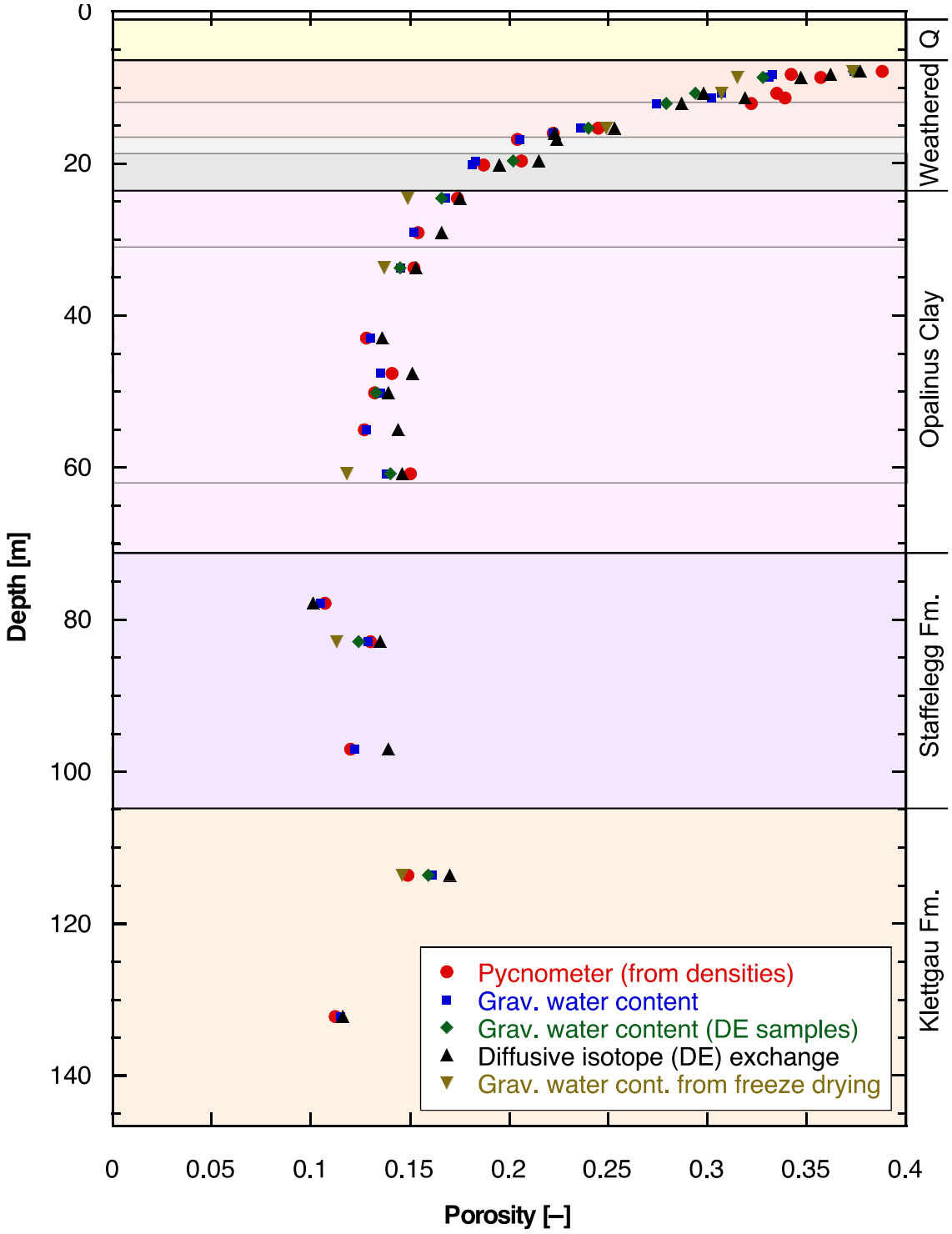

Fig. 4-27: Porosity as a function of depth.

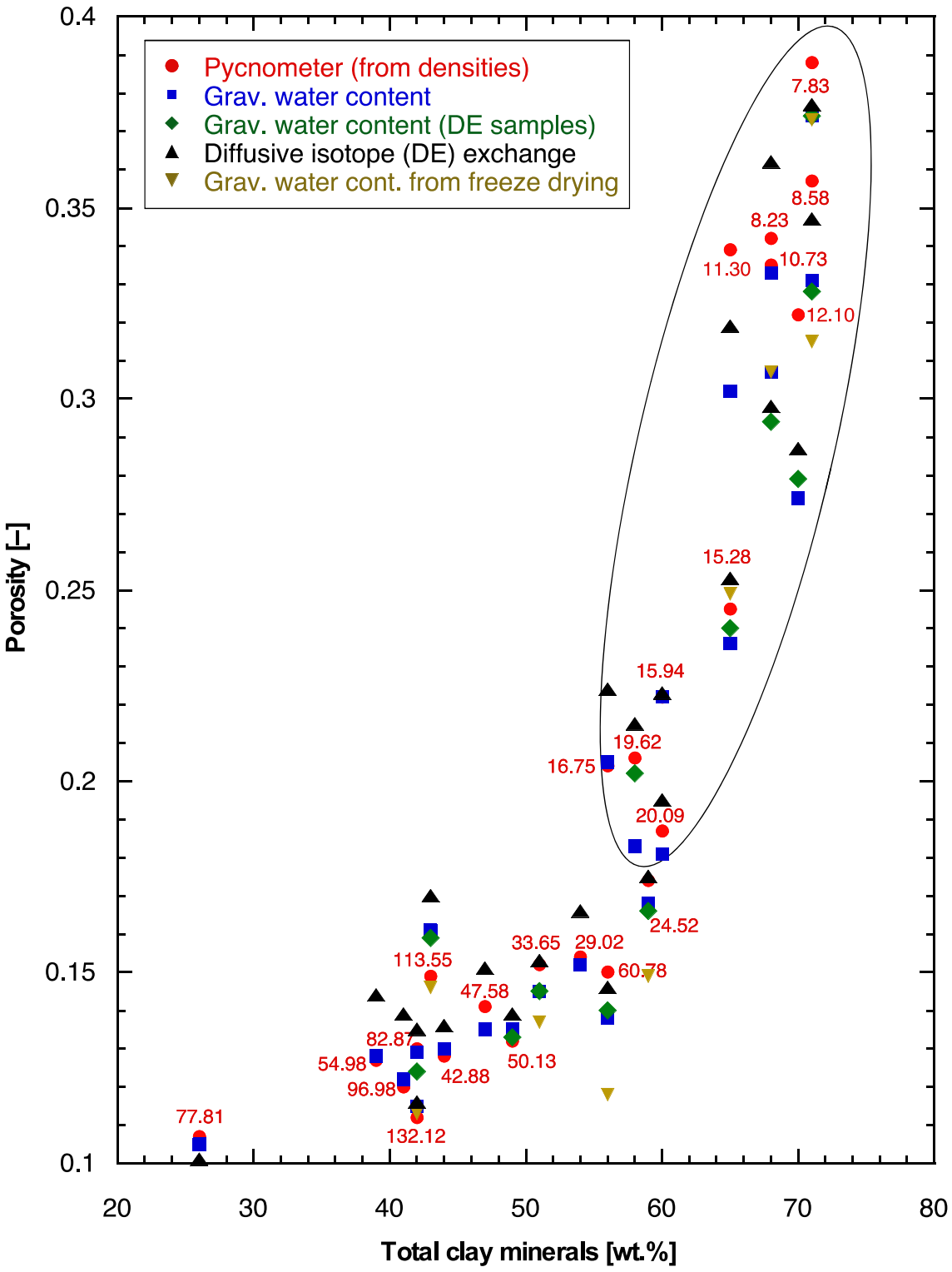

Fig. 4-28: Porosity as a function of clay-mineral content.

Numbers indicate sample depths. Ellipse identifies samples from the weathered zone.

4.8 Aqueous extraction

Saturated rock samples were used for aqueous extraction, and a water mass equivalent to that of the saturated sample was added. This means that S^*/L = *(mass of dry rock + mass of pore water)/mass of water added* was about 1. The solid/liquid ratio must be corrected using the measured water content. The relevant S/L^* ratio is the mass of dry rock/(mass of pore water + mass of water added) and varies between 0.699 and 0.923.

The S/L^* data and the chemical compositions of the aqueous extracts are shown in Tab. 4-15 and illustrated in Fig. 4-29. The main observations are as follows:

- Cl^- concentrations are low and show no systematic depth trend within the weathered zone, i.e. to about 20 – 24 m depth. A strong increase is identified below this depth until about 47 m, below which depth concentrations remain largely constant.
- A similar profile is identified for Na^+ and SO_4^{2-}, even though, unlike Cl^-, the concentration starts increasing within and not below the weathered zone.
- Ca^{2+} concentrations are largely constant and higher than those of Na^+ in the upper part of the weathered zone, until about 16 m. Then, they strongly drop to low values within the lower part of the weathered zone and remain low over the entire profile, with no apparent depth trend.
- Depth trends for K^+ and Mg^{2+} differ slightly from the overall profiles in the upper part of the weathered zone but are not clearly systematic.
- In comparison to the rest of the profile, total Mn contents are higher in the weathered zone, as are 2 data points for total Fe.
- TOC is below detection in the upper part of the weathered zone, with unsystematic distribution over the entire profile.
- Fe and Mn concentrations are low but variable, ranging from a few to max. about 100 µg/L. No clear trend with depth is found. Because extraction conditions were not carried out under a rigorously controlled anoxic conditions, these components may have been affected by oxidation. Note that photometrically determined Fe(II) concentrations are below detection of 1.5 mg/L.
- The ratio NH_4^+/NO_3^- shows no systematic depth evolution below about 25 – 30 m, i.e. below the base of the weathered zone. Within the weathered zone, a systematic decrease towards the surface is identified (Fig. 4-30). This trend is mainly due to a decrease of NH_4^+ towards the surface, whereas the trend of NO_3^- is less clear. It appears that bacterially mediated oxidation of NH_4^+ took place at shallow levels. It is noteworthy that the ratio NH_4^+/NO_3^- is diminished to a depth well below that in which rock oxidation phenomena were identified (16.4 m).

Tab. 4-15: Chemical composition of aqueous extracts.

Analytical errors of the respective instruments are also given.

Depth [m]	Geological unit	Mass of wet rock [g]	Mass of dry rock [g]	Mass of pore water [g]	Mass of water added [g]	S:L* (g dry rock/g pore + added water)	S*:L* (g wet rock/g pore + added water)	Na [mg/L]	Error [mg/L]	K [mg/L]	Error [mg/L]	NH4 [mg/L]	Error [mg/L]	Ca [mg/L]	Error [mg/L]	Mg [mg/L]	Error [mg/L]	Sr ICP-OES [mg/L]	Error [mg/L]	Ba ICP-OES [mg/L]	Error [mg/L]	Fe(tot) ICP-OES [mg/L]	Error [mg/L]	Fe2+ Photom [mg/L]	Mn(tot) ICP-OES [mg/L]	Error [mg/L]
7.83	Opalinus Clay	29.758	24.371	5.387	29.503	0.699	0.853	6.26	0.31	5.34	0.27	0.15	0.03	48.05	2.40	5.61	0.28	0.230	0.012	0.016	0.003	0.009	0.002	<1.5	0.037	0.002
8.23	Opalinus Clay	29.820	25.166	4.654	30.030	0.726	0.860	5.82	0.29	3.79	0.19	0.13	0.03	40.68	2.03	5.01	0.25	0.190	0.009							
8.58	Opalinus Clay	30.564	25.804	4.760	29.294	0.758	0.898	5.88	0.29	5.80	0.29	0.13	0.03	48.47	2.42	5.96	0.30	0.229	0.011	0.017	0.003	0.007	0.001	<1.5	0.039	0.002
10.73	Opalinus Clay	28.598	24.555	4.043	28.870	0.746	0.869	6.48	0.32	6.44	0.32	0.19	0.04	47.81	2.39	5.98	0.30	0.238	0.012	0.033	0.002	0.031	0.002	<1.5	0.040	0.002
11.30	Opalinus Clay	29.920	25.776	4.144	30.220	0.750	0.871	6.38	0.32	4.78	0.24	0.15	0.03	40.54	2.03	5.33	0.27	0.224	0.011							
12.10	Opalinus Clay	29.349	25.726	3.623	29.276	0.782	0.892	8.06	0.40	9.06	0.45	0.31	0.02	54.83	2.74	7.75	0.39	0.408	0.020	0.047	0.002	0.083	0.004	<1.5	0.069	0.003
15.28	Opalinus Clay	29.627	26.568	3.059	29.540	0.815	0.909	18.78	0.94	11.06	0.55	0.60	0.03	54.30	2.72	12.71	0.64	0.770	0.039	0.015	0.003	0.010	0.002	<1.5	0.110	0.006
15.94	Opalinus Clay	30.260	27.359	2.901	30.310	0.824	0.911	14.19	0.71	6.45	0.32	0.38	0.02	22.95	1.15	5.39	0.27	0.382	0.019							
16.75	Opalinus Clay	29.990	27.377	2.613	30.100	0.837	0.917	15.65	0.78	8.83	0.44	0.50	0.02	23.61	1.18	6.20	0.31	0.529	0.026							
19.62	Opalinus Clay	29.786	27.503	2.283	29.824	0.857	0.928	46.57	2.33	11.15	0.56	<1		17.52	0.88	6.69	0.33	1.179	0.059	0.003	0.001	0.003	0.001	<1.5	0.016	0.003
20.09	Opalinus Clay	30.330	28.026	2.304	30.250	0.861	0.932	44.34	2.22	8.58	0.43	<1		8.98	0.45	3.58	0.18	0.683	0.034							
24.52	Opalinus Clay	30.185	28.093	2.092	28.921	0.906	0.973	126.29	6.31	8.63	0.43	1.50	0.30	5.87	0.29	2.76	0.14	0.310	0.015	0.010	0.002	0.002	0.000	<1.5	0.003	0.001
29.02	Opalinus Clay	29.700	27.848	1.852	29.680	0.883	0.942	168.53	8.43	7.73	0.39	1.54	0.31	4.70	0.24	2.10	0.11	0.146	0.007							
33.65	Opalinus Clay	29.877	28.115	1.762	28.935	0.916	0.973	228.50	11.43	9.59	0.48			5.66	0.28	2.78	0.14	0.196	0.010	0.021	0.001	0.002	0.000	<1.5	0.006	0.001
42.88	Opalinus Clay	30.500	28.893	1.607	30.020	0.914	0.964	239.83	11.99	10.01	0.50	<1		6.97	0.35	3.20	0.16	0.642	0.032							
47.58	Opalinus Clay	30.050	28.411	1.639	30.080	0.896	0.947	227.23	11.36	8.41	0.42	1.70	0.34	5.26	0.26	2.19	0.11	0.234	0.012							
50.13	Opalinus Clay	28.728	27.159	1.569	28.927	0.891	0.942	246.56	12.33	9.74	0.49			5.63	0.28	2.65	0.13	0.221	0.011	0.023	0.001	0.015	0.003	<1.5	0.005	0.001
54.98	Opalinus Clay	30.130	28.595	1.535	30.070	0.905	0.953	269.62	13.48	10.65	0.53	<1		9.52	0.48	4.39	0.22	1.952	0.098							
60.78	Opalinus Clay	29.792	28.121	1.671	29.990	0.888	0.941	260.53	13.03	9.60	0.48			5.66	0.28	2.77	0.14	0.171	0.009	0.010	0.002	0.002	0.000	<1.5	0.006	0.001
77.81	Staffelegg-Fm	30.290	29.044	1.246	30.210	0.923	0.963	231.67	11.58	9.78	0.49	2.05	0.10	6.58	0.33	2.94	0.15	0.184	0.009							
82.87	Staffelegg-Fm	30.273	28.703	1.570	30.028	0.908	0.958	250.31	12.52	9.20	0.46			5.42	0.27	2.79	0.14	0.148	0.007	0.007	0.001	0.005	0.001	<1.5	<0.002	
96.98	Staffelegg-Fm	30.360	28.873	1.487	30.290	0.909	0.955	219.77	10.99	7.79	0.39	2.09	0.10	4.01	0.20	1.86	0.37	0.079	0.004							
113.55	Klettgau-Fm	30.544	28.577	1.967	30.162	0.889	0.951	305.72	15.29	10.02	0.50			7.83	0.39	3.89	0.19	0.391	0.020	0.049	0.002	<0.002		<1.5	<0.002	
132.12	Klettgau-Fm	29.980	28.639	1.341	29.990	0.914	0.957	359.86	17.99	14.30	0.72	<1		20.13	1.01	9.61	0.48	10.252	0.513							

Depth [m]	Geological unit	F [mg/L]	Error [mg/L]	Cl [mg/L]	Error [mg/L]	Br [mg/L]	NO3 [mg/L]	Error [mg/L]	SO4 [mg/L]	Error [mg/L]	Tot. alkalinity (titration) [meq/L]	Error [mg/L]	Tot. alkalinity (titration) as HCO3 [mg/L]	Error [mg/L]	TOC C analyser[mg/L]	Error [mg/L]	TIC C analyser[mg/L]	Error [mg/L]	TIC C analyser as HCO3 [mg/L]	Error [mg/L]	pH	TDS [mg/L]	Sum cations [meq/L]	Sum anions [meq/L]	Charge balance [%]
7.83	Opalinus Clay	0.50	0.03	1.45	0.07	<0.016	0.56	0.03	8.49	0.42	3.10	0.16	189.2	9.5	<1		41.6	2.1	211.4	10.6	7.84	307.5	3.28	-3.35	-1.04
8.23	Opalinus Clay	0.47	0.02	1.88	0.09	<0.016	0.43	0.02	7.19	0.36	3.14	0.16	191.6	9.6	<1		35.5	1.8	180.2	9.0	8.09	292.8	2.80	-3.19	-6.40
8.58	Opalinus Clay	0.48	0.02	2.15	0.11	<0.016	0.27	0.01	8.84	0.44	3.17	0.16	193.4	9.7	<1		41.9	2.1	212.8	10.6	7.86	313.6	3.33	-3.44	-1.72
10.73	Opalinus Clay	0.40	0.02	2.44	0.12	<0.016	0.23	0.01	16.95	0.85	2.93	0.15	178.8	8.9	<1		38.7	1.9	196.7	9.8	7.84	304.7	3.34	-3.38	-0.51
11.30	Opalinus Clay	0.44	0.02	2.22	0.11	<0.016	0.31	0.02	8.25	0.41	3.11	0.16	189.8	9.5	<1		36.5	1.8	185.4	9.3	8.09	295.8	2.88	-3.30	-6.89
12.10	Opalinus Clay	0.36	0.02	2.03	0.10	<0.016	0.21	0.01	11.01	0.55	3.74	0.19	228.2	11.4	1.63	0.33	49.2	2.5	249.8	12.5	7.86	373.2	3.99	-4.05	-0.75
15.28	Opalinus Clay	0.32	0.02	1.62	0.08	<0.016	0.39	0.02	29.98	1.50	4.33	0.22	264.2	13.2	<1		56.7	2.8	287.9	14.4	8.05	451.9	4.91	-5.02	-1.13
15.94	Opalinus Clay	0.60	0.03	1.42	0.07	<0.016	0.41	0.02	24.45	1.22	2.42	0.12	147.7	7.4	4.79	0.05	25.3	1.3	128.8	6.4	8.06	254.4	2.40	-2.70	-5.83
16.75	Opalinus Clay	0.59	0.03	1.03	0.05	<0.016	0.64	0.03	39.73	1.99	2.30	0.12	140.3	7.0	2.95	0.03	24.7	1.2	125.6	6.3	8.10	265.3	2.63	-2.96	-5.76
19.62	Opalinus Clay	0.72	0.04	1.92	0.10	<0.016	0.05	0.00	66.26	3.31	2.42	0.12	147.7	7.4	<1		31.5	1.6	160.1	8.0	8.32	332.2	3.81	-3.89	-1.02
20.09	Opalinus Clay	1.16	0.06	1.94	0.10	<0.016	0.54	0.03	59.44	2.97	2.02	0.10	123.3	6.2	2.57	0.03	22.6	1.1	114.9	5.7	8.27	278.5	2.95	-3.25	-4.72
24.52	Opalinus Clay	1.94	0.10	19.94	1.00	<0.16	0.61	0.03	178.51	8.93	2.62	0.13	159.9	8.0	4.34	0.87	23.4	1.2	119.1	6.0	8.81	534.0	6.32	-7.01	-5.15
29.02	Opalinus Clay	2.00	0.10	36.36	1.82	<0.16	0.60	0.03	226.02	11.30	2.29	0.11	139.7	7.0	11.87	0.12	27.5	1.4	139.9	7.0	8.83	628.7	8.02	-8.14	-0.71
33.65	Opalinus Clay	1.57	0.08	56.12	2.81	<0.16	0.30	0.06	272.83	13.64	3.35	0.17	204.4	10.2	1.48	0.30	41.4	2.1	210.4	10.5	8.81	824.9	10.70	-10.70	0.00
42.88	Opalinus Clay	1.41	0.07	81.63	4.08	<0.16	0.58	0.03	302.40	15.12	3.29	0.16	200.7	10.0	2.50	0.03	37.2	1.9	188.9	9.4	8.66	887.3	11.31	-11.78	-2.01
47.58	Opalinus Clay	2.00	0.10	85.29	4.26	<0.16	0.65	0.03	284.23	14.21	2.62	0.13	159.9	8.0	<1		28.3	1.4	143.6	7.2	8.83	806.0	10.64	-10.79	-0.71
50.13	Opalinus Clay	1.72	0.09	85.73	4.29	<0.16	0.24	0.05	283.53	14.18	3.23	0.16	197.1	9.9	<1		37.7	1.9	191.4	9.6	8.80	870.9	11.48	-11.65	-0.73
54.98	Opalinus Clay	1.52	0.08	86.52	4.33	<0.16	0.56	0.03	403.18	20.16	2.48	0.12	151.3	7.6	<1		31.0	1.6	157.7	7.9	8.67	971.3	12.88	-13.51	-2.38
60.78	Opalinus Clay	2.27	0.11	88.65	4.43	<0.16	0.32	0.06	286.67	14.33	3.54	0.18	216.0	10.8	<1		44.3	2.2	225.2	11.3	8.78	917.5	12.09	-12.14	-0.17
77.81	Staffelegg-Fm	2.75	0.14	73.11	3.66	<0.16	0.37	0.07	364.00	18.20	1.44	0.07	87.9	4.4	2.69	0.03	14.6	0.7	74.0	3.7	9.08	798.4	11.02	-11.00	0.05
82.87	Staffelegg-Fm	3.00	0.15	87.12	4.36	<0.16	0.61	0.03	337.61	16.88	1.76	0.09	107.4	5.4	0.71	0.14	15.4	0.8	78.5	3.9	9.16	819.9	11.63	-11.42	0.92
96.98	Staffelegg-Fm	3.58	0.18	82.97	4.15	<0.16	0.68	0.03	295.55	14.78	1.62	0.08	98.8	4.9	6.31	0.06	15.4	0.8	78.3	3.9	9.29	738.9	10.23	-9.98	1.25
113.55	Klettgau-Fm	3.19	0.16	103.31	5.17	<0.16	0.37	0.07	421.14	21.06	2.79	0.14	170.2	8.5	2.67	0.53	27.2	1.4	138.2	6.9	9.48	1056.2	14.27	-14.65	-1.29
132.12	Klettgau-Fm	2.53	0.13	85.68	4.28	<0.16	0.54	0.03	672.79	33.64	1.85	0.09	112.9	5.6	2.78	0.03	20.7	1.0	105.0	5.2	8.87	1312.1	18.05	-18.29	-0.66

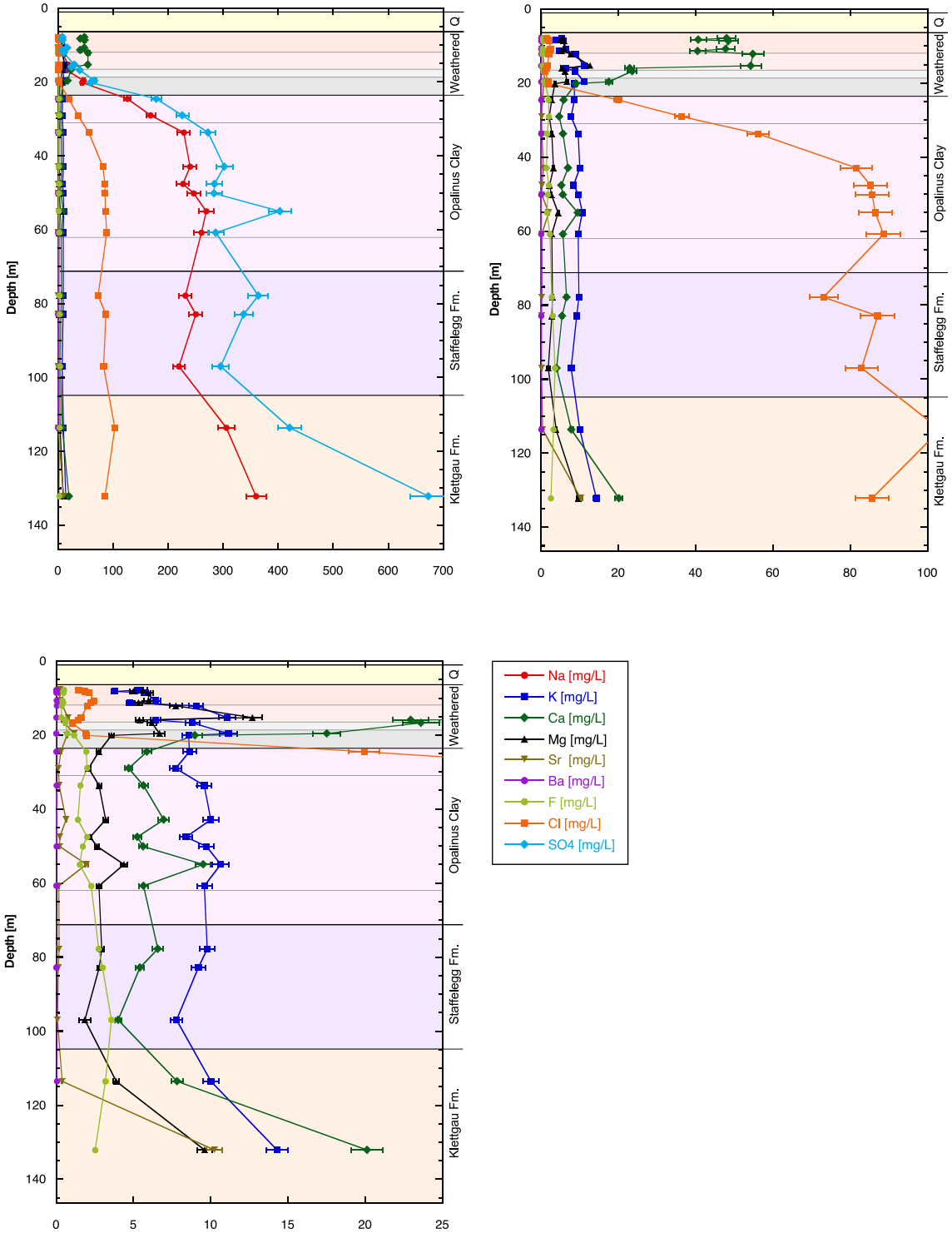

Fig. 4-29: Ion concentrations in aqueous extracts as a function of depth.

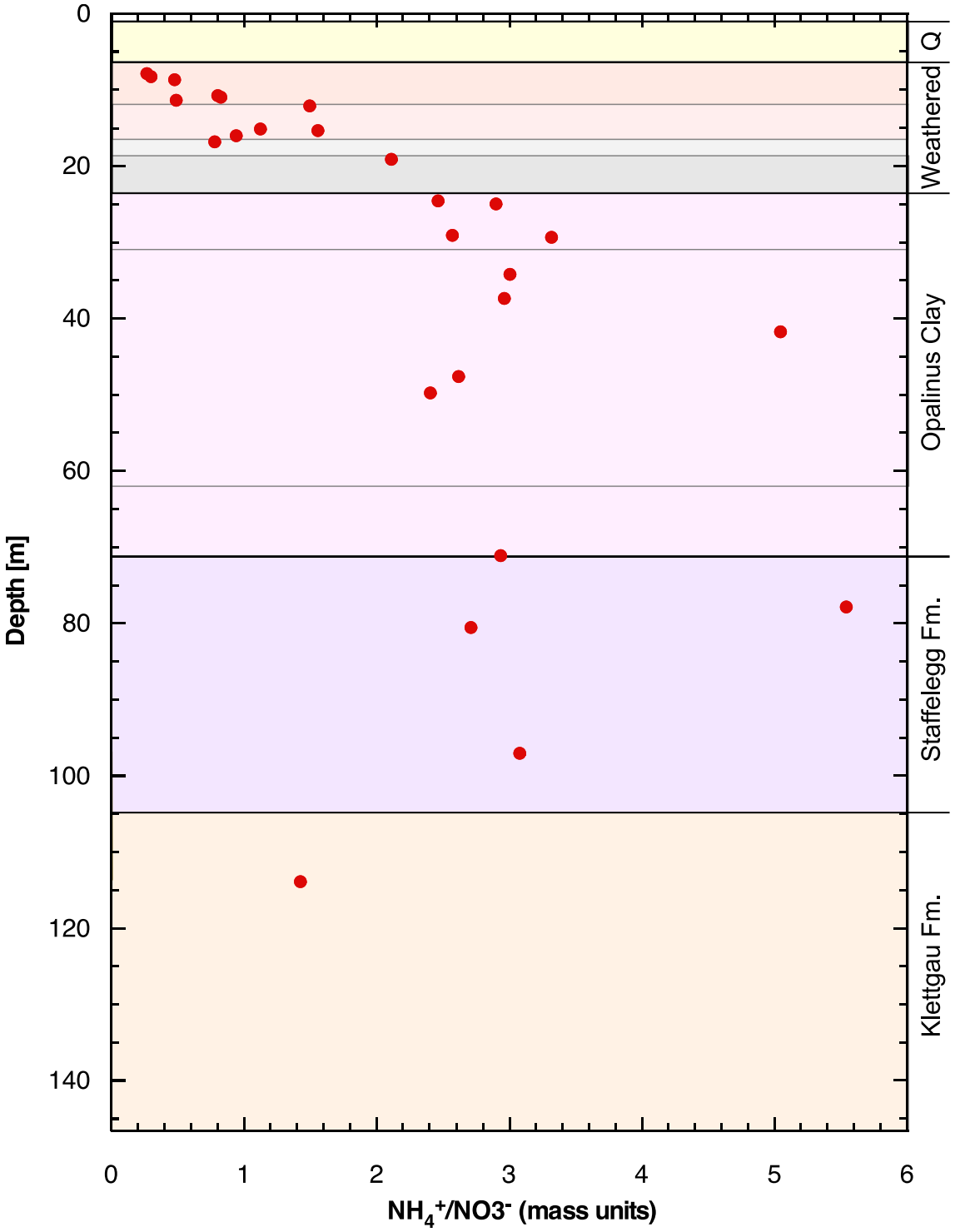

Fig. 4-30: Ratio NH_4^+/NO_3^- in aqueous extracts as a function of depth.

4.9 Pore-water squeezing: Major ions

4.9.1 Squeezing pressure and water yield

A total of 12 samples were taken over the entire profile, with a denser sampling at shallow levels. The lowermost two samples are from units underlying the Opalinus Clay (an argillaceous siltstone from the Staffelegg Fm. and a dolomitic claystone from the Klettgau Fm.). Given the higher water content of the Opalinus Clay within the uppermost 20 – 30 m (Section 4.7), the lowest squeezing pressure was chosen at 10 – 20 MPa, whereas it was 100 MPa in the underlying unweathered rocks. The squeezing conditions are summarised in Tab. 4-16. The cumulative mass of squeezed water is also listed in Tab. 4-16 and is illustrated in Fig. 4-31. Samples of Opalinus Clay yielded a total of 8 – 33 g water, with a decreasing trend with depth. The water mass remaining in samples of Opalinus Clay after squeezing was in the range 11 – 15 g, corresponding to water contents of 2.6 – 3.9 wt.-%. Fig. 4-32 shows the linear relationship between the total squeezed water mass and the original water content.

Fig. 4-33 shows the water content in the samples as a function of squeezing pressure. The following observations can be made:

- In relative terms, the squeezing behaviour of all Opalinus Clay samples is similar, indicated by the fact that the the lines in Fig. 4-33 do not cross cut each other (or only marginally). In contrast, the samples from the Lias and Keuper show a distinctly lower compressibility and water yield, and the lines cross cut those of Opalinus Clay.
- Samples from the clay-rich Opalinus Clay (10.88, 15.05, 19.05, 24.93, 29.28, 71.08) show a decreasing trend of the initial as well as the final water content with depth. This means that the shallowest samples with the highest initial water content also have the highest water content remaining in the sample after squeezing. It follows that the surficial increase of porosity due to decompaction and infiltration of low-salinity water is not fully reversible. This is most likely due to mineral dissolution (calcite, pyrite) and related fabric changes.

Tab. 4-16: Water content of rock samples prior to squeezing, water mass squeezed and water mass remaining after squeezing.

The wet water content prior to squeezing was calculated by adding the squeezed water mass with the mass of the water remaining in the sample after squeezing (determined by drying at 105 °C).

Depth [m]	Geological unit	Wet water content prior to squeezing [wt%]	Dry rock mass [g]	Mass of water in squeezed core [g]	Squeezing pressure [Mpa]	Mass squeezed [g]	Cumulative mass squeezed [g]
10.88	Opalinus Clay	13.95	280.92	12.63	10	3.74	3.74
					20	5.81	9.55
					50	9.40	18.95
					100	4.32	23.27
					150	2.32	25.59
					200	2.23	27.82
					300	1.81	29.63
					400	1.43	31.06
					500	1.84	32.90
15.05	Opalinus Clay	11.84	261.44	11.10	10	3.71	3.71
					20	4.13	7.84
					50	5.37	13.21
					100	3.09	16.30
					150	1.57	17.87
					200	1.69	19.56
					300	1.58	21.14
					400	1.42	22.56
					500	1.45	24.01
19.05	Opalinus Clay	7.67	384.38	14.59	20	2.33	2.33
					50	3.61	5.94
					100	3.12	9.06
					150	1.99	11.05
					200	1.35	12.40
					300	1.96	14.36
					400	1.54	15.90
					500	1.42	17.32
24.93	Opalinus Clay	6.69	376.22	13.87	20	0.00	0.00
					50	2.06	2.06
					100	3.09	5.15
					150	1.85	7.00
					200	1.57	8.57
					300	1.82	10.39
					400	1.51	11.90
					500	1.22	13.12
29.28	Opalinus Clay	5.92	415.91	14.19	100	3.72	3.72
					150	2.08	5.80
					200	1.37	7.17
					300	1.90	9.07
					400	1.95	11.02
					500	0.95	11.97

Depth [m]	Geological unit	Wet water content prior to squeezing [wt%]	Dry rock mass [g]	Mass of water in squeezed core [g]	Squeezing pressure [Mpa]	Mass squeezed [g]	Cumulative mass squeezed [g]
34.13	Opalinus Clay	5.70	394.66	13.27	100	2.28	2.28
					150	2.18	4.46
					200	1.45	5.91
					300	2.05	7.96
					400	1.68	9.64
					500	0.93	10.57
37.30	Opalinus Clay	4.87	373.12	10.73	100	0.97	0.97
					150	1.74	2.71
					200	1.40	4.11
					300	2.04	6.15
					400	1.20	7.35
					500	1.01	8.36
41.68	Opalinus Clay	4.41	406.05	11.20	100	0.00	0.00
					150	1.36	1.36
					200	1.30	2.66
					300	2.37	5.03
					400	1.39	6.42
					500	1.13	7.55
49.75	Opalinus Clay	5.38	328.99	11.20	100	0.48	0.48
					150	1.66	2.14
					200	1.57	3.71
					300	1.47	5.18
					400	1.32	6.50
					500	1.01	7.51
71.08	Opalinus Clay	6.15	363.83	13.20	100	1.77	1.77
					150	2.12	3.89
					200	1.66	5.55
					300	2.12	7.67
					400	1.63	9.30
					500	1.33	10.63
80.47	Staffelegg-Fm	3.91	465.23	15.12	100	0.00	0.00
					150	0.00	0.00
					200	0.00	0.00
					300	1.29	1.29
					400	1.28	2.57
					500	1.26	3.83
113.79	Klettgau-Fm	5.71	414.38	20.64	100	0.00	0.00
					150	0.00	0.00
					200	0.00	0.00
					300	1.30	1.30
					400	1.63	2.93
					500	1.51	4.44

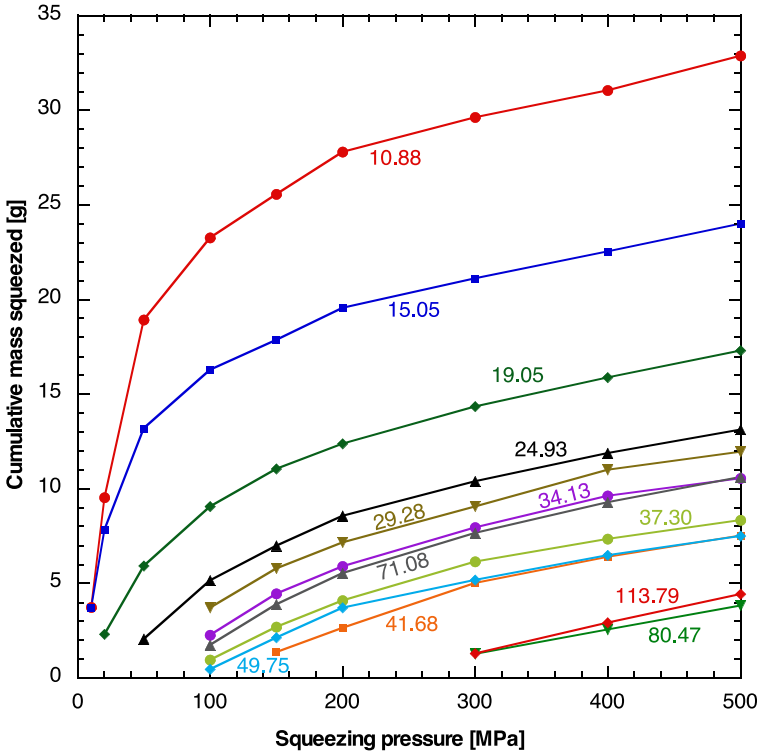

Fig. 4-31: Cumulative mass of squeezed water as a function of pressure.

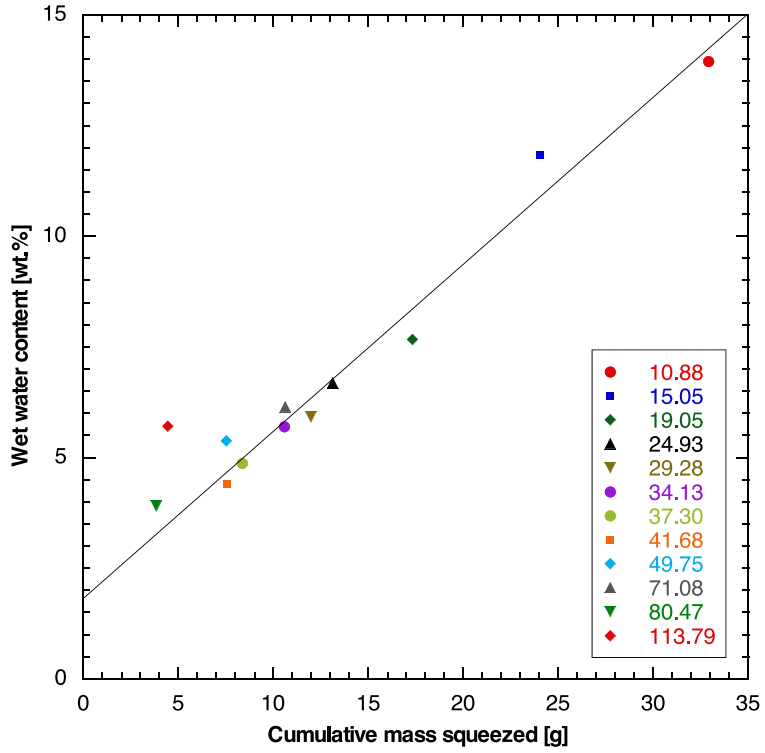

Fig. 4-32: Relationship between the total squeezed water mass and the water content of the unsqueezed samples.

Regression line refers to Opalinus Clay only, i.e. neglects the lowermost two samples.

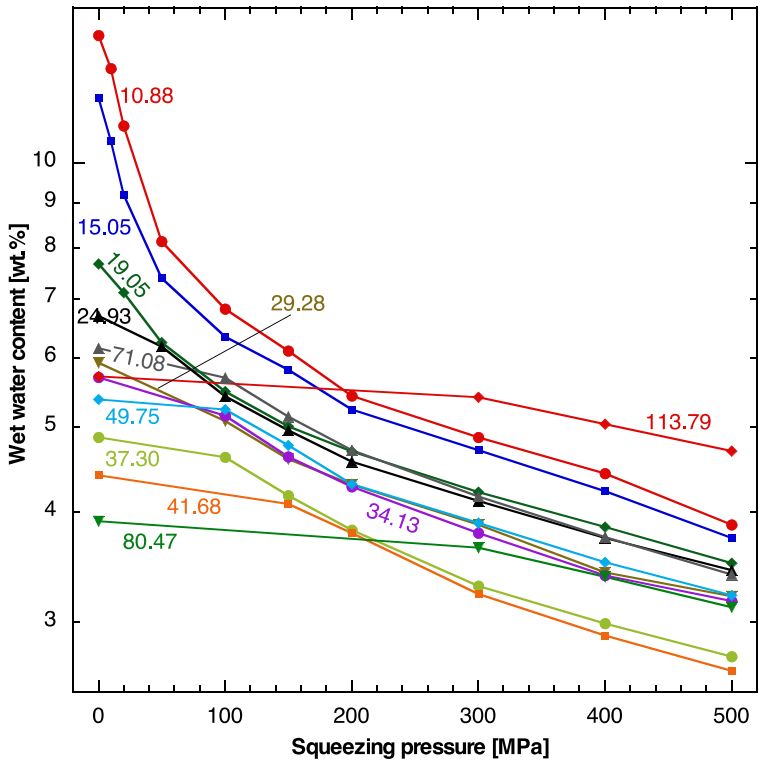

Fig. 4-33: Residual water content of the rock samples as a function of squeezing pressure. Values at 0 MPa represent the original water content prior to squeezing.

4.9.2 Chemical composition of squeezed waters – dependence on pressure

The chemical composition of squeezed waters is listed in Tab. 4-17 and shown graphically in Fig. 4-34. The concentrations of Na^+, K^+, Cl^- and Br^- decrease with increasing squeezing pressure, an observation already made and discussed in Mazurek et al. (2015) for samples from the Schlattingen borehole. Those authors argued that the water obtained at the lowest pressure is the closest representation of the pore-water composition. The relative decrease of monovalent-ion concentrations at Lausen is similar to that observed at Schlattingen, with the exception of the three shallowest samples in the weathered zone (10.88, 15.05, 19.05), where salinity is much lower than in the deeper samples.

In the shallow samples, Cl^- concentration drops dramatically by about 60 – 70 % between the first (10 – 20 MPa) and the second (20 – 50 MPa) squeezing step. Cl^- concentration drops further up to 150 MPa and then increases slightly at higher pressures. A similar behaviour is seen for Na^+, even though concentrations tend to be constant instead of increasing as those of Cl^-. Such pressure trends for both Cl^- and Na^+ have not been identified in past campaigns. Interestingly, the relative decrease of K^+ in the uppermost three samples is indistinguishable from that of the deeper samples. Hypotheses explaining the behaviour of Na^+ and Cl^- in the shallow samples include:

1. Contamination of Na^+ and Cl^- from an unknown source during squeezing would have the relatively strongest effects in samples with a low pore-water salinity. The possible contamination by fiberglass filters attached to the end pieces of the squeezed core is duscussed in Section 4.9.4.

2. Porosity and pore-space architecture differ between shallow and deeper samples of Opalinus Clay, i.e. the material has distinct fabrics. The low salinity of the pore water in the shallow samples tends to amplify the effects of membrane filtration, while larger apertures have the opposite effect. These features may affect ion transport through the material, even though a simple model is not at hand to explain the ensemble of all observations.

For other pore-water constituents, the following observations can be made:

- Concentrations of Ca^{2+} and Mg^{2+} generally increase slightly with pressure, most probably due to the dissolution of carbonate minerals at higher pressures. However, this is not the case for the 3 samples from the weathered zone where concentrations remain nearly constant. Note that calcite contents in those samples are lower but not zero.
- F^- concentrations in the first water squeezed are substantially higher than in waters squeezed at higher pressures. Mazurek et al. (2015) suspected that F^- is contaminated by the equipment, possibly the fiberglass filters on both sides of each sample. This is confirmed by an aqueous-extraction test described in Section 4.9.4. Again, the 3 samples from the weathered zone behave differently in that F^- contents increase slightly with pressure after the initial drop.
- SO_4^{2-} concentrations decrease slightly with pressure, except for the samples in the weathered zone where they remain constant (with the exception of sample 15.05 that shows a slight increase).
- TOC concentrations in the first water aliquot are always substantially higher when compared to those obtained at higher pressures. In the first aliquot squeezed from samples of Opalinus Clay, low-molecular weight organic acids account for 18 – 41 % of the measured TOC (sample 71.08: 2.5 %). This finding is consistent with previous observations, and a similar behaviour has also been identified in water samples obtained by advective displacement (Mäder et al. 2017). Again, release from the fiberglass filters may contribute at least to the measured acetate and propionate concentrations (Section 4.9.4).

Tab. 4-17: Chemical composition of squeezed waters.

Precipitated calcite was observed in waters 15.05 m/50 MPa and 15.05 m/150 MPa. Values in [brackets] are affected substantially, those in italics to a lesser degree by contamination.

Depth [m]	Geological unit	Squeezing pressure	Na [mg/L]	Error	K [mg/L]	Error	Ca [mg/L]	Error	Mg [mg/L]	Error	Sr [mg/L]	Error	F [mg/L]	Error	Cl [mg/L]	Error	Br [mg/L]	Error	NO3 [mg/L]	Error	SO4 [mg/L]	Error	TIC (direct) [mg/L]	Error	TIC (direct) as HCO3 [mg/L]	Error	TOC (direct) [mg/L]	Error	lactate [mg/L]	Error	Acetate [mg/L]	Error	Propionate [mg/L]	Error	Formate [mg/L]	Error	pH
10.88	Opalinus Clay	10	*[133.4]*	6.7	*13.83*	0.69	*198.7*	9.9	36.27	1.81	*0.92*	0.05	*3.81*	0.19	*[98.36]*	4.92	<0.16		4.22	0.21	671.1	33.6	*37.12*	1.86	*188.7*	9.4	57.07	5.71	2.6	0.5	24.5	1.2	<2				5.5	0.3	7.83
10.88	Opalinus Clay	20	65.21	3.26	14.84	0.74	200.4	10.0	35.53	1.78	0.96	0.05	1.24	0.06	41.39	2.07	<0.16		1.14	0.06	547.5	27.4	44.29	2.21	225.2	11.3	18.24	1.82	<2		<2		<2		2.6	0.5	7.99
10.88	Opalinus Clay	50	47.48	2.37	11.29	0.56	198.0	9.9	37.33	1.87	0.94	0.05	1.01	0.05	28.59	1.43	<0.16		0.67	0.03	518.1	25.9	49.51	2.48	251.7	12.6	14.13	1.41	<2		2.4	0.5	<2		5.6	0.3	7.82
10.88	Opalinus Clay	100	41.90	2.10	8.33	0.42	201.8	10.1	39.06	1.95	0.84	0.04	1.45	0.07	25.08	1.25	<0.16		0.67	0.03	521.6	26.1	44.69	2.23	227.2	11.4	25.88	2.59	<2		4.8	1.0	<2		5.5	0.3	8.15
10.88	Opalinus Clay	150	35.79	1.79	6.40	0.32	167.6	8.4	39.95	2.00	0.72	0.04	1.52	0.08	24.18	1.21	<0.16		0.54	0.03	516.8	25.8	30.58	1.53	155.5	7.8	22.55	2.25	<2		2.1	0.4	<2		9.1	0.5	8.07
10.88	Opalinus Clay	200	37.49	1.87	5.97	0.30	173.0	8.6	39.49	1.97	0.57	0.03	2.10	0.11	24.78	1.24	<0.16		<0.16		508.9	25.4	23.86	1.19	121.3	6.1	33.76	3.38	<2		4.6	0.9	<2		3.0	0.6	8.03
10.88	Opalinus Clay	300	30.28	1.51	4.51	0.23	163.1	8.2	38.94	1.95	0.47	0.02	2.35	0.12	23.75	1.19	<0.16		1.00	0.05	495.3	24.8	21.22	1.06	107.9	5.4	26.24	2.62	<2		2.3	0.5	<2		5.9	0.3	7.99
10.88	Opalinus Clay	400	29.22	1.46	4.28	0.21	163.7	8.2	39.87	1.99	0.39	0.02	2.65	0.13	24.76	1.24	<0.16		0.42	0.02	500.4	25.0	17.06	0.85	86.7	4.3	31.43	3.14	<2		2.4	0.5	<2		4.9	1.0	7.86
10.88	Opalinus Clay	500	33.05	1.65	4.59	0.23	152.9	7.6	38.00	1.90	0.28	0.01	3.34	0.17	26.14	1.31	<0.16		0.39	0.08	484.5	24.2	17.94	0.90	91.2	4.6	32.10	3.21	<2		2.6	0.5	<2		23.4	1.2	7.77
15.05	Opalinus Clay	10	*[148.2]*	7.4	9.14	0.46	36.9	1.8	14.67	0.73	0.73	0.04	*5.35*	0.27	*[89.29]*	4.46	<0.16		4.12	0.21	98.13	4.91	58.70	2.94	298.4	14.9	58.77	5.88	2.7	0.5	25.3	1.3	<2		2.4	0.5	8.45
15.05	Opalinus Clay	20	82.12	4.11	8.32	0.42	43.7	2.2	17.41	0.87	0.83	0.04	1.60	0.08	30.05	1.50	<0.16		1.18	0.06	94.90	4.75	65.92	3.30	335.1	16.8	15.62	1.56	<2		<2		<2		<2		8.52
15.05	Opalinus Clay	50	64.38	3.22	7.66	0.38	35.5	1.8	17.87	0.89	0.84	0.04	1.27	0.06	21.28	1.06	<0.16		0.63	0.03	89.43	4.47	61.85	3.09	314.4	15.7	11.51	1.15	<2		<2		<2		6.1	0.3	8.46
15.05	Opalinus Clay	100	60.43	3.02	6.64	0.33	58.7	2.9	19.93	1.00	0.88	0.04	1.99	0.10	19.90	1.00	<0.16		0.49	0.02	92.98	4.65	58.62	2.93	298.0	14.9	21.57	2.16	<2		4.5	0.9	<2		<2		8.47
15.05	Opalinus Clay	150	51.53	2.58	5.61	0.28	30.2	1.5	19.83	0.99	0.80	0.04	2.06	0.10	19.20	0.96	<0.16		0.71	0.04	96.66	4.83	54.42	2.72	276.6	13.8	18.74	1.87	<2		<2		<2		6.3	0.3	8.38
15.05	Opalinus Clay	200	52.00	2.60	5.97	0.30	53.7	2.7	20.04	1.00	0.78	0.04	2.79	0.14	21.52	1.08	<0.16		0.54	0.03	101.2	5.1	44.46	2.22	226.0	11.3	24.75	2.48	<2		3.7	0.7	<2		6.1	0.3	8.41
15.05	Opalinus Clay	300	42.68	2.13	4.58	0.23	57.0	2.8	20.67	1.03	0.70	0.03	3.25	0.16	22.16	1.11	<0.16		0.36	0.07	104.1	5.2	41.74	2.09	212.2	10.6	24.29	2.43	<2		<2		<2		<2		8.38
15.05	Opalinus Clay	400	39.20	1.96	4.32	0.22	53.8	2.7	20.40	1.02	0.60	0.03	3.40	0.17	23.13	1.16	<0.16		0.28	0.06	105.9	5.3	37.25	1.86	189.4	9.5	26.74	2.67	<2		<2		<2		6.1	0.3	8.24
15.05	Opalinus Clay	500	40.83	2.04	4.55	0.23	48.8	2.4	19.39	0.97	0.47	0.02	4.20	0.21	26.55	1.33	<0.16		0.59	0.03	107.5	5.4	34.18	1.71	173.7	8.7	24.85	2.48	<2		<2		<2		2.1	0.4	8.30
19.05	Opalinus Clay	20	*[306.5]*	15.3	*14.48*	0.72	*47.7*	2.4	33.89	1.69	*3.41*	0.17	*7.79*	0.39	*[141.7]*	7.08	<0.8		*7.77*	0.39	*402.7*	20.1	*67.21*	3.36	*341.6*	17.1	*90.99*	9.10	*5.9*	0.3	*44.7*	2.2	<2		*26.5*	1.3	*8.53*
19.05	Opalinus Clay	50	175.2	8.8	13.04	0.65	58.1	2.9	35.93	1.80	3.87	0.19	2.40	0.12	38.90	1.95	<0.8		2.45	0.12	402.1	20.1	55.61	2.78	282.7	14.1	28.14	2.81	2.2	0.4	7.8	0.4	<2		7.3	0.4	8.48
19.05	Opalinus Clay	100	134.3	6.7	10.36	0.52	64.5	3.2	35.79	1.79	4.00	0.20	2.72	0.14	25.52	1.28	<0.8		1.36	0.07	368.4	18.4	50.10	2.51	254.7	12.7	23.71	2.37	<2		4.7	0.9	<2		6.3	0.3	8.40
19.05	Opalinus Clay	150	104.5	5.2	8.07	0.40	58.0	2.9	37.55	1.88	3.86	0.19	2.69	0.13	22.79	1.14	<0.8		0.78	0.04	360.6	18.0	36.02	1.80	183.1	9.2	21.95	2.19	<2		2.5	0.5	<2		5.7	0.3	8.27
19.05	Opalinus Clay	200	93.38	4.67	7.19	0.36	57.6	2.9	40.41	2.02	3.86	0.19	2.91	0.15	23.91	1.20	<0.8		0.92	0.05	366.5	18.3	29.78	1.49	151.4	7.6	24.01	2.40	<2		3.5	0.7	<2		7.3	0.4	8.18
19.05	Opalinus Clay	300	67.91	3.40	5.32	0.27	66.5	3.3	42.43	2.12	3.78	0.19	3.34	0.17	24.60	1.23	<0.8		0.81	0.04	360.0	18.0	27.49	1.37	139.7	7.0	25.53	2.55	<2		<2		<2		5.8	0.3	8.10
19.05	Opalinus Clay	400	54.00	2.70	4.66	0.23	74.2	3.7	46.78	2.34	3.83	0.19	3.05	0.15	26.29	1.31	<0.8		1.05	0.05	353.8	17.7	25.86	1.29	131.4	6.6	25.81	2.58	<2		2.9	0.6	<2		6.1	0.3	8.13
19.05	Opalinus Clay	500	51.09	2.55	4.50	0.23	79.7	4.0	49.88	2.49	3.69	0.18	3.15	0.16	29.56	1.48	<0.8		0.73	0.04	367.5	18.4	30.77	1.54	156.4	7.8	28.15	2.82	<2		3.3	0.7	<2		7.7	0.4	8.17
24.93	Opalinus Clay	50	1167	58.3	37.00	1.85	178.5	8.9	102.6	5.1	6.30	1.26	7.95	0.40	739.1	37.0	<0.8		7.60	0.38	2270	114	35.05	1.75	178.2	8.9	82.21	8.22	<10		44.7	2.2	<10		25.6	1.3	8.22
24.93	Opalinus Clay	100	917	45.8	26.20	1.31	176.6	8.8	106.1	5.3	8.00	1.60	3.20	0.16	566.5	28.3	<0.8		2.20	0.11	2040	102	28.11	1.41	142.9	7.1	38.31	3.83	<10		13.1	2.6	<10		<10		8.25
24.93	Opalinus Clay	150	763	38.2	18.60	0.93	182.9	9.1	116.3	5.8	7.55	1.51	2.75	0.14	487.4	24.4	<0.8		2.15	0.11	1871	94	26.85	1.34	136.5	6.8	29.25	2.92	<10		<10		<10		<10		8.12
24.93	Opalinus Clay	200	655	32.8	14.50	0.73	206.6	10.3	128.2	6.4	8.80	1.76	2.70	0.14	443.7	22.2	<0.8		1.60	0.32	1785	89	26.18	1.31	133.1	6.7	30.83	3.08	<10		<10		<10		<10		8.12
24.93	Opalinus Clay	300	483	24.2	10.00	0.50	230.4	11.5	144.2	7.2	9.20	1.84	2.80	0.14	388.2	19.4	<0.8		1.65	0.33	1663	83	27.47	1.37	139.6	7.0	31.68	3.17	<10		<10		<10		<10		8.27
24.93	Opalinus Clay	400	358	17.9	8.00	1.60	263.9	13.2	169.6	8.5	9.50	1.90	2.65	0.13	351.7	17.6	<0.8		1.25	0.25	1628	81	28.55	1.43	145.1	7.3	29.49	2.95	<10		<10		<10		<10		8.20
24.93	Opalinus Clay	500	286	14.3	7.55	1.51	284.4	14.2	185.2	9.3	9.90	1.98	2.45	0.12	337.7	16.9	<0.8		5.65	0.28	1616	81	29.62	1.48	150.6	7.5	31.25	3.12	<10		<10		<10		10.1	2.0	8.21
29.28	Opalinus Clay	100	1880	94.0	44.30	2.22	355.0	17.8	194.7	9.7	9.50	1.90	6.80	0.34	1269	63	1.50	0.30	4.25	0.21	4042	202	28.27	1.41	143.7	7.2	64.82	6.48	<10		24.3	4.9	11.2	2.2	17.3	3.5	8.06
29.28	Opalinus Clay	150	1599	79.9	29.75	1.49	344.2	17.2	191.0	9.6	9.75	1.95	3.30	0.17	1047	52	1.25	0.25	3.20	0.16	3664	183	28.25	1.41	143.6	7.2	35.26	3.53	<10		11.1	2.2	10.9	2.2	10.9	2.2	8.08
29.28	Opalinus Clay	200	1439	72.0	22.50	1.13	367.1	18.4	205.8	10.3	9.00	1.80	3.10	0.16	965.7	48.3	1.15	0.23	1.55	0.31	3518	176	30.09	1.50	153.0	7.6	30.77	3.08	<10		<10		<10		12.7	2.5	8.14
29.28	Opalinus Clay	300	1112	55.6	15.40	0.77	383.9	19.2	213.3	10.7	8.25	1.65	3.15	0.16	817.4	40.9	<0.8		1.75	0.35	3137	157	30.21	1.51	153.6	7.7	24.13	2.41	<10		<10		<10		<10		8.24
29.28	Opalinus Clay	400	852	42.6	11.25	0.56	447.5	22.4	259.3	13.0	9.05	1.81	2.80	0.14	756.7	37.8	<0.8		1.25	0.25	3043	152	27.28	1.36	138.7	6.9	24.41	2.44	<10		<10		<10		<10		8.28
29.28	Opalinus Clay	500	771	38.6	10.95	0.55	499.2	25.0	273.0	13.7	8.90	1.78	2.80	0.14	764.4	38.2	<0.8		2.00	0.10	3088	154	32.29	1.61	164.1	8.2	33.66	3.37	<10		<10		<10		<10		8.15

Tab. 4-17: Cont.

Depth [m]	Geological unit	Squeezing pressure	Na [mg/L]	Error	K [mg/L]	Error	Ca [mg/L]	Error	Mg [mg/L]	Error	Sr [mg/L]	Error	F [mg/L]	Error	Cl [mg/L]	Error	Br [mg/L]	Error	NO3 [mg/L]	Error	SO4 [mg/L]	Error	TIC (direct) [mg/L]	Error	TIC (direct) as HCO3 [mg/L]	Error	TOC (direct) [mg/L]	Error	lactate [mg/L]	Error	Acetate [mg/L]	Error	Propionate [mg/L]	Error	Formate [mg/L]	Error	pH
34.13	Opalinus Clay	100	2408	120.4	51.75	2.59	416.7	20.8	231.5	11.6	10.65	0.53	7.85	0.39	1936	97	2.15	0.11	3.40	0.17	4649	232	26.37	1.32	134.0	6.7	69.84	6.98	<10		43.9	2.2	11.5	2.3	18.7	3.7	7.88
34.13	Opalinus Clay	150	2151	107.6	36.15	1.81	393.1	19.7	227.7	11.4	9.15	1.83	4.25	0.21	1647	82	1.80	0.04	1.55	0.31	4319	216	27.11	1.36	137.8	6.9	40.39	4.04	<10		16.2	3.2	10.5	2.1	13.9	2.8	8.08
34.13	Opalinus Clay	200	1967	98.4	27.25	1.36	409.5	20.5	235.1	11.8	8.10	1.62	3.55	0.18	1539	77	1.75	0.04	3.15	0.16	4219	211	27.90	1.40	141.8	7.1	33.36	3.34	<10		<10		10.5	2.1	<10		8.11
34.13	Opalinus Clay	300	1570	78.5	19.90	1.00	422.8	21.1	244.5	12.2	9.00	1.80	3.25	0.16	1281	64	1.50	0.03	4.70	0.24	3753	188	28.57	1.43	145.2	7.3	27.34	2.73	<10		<10		<10		<10		8.34
34.13	Opalinus Clay	400	1286	64.3	13.95	0.70	471.4	23.6	279.2	14.0	9.35	1.87	3.05	0.15	1184	59	1.40	0.03	1.05	0.21	3739	187	27.39	1.37	139.2	7.0	27.77	2.78	<10		<10		<10		<10		8.21
34.13	Opalinus Clay	500	1215	60.8	13.10	0.66	515.7	25.8	305.5	15.3	8.10	1.62	3.20	0.16	1203	60	1.45	0.03	1.00	0.20	3676	184	32.18	1.61	163.6	8.2	36.33	3.63	<10		10.6	2.1	<10		<10		8.16
37.30	Opalinus Clay	100	2923	146.1	59.00	2.95	446.5	22.3	230.1	11.5	6.95	1.39	14.05	0.70	2360	118	2.65	0.13	5.75	0.29	4634	232	32.28	1.61	164.1	8.2	137.83	13.78	<10		51.5	2.6	13.7	2.7	<10		8.12
37.30	Opalinus Clay	150	2338	116.9	37.70	1.89	433.0	21.7	219.2	11.0	8.20	1.64	4.50	0.23	1825	91	2.15	0.11	2.70	0.14	4209	210	28.11	1.41	142.9	7.1	49.06	4.91	<10		<10		10.9	2.2	<10		8.30
37.30	Opalinus Clay	200	2057	102.9	26.05	1.30	459.0	23.0	230.7	11.5	9.05	1.81	3.20	0.16	1688	84	2.00	0.10	1.05	0.21	4113	206	28.05	1.40	142.6	7.1	37.78	3.78	<10		<10		10.5	2.1	<10		8.22
37.30	Opalinus Clay	300	1702	85.1	18.45	0.92	481.3	24.1	262.8	13.1	8.85	1.77	2.90	0.15	1508	75	1.90	0.38	0.90	0.18	3829	191	27.51	1.38	139.8	7.0	33.66	3.37	<10		<10		<10		<10		8.39
37.30	Opalinus Clay	400	1493	74.7	14.80	0.74	557.4	27.9	307.0	15.3	9.60	1.92	3.05	0.15	1449	72	1.75	0.35	<0.8		3704	185	30.49	1.52	155.0	7.7	34.87	3.49	<10		<10		<10		<10		8.15
37.30	Opalinus Clay	500	1249	62.4	13.10	0.66	596.6	29.8	336.0	16.8	9.00	1.80	3.30	0.17	1352	68	1.75	0.35	<0.8		3517	176	32.70	1.63	166.2	8.3	36.81	3.68	<10		<10		<10		<10		8.20
41.68	Opalinus Clay	150	3090	154.5	59.55	2.98	535.9	26.8	232.2	11.6	10.20	0.51	7.75	0.39	2566	128	2.90	0.15	3.30	0.17	5261	263	33.75	1.69	171.5	8.6	88.91	8.89	<10		23.3	4.7	13.3	2.7	<10		8.41
41.68	Opalinus Clay	200	2802	140.1	45.00	2.25	568.3	28.4	279.0	14.0	11.40	0.57	4.30	0.22	2417	121	3.00	0.15	1.85	0.37	5026	251	34.37	1.72	174.7	8.7	51.13	5.11	<10		<10		14.7	2.9	<10		8.30
41.68	Opalinus Clay	300	2386	119.3	31.30	1.57	615.7	30.8	320.1	16.0	11.15	0.56	3.05	0.15	2213	111	2.65	0.13	1.55	0.31	4839	242	24.53	1.23	124.7	6.2	36.01	3.60	<10		<10		14.4	2.9	<10		8.39
41.68	Opalinus Clay	400	2122	106.1	23.95	1.20	608.1	30.4	325.1	16.3	8.70	1.74	3.00	0.15	2066	103	2.65	0.13	<0.8		4465	223	33.59	1.68	170.8	8.5	32.90	3.29	<10		<10		13.7	2.7	<10		8.37
41.68	Opalinus Clay	500	1929	96.4	19.65	0.98	623.1	31.2	330.6	16.5	10.00	0.50	2.65	0.13	1933	97	2.40	0.12	<0.8		4291	215	33.23	1.66	168.9	8.4	33.90	3.39	<10		<10		13.7	2.7	<10		8.43
49.75	Opalinus Clay	100	3224	161.2	70.85	3.54	453.5	22.7	242.4	12.1	6.25	1.25	13.75	0.69	3180	159	3.80	0.19	<0.8		4387	219							<10		<10		<10	1.5	30.3	1.5	8.11
49.75	Opalinus Clay	150	2710	135.5	46.80	2.34	470.4	23.5	248.9	12.4	9.65	0.48	5.00	0.25	2804	140	3.35	0.17	3.05	0.15	4125	206	34.09	1.70	173.3	8.7	62.71	6.27	<10		<10		<10		<10		7.98
49.75	Opalinus Clay	200	2278	113.9	30.85	1.54	516.4	25.8	279.5	14.0	8.95	0.45	4.15	0.21	2527	126	3.00	0.15	1.35	0.27	3871	194	32.07	1.60	163.0	8.2	38.34	3.83	<10		<10		<10		<10		8.09
49.75	Opalinus Clay	300	1930	96.5	21.25	1.06	520.7	26.0	280.3	14.0	8.85	0.44	3.55	0.18	2169	108	2.55	0.13	0.00		3537	177	38.83	1.94	197.4	9.9	25.64	2.56	<10		<10		<10		<10		8.20
49.75	Opalinus Clay	400	1485	74.2	16.30	0.82	599.9	30.0	321.6	16.1	8.25	0.41	3.70	0.19	1933	97	2.35	0.12	0.00		3301	165	32.40	1.62	164.7	8.2	30.04	3.00	<10		<10		<10		<10		8.26
49.75	Opalinus Clay	500	1294	64.7	13.75	0.69	634.1	31.7	349.3	17.5	7.95	0.40	3.55	0.18	1830	92	2.30	0.12	0.00		3222	161	30.55	1.53	155.3	7.8	27.52	2.75	<10		<10		<10		<10		8.17
71.08	Opalinus Clay	100	3047	152.4	54.25	2.71	452.5	22.6	264.1	13.2	7.85	0.39	10.85	0.54	3242	162	4.10	0.21	12.10	0.61	4221	211	33.02	1.65	167.9	8.4	118.74	11.87	<10		<10		<10	2.2	11.0	2.2	7.88
71.08	Opalinus Clay	150	2619	130.9	36.30	1.82	478.1	23.9	268.0	13.4	8.40	0.42	4.95	0.25	2853	143	3.60	0.18	4.40	0.22	4133	207	24.22	1.21	123.1	6.2	44.83	4.48	<10		<10		<10		<10		7.90
71.08	Opalinus Clay	200	2387	119.3	26.45	1.32	528.5	26.4	284.2	14.2	8.10	0.41	4.25	0.21	2667	133	3.40	0.17	3.00	0.15	4064	203	25.77	1.29	131.0	6.5	103.05	10.31	<10		<10		<10		<10		8.02
71.08	Opalinus Clay	300	1984	99.2	19.50	0.98	570.2	28.5	306.0	15.3	8.40	0.42	3.60	0.18	2332	117	3.05	0.15	4.75	0.24	3827	191	23.93	1.20	121.6	6.1	36.21	3.62	<10		<10		<10		<10		8.34
71.08	Opalinus Clay	400	1620	81.0	14.45	0.72	661.3	33.1	368.2	18.4	8.60	0.43	3.70	0.19	2137	107	2.85	0.14	<0.8		3725	186	24.38	1.22	123.9	6.2	30.07	3.01	<10		<10		<10		<10		8.07
71.08	Opalinus Clay	500	1343	67.1	12.60	0.63	711.1	35.6	393.2	19.7	8.70	0.44	3.45	0.17	1989	99	2.75	0.14	<0.8		3607	180	26.84	1.34	136.5	6.8	30.65	3.07	<10		<10		<10		<10		8.08
80.47	Staffelegg-Fm	300	3313	165.7	57.45	2.87	547.9	27.4	299.4	15.0	10.25	0.51	10.10	0.51	3428	171	4.55	0.23	6.15	0.31	5033	252	31.62	1.58	160.8	8.0	83.80	8.38	<10		<10		<10	1.8	36.7	1.8	8.03
80.47	Staffelegg-Fm	400	3037	151.9	48.55	2.43	569.7	28.5	317.1	15.9	9.70	1.94	6.20	0.31	3268	163	4.55	0.23	3.65	0.18	4859	243	29.62	1.48	150.6	7.5	60.27	6.03	<10		<10		<10		<10		7.92
80.47	Staffelegg-Fm	500	2774	138.7	38.10	1.91	601.0	30.1	341.0	17.1	8.85	0.44	4.75	0.24	3124	156	4.40	0.22	2.15	0.11	4650	233	24.80	1.24	126.1	6.3	43.77	4.38	<10		<10		<10		<10		7.95
113.79	Klettgau-Fm	300	3469	173.4	59.55	2.98	474.8	23.7	231.9	11.6	8.00	0.40	8.40	0.42	3441	172	5.00	0.25	6.05	0.30	4905	245	31.30	1.57	159.1	8.0	69.41	6.94	<10		<10		<10		21.0	4.2	8.04
113.79	Klettgau-Fm	400	3029	151.4	44.55	2.23	500.6	25.0	246.7	12.3	8.05	0.40	5.45	0.27	3009	150	4.40	0.22	3.70	0.19	4729	236	27.88	1.39	141.7	7.1	35.28	3.53	<10		<10		<10		<10		7.89
113.79	Klettgau-Fm	500	2853	142.7	36.75	1.84	520.2	26.0	264.9	13.2	7.15	0.36	4.60	0.23	2865	143	4.05	0.20	3.00	0.15	4756	238	26.78	1.34	136.1	6.8	35.58	3.56	<10		<10		<10		<10		7.96

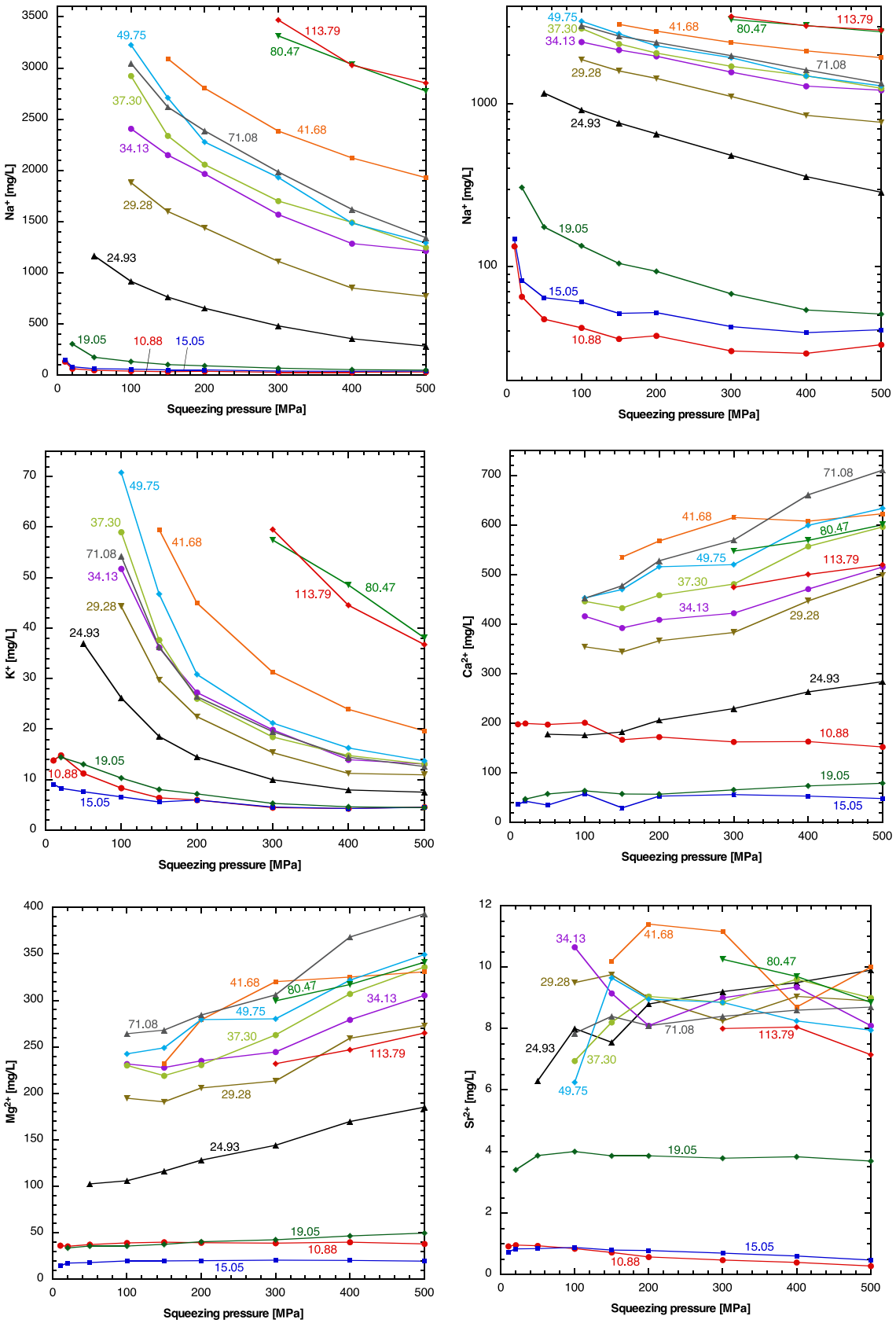

Fig. 4-34: Chemical composition of squeezed waters as a function of squeezing pressure.

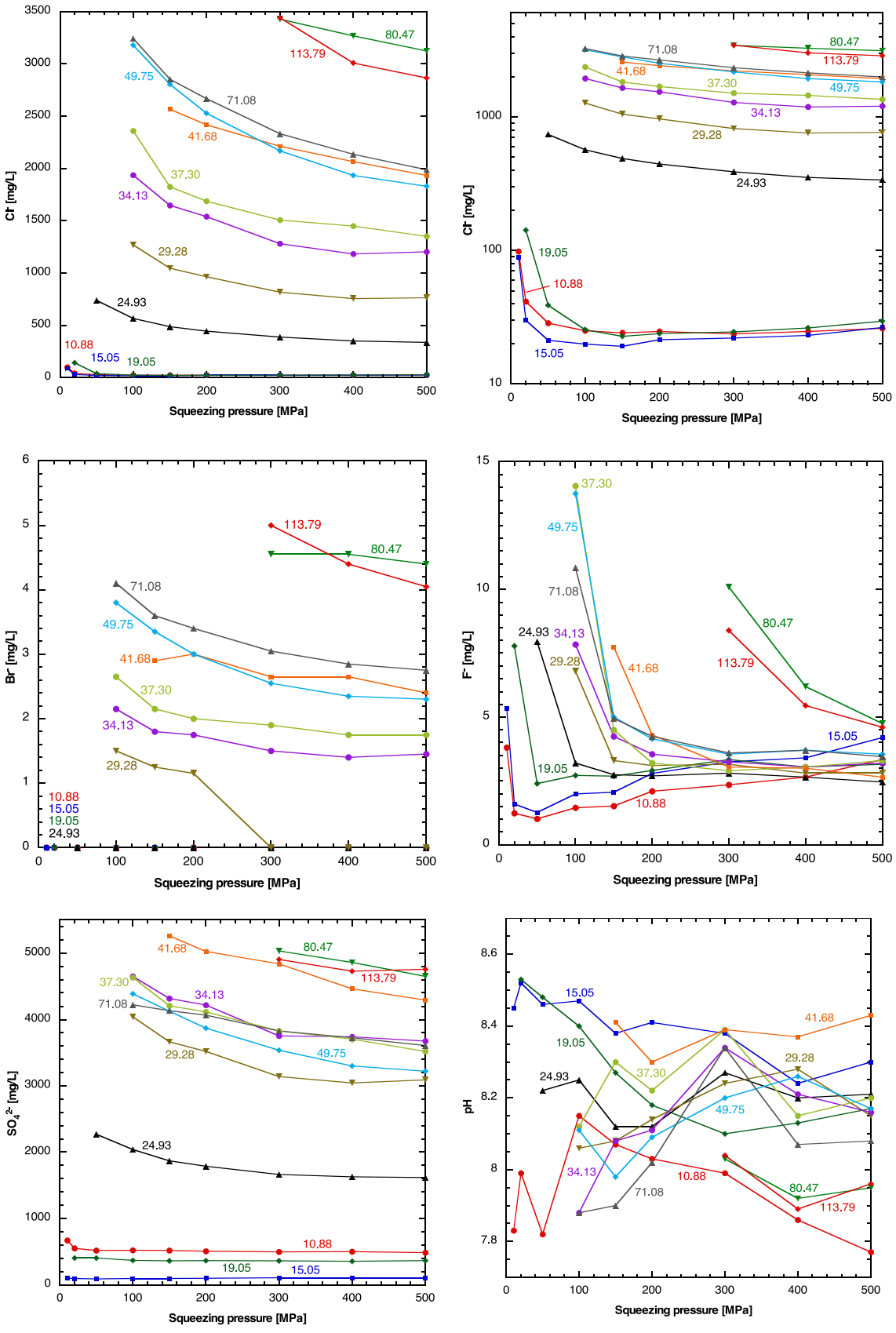
Cl⁻ [mg/L]
Squeezing pressure [MPa]
80.47
113.79
49.75
71.08
41.68
37.30
34.13
29.28
24.93
10.88
15.05
19.05
Br⁻ [mg/L]
F⁻ [mg/L]
SO4 2- [mg/L]
pH

Fig. 4-34: Cont.

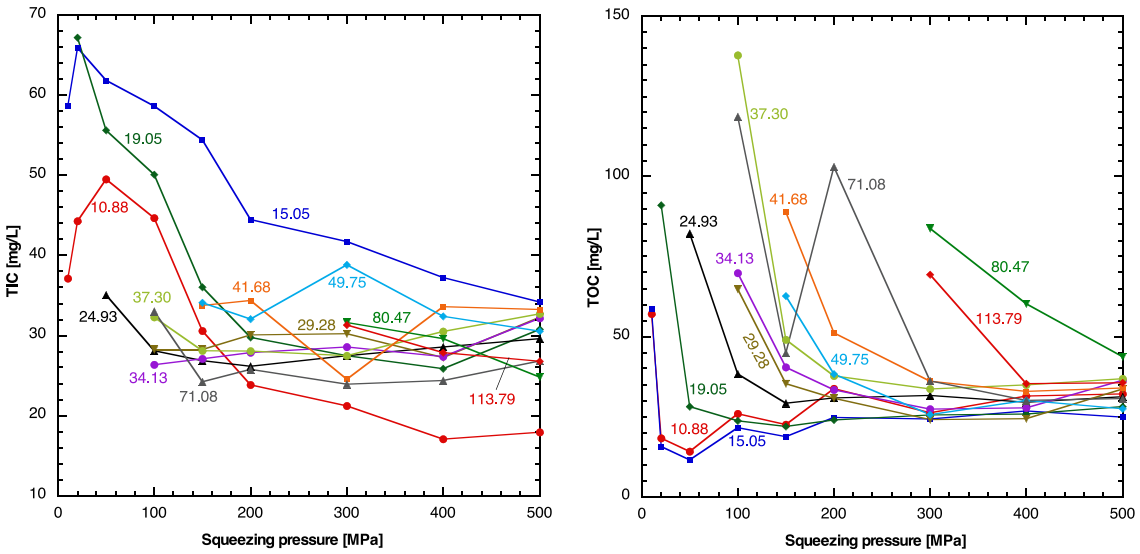

Fig. 4-34: Cont.

4.9.3 Cl^- and water budgets, anion-accessible porosity

The total mass of pore water in a sample can be obtained by adding the mass of water squeezed and the mass of water remaining in the sample after squeezing, the latter quantified by drying at 105 °C. Similarly, the total mass of Cl^- is obtained from the addition of Cl^- squeezed and Cl^- remaining in the squeezed sample. The remaining Cl^- can be calculated from the Cl^- concentration in aqueous extracts ($C_{Cl\ in\ aq.ex.}$) of previously squeezed rock. As only a fraction ($m_{rock\ in\ aq.\ ex.}$) of the total dry rock mass ($m_{rock\ in\ total\ sample}$) is used for extraction, the following formalism applies:

$$m_{Cl\ in\ total\ sample} = \frac{m_{Cl\ in\ aq.ex.} * m_{rock\ in\ total\ sample}}{m_{rock\ in\ aq.ex.}} \quad (1)$$

$$m_{Cl\ in\ aq.ex.} = C_{Cl\ in\ aq.ex.} * m_{water\ in\ aq.ex.} \quad (2)$$

$$S/L = \frac{m_{rock\ in\ aq.ex.}}{m_{water\ in\ aq.ex.}} \quad (3)$$

Insertion of (2) and (3) into (1) yields

$$m_{Cl\ in\ total\ sample} = \frac{C_{Cl\ in\ aq.ex.} * m_{rock\ in\ total\ sample}}{S/L} \quad (4)$$

Dividing the mass of total Cl^- by the total mass of water yields the Cl^- concentration in bulk pore water. Comparison of this concentration with that in the first water aliquot squeezed at the lowest pressure can be used to calculate the anion-accessible porosity fraction. The underlying assumption is that the Cl^- concentration in water squeezed at the lowest pressure represents the Cl^- concentration in the free pore water.

Data and calculations are listed in Tab. 4-18, and the anion-accessible porosity fraction is shown as a function of depth in Fig. 4-35. Values vary in the range 0.48 – 0.66. The average value for Opalinus Clay below the weathered zone is 0.58, which is slightly higher than the value of 0.54 ± 0.04 reported from the Mont Terri URL (Pearson et al. 2003). There is no evident correlation with clay-mineral content based on analyses of adjacent samples or obtained from geophysical borehole logging. Similarly, correlations with porosity, pore-water salinity or depth are not identified. This is remarkable, given the wide variability of these parameters. At shallow levels, salinity is lower (resulting in a reduced anion accessibility) but porosity and therefore pore apertures are higher (resulting in an enhanced anion accessibility), so possibly these effects cancel out each other.

Tab. 4-18: Budgets of water and Cl^- in squeezed water and in the total pore water, and calculated anion-accessible porosity fraction.

				Water budget			Cl budget			Calculation of anion-accessible porosity fraction (AAPF)		
Depth [m]	Geological unit	Dry rock mass [g]	S:L for aq. extraction [g dry rock/g added water]	Water mass squeezed [g]	Water mass remanining in squeezed core (drying @ 105 °C) [g]	Total water mass in sample [g]	Cl squeezed [mg]	Cl mass remaining in squeezed core (based on aq. extraction) [mg]	Total Cl in sample [mg]	Cl in bulk pore water [mg/L]	Cl squeezed at lowest pressure [mg/L]	AAPF based on lowest pressure
10.88	Opalinus Clay	280.92	0.994	32.90	12.63	45.53	1.223	0.940	2.163	47.50	98.36	0.483
15.05	Opalinus Clay	261.44	0.997	24.01	11.10	35.11	0.804	1.122	1.926	54.85	89.29	0.614
19.05	Opalinus Clay	384.38	0.995	17.32	14.59	31.91	0.758	1.941	2.700	84.60	141.7	0.597
24.93	Opalinus Clay	376.22	0.996	13.12	13.87	26.99	6.521	4.386	10.91	404.2	739.1	0.547
29.28	Opalinus Clay	415.91	0.993	11.97	14.19	26.16	11.98	7.809	19.78	756.4	1269	0.596
34.13	Opalinus Clay	394.66	0.993	10.57	13.27	23.84	15.97	10.02	25.98	1090	1936	0.563
37.30	Opalinus Clay	373.12	0.991	8.36	10.73	19.09	14.01	12.47	26.47	1387	2360	0.588
41.68	Opalinus Clay	406.05	0.994	7.55	11.20	18.75	16.93	14.88	31.81	1697	2566	0.661
49.75	Opalinus Clay	328.99	0.995	7.51	11.20	18.71	17.74	13.06	30.80	1646	3180	0.518
71.08	Opalinus Clay	363.83	0.996	10.63	13.20	23.83	27.29	16.54	43.82	1839	3242	0.567
80.47	Staffelegg-Fm	465.23	0.997	3.83	15.12	18.95	12.54	29.73	42.27	2230	3428	0.651
113.79	Klettgau-Fm	414.38	0.996	4.44	20.64	25.08	13.70	33.17	46.87	1869	3441	0.543

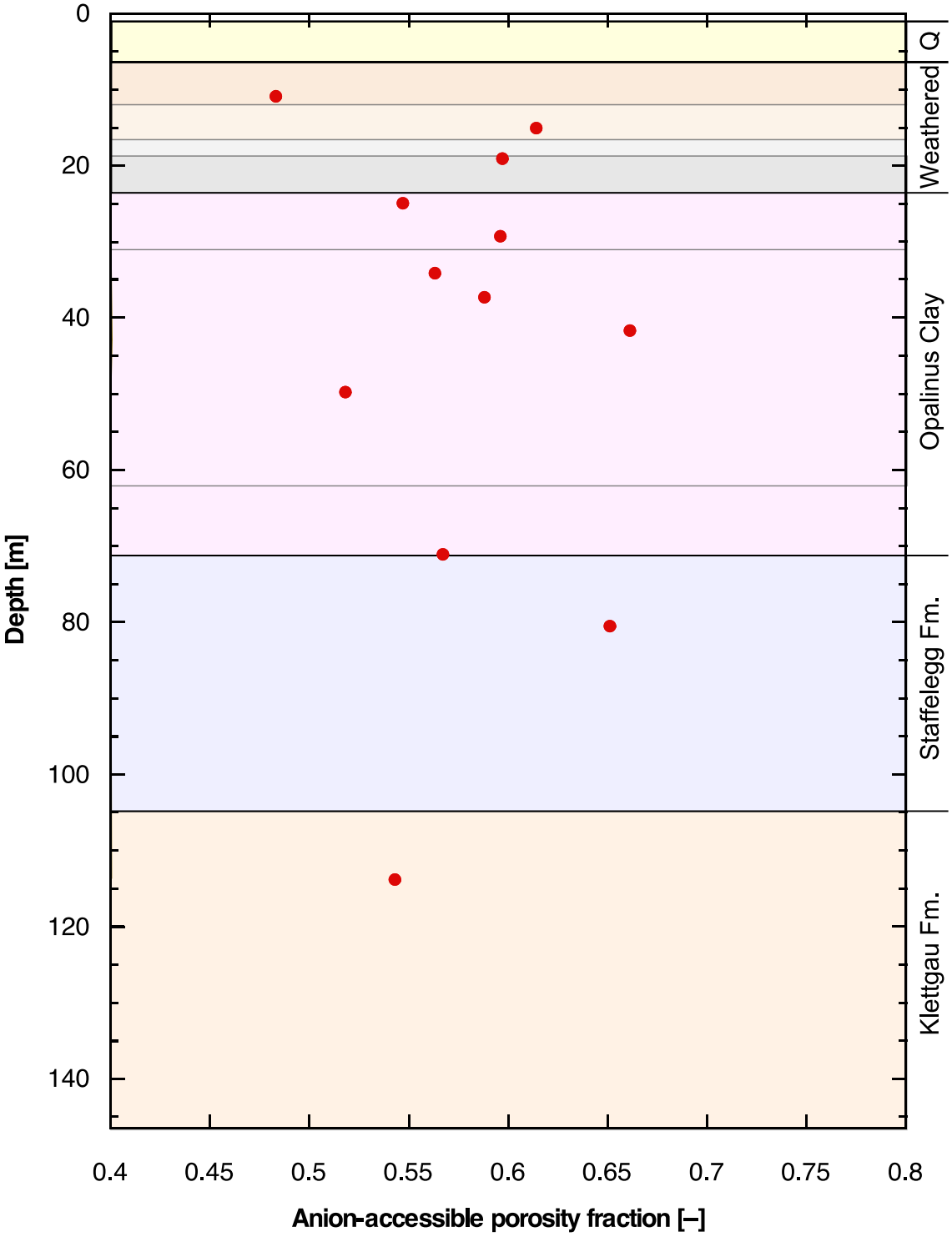

Fig. 4-35: Anion-accessible porosity fraction as a function of depth.

4.9.4 Evaluation of Cl^- data from the weathered zone

As stated in Section 4.9.2, Cl^- and Na^+ data for the three samples from the weathered zone are distinct in that concentrations drop much more strongly from the first to the second squeezing pressure than in the deeper samples and also in comparison with previous squeezing campaigns. Fig. 4-36 shows Cl^- concentrations in the weathered zone based on squeezing in comparison with data obtained from aqueous extraction as well as from ground-water sampling. Pore-water Cl^- concentration based on aqueous extraction recalculated using an anion-accessible porosity fraction of 0.58 is only slightly higher when compared to ground waters, which is considered to be plausible. On the other hand, the data obtained from the first squeezing step are a factor of about 3 higher and would require an unusually low accessible porosity if such values should be attained on the basis of aqueous-extraction data. In contrast, the Cl^- data from higher pressure steps are much closer to concentrations obtained by the other methods. This comparison suggests that the squeezing data are not representative, probably affected by an artefact, such as contamination. The same effect may also be present for all other samples but, given the much higher salinities, becomes less significant. It is concluded that for the samples from the weathered zone Cl^- in the first water obtained at the lowest pressure is not an adequate representation of the pore-water concentration. As Na^+ shows the same drop of concentration between the first and second pressure steps, this conclusion also applies to Na^+. All other constituents show pressure evolutions as described earlier and so may be less affected, even though some uncertainty remains. For this reason, Cl^- and Na^+ data from the first squeezing step for the three shallowest samples in Tab. 4-17 are considered inadequate, and those for the other constituents are considered uncertain.

In order to explore the potential sources of contamination, the fiberglass filters that are placed along both end pieces of the squeezed core were subjected to aqueous extraction. On the one hand, the filter material was scratched off from previously squeezed samples using a knife. The filters sticked firmly to the rock material. A proper separation was not possible, meaning that the scratched-off powder was contaminated by rock material to some degree. In order to obtain sufficient material for extraction, the filters from all 12 samples were pooled, and extraction was performed at a S/L ratio of 1. On the other hand, unused filters obtained from CRIEPI were also subjected to aqueous extraction at a S/L ratio of 1/20 (the dry mass of one filter is 0.234 g). The results are shown in Tab. 4-19. The filters contain surprisingly high contents of several ions, also including organic acids. A mass-balance calculation was performed, allocating the whole ion mass leached from the filters to the first water aliquot obtained at the lowest pressure. The calculation shows that in the low-salinity samples from the weathered zone, the relative contribution of filter leaching to the measured ion concentrations in the lowest-pressure water aliquots may be substantial for Na^+, K^+, F^-, Cl^-, NO_3^-, acetate and formate. For the higher-salinity samples below the weathered zone, this contamination becomes insignificant for several ions but remains high for some anions, in particular F^-, NO_3^-, acetate and formate. Because filters were crushed prior to extraction, which increased their surface area, and also due to the low S/L ratio chosen for the extraction of the unused filters, the measured contamination probably is a maximum for what may have happened in the squeezed samples. Efforts are under way to identify alternative filter materials and to quantify the potential contamination by performing aqueous extractions at different S/L ratios.

Tab. 4-19: Chemical composition of aqueous extracts of fiberglass filters used for squeezing experiments.

Units are mg per kg of solid filter material.

Material	Mass of dry filter material [g]	Mass of water added [g]	S:L [g/g]	Na [mg/kg]	K [mg/kg]	NH4 [mg/kg]	Ca [mg/kg]	Mg [mg/kg]	Sr [mg/kg]	F [mg/kg]	Cl [mg/kg]	Br [mg/kg]	NO3 [mg/kg]	SO4 [mg/kg]	Tot. alkalinity (titration) [meq/kg]	TOC [mg/kg]	TIC [mg/kg]	Lactate [mg/kg]	Acetate [mg/kg]	Propionate [mg/kg]	Formate [mg/kg]	pH
Filter scraped off all squeezed cores	2.001	2.003	0.999	500	25.3	<0.1	17.1	4.97	0.800	27.29	91.1	1.94	10.30	123	n.d.	n.d.	n.d.	<2	104.5	<2	83.20	n.d.
Unused filter for squeezing tests, A	1.436	27.875	0.052	464	16.1	<1.94	<1.94	<1.94	<1.94	27.86	255.5	<0.31	7.98	2.89	13.01	153.3	43.23	4.86	52.89	<3.88	19.01	9.16
Unused filter for squeezing tests, B	1.340	27.979	0.048	467	16.4	<2.09	<2.09	<2.09	<2.09	28.31	256.4	<0.33	8.44	2.74	15.03	152.3	53.04	4.36	53.01	<4.18	19.57	9.07

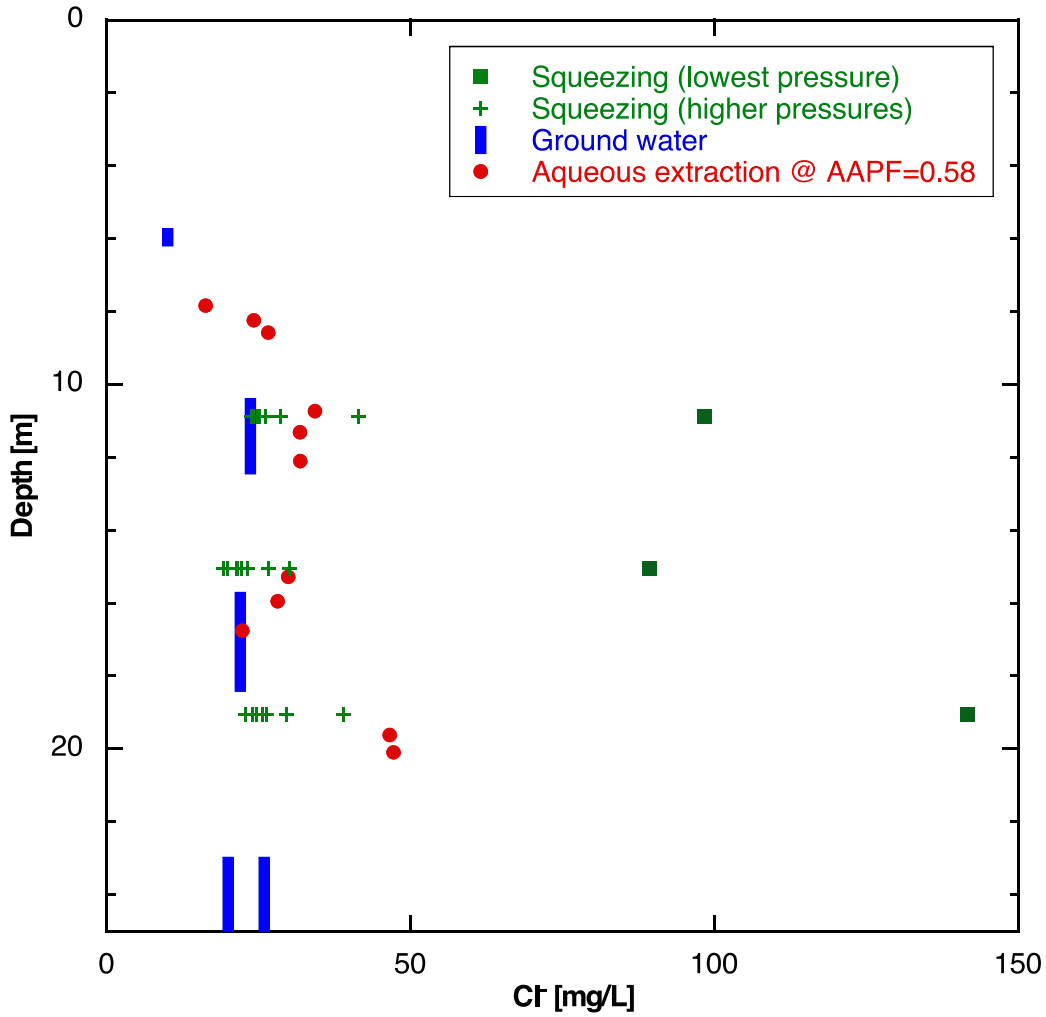

Fig. 4-36: Cl^- concentration in the weathered zone, based on different methods.

4.10 Stable water isotopes

The isotopic composition of the pore water was studied by the diffusive exchange method, and water samples obtained by squeezing were also analysed for stable isotopes.

4.10.1 Data based on diffusive isotope exchange

Data obtained by the diffusive exchange method are listed in Tab. 4-20. In total, 24 samples were analysed over the entire core profile. As shown in Fig. 4-37, δ values increase with depth in the upper part of the borehole and reach near-constant values in the deeper part of the Opalinus Clay and below. A marked negative excursion of both isotopes is identified at a depth of about 30 m.

Tab. 4-20: Water-isotope data based on diffusive exchange.

Depth [m]	Geological unit	δ18O [‰V-SMOW]	δ18O, error [‰V-SMOW]	δ2H [‰V-SMOW]	δ2H, error [‰V-SMOW]
7.83	Opalinus Clay	-8.58	0.13	-63.60	1.28
8.23	Opalinus Clay	-8.54	0.13	-63.57	1.30
8.58	Opalinus Clay	-8.52	0.13	-63.97	1.30
10.73	Opalinus Clay	-8.37	0.13	-63.80	1.28
11.30	Opalinus Clay	-8.35	0.14	-63.58	1.32
12.10	Opalinus Clay	-8.21	0.14	-63.20	1.34
15.28	Opalinus Clay	-8.07	0.15	-61.27	1.40
15.94	Opalinus Clay	-7.88	0.15	-60.45	1.43
16.75	Opalinus Clay	-7.78	0.14	-59.84	1.38
19.62	Opalinus Clay	-7.80	0.15	-59.65	1.47
20.09	Opalinus Clay	-7.64	0.16	-59.85	1.53
24.52	Opalinus Clay	-8.35	0.16	-63.23	1.54
29.02	Opalinus Clay	-8.74	0.16	-65.23	1.55
33.65	Opalinus Clay	-8.67	0.17	-63.17	1.64
42.88	Opalinus Clay	-7.89	0.19	-56.18	1.84
47.58	Opalinus Clay	-7.80	0.17	-54.07	1.74
50.13	Opalinus Clay	-7.56	0.18	-52.24	1.76
54.98	Opalinus Clay	-7.79	0.18	-52.94	1.81
60.78	Opalinus Clay	-7.47	0.18	-49.37	1.88
77.81	Staffelegg-Fm	-6.53	0.22	-45.74	2.20
82.87	Staffelegg-Fm	-7.33	0.17	-47.16	1.81
96.98	Staffelegg-Fm	-7.32	0.18	-46.31	1.90
113.55	Klettgau-Fm	-7.63	0.17	-46.24	1.74
132.12	Klettgau-Fm	-7.08	0.21	-43.89	2.17

4.10.2 Data based on squeezing

Squeezed waters were filled into plastic containers at CRIEPI, Japan. In order to minimise the air-filled head space, a range of container types were used, depending on the mass of the squeezed water:

- Broad vessel, 10 mL
- Cryovial, 4 mL
- Cryovial, 2 mL
- Cryovial, 1.2 mL

All containers were sent to RWI, Bern, for chemical and isotope analysis. While chemical analysis was performed within 3 months, isotope analysis was delayed due to an extended breakdown period of the Picarro instrument, followed by a period of testing and calibration. The sample history is as follows:

- End of August 2016: Squeezed waters received by RWI, Bern. Storage of all waters at 4 °C. Analysis of pH, TIC and TOC in early September.
- Mid-December 2016: Major-ion analysis of the waters. Since then, samples were stored under laboratory conditions.
- End March 2017: First campaign of isotope analysis. The large majority of the results were considered adequate from the analytical viewpoint. A minority of the data were considered uncertain (larger analytical error). Therefore, it was decided to re-analyse all waters after another instrument-calibration effort. Samples were stored under laboratory conditions.
- Beginning July 2017: Re-analysis of all waters. These data are considered adequate from the analytical perspective.
- In summary, waters were stored about 3 months at 4 °C, then 3.5 months in the laboratory until the first campaign, followed by another 3 months under laboratory conditions until the second campaign. The results of both campaigns are shown in Fig. 4-37 as a function of squeezing pressure, together with the data obtained from diffusive exchange. The following observations can be made:
- All δ values obtained from squeezed waters are higher than those from diffusive exchange. This is unexpected, as the experience from the Schlattingen core indicates good correspondence between the two methods or slightly lower δ values for squeezed waters (Wersin et al. 2013).
- There is no systematic evolution of δ values with squeezing pressure, which again contrasts the experience from Schlattingen where δ values become lower with pressure.
- The results of the first and the second campaign differ substantially. The data of the second campaign yield higher δ values and so deviate more strongly from the diffusive-exchange data than the data of the first campaign.
- Fig. 4-38 shows the same data as a function of the type of sample container for δ^2H, leading to the following observations:
- Data obtained from waters stored in the broad 10 mL containers are consistent with the diffusive-exchange data. This container type was used only in the weathered zone where large water volumes could be collected.

- The deviation of the δ values from the diffusive-exchange data becomes larger with decreasing volume of the cryovials. The 4 mL cryovials show a moderate shift to higher δ values, whereas the shift is much more substantial for the 1.2 mL vials. The shifts become much larger in the second campaign in comparison to the first campaign.

We come to the surprising conclusion that sample storage in cryovials over several months results in shifts of the water-isotope composition. This cannot be due to the variable filling level of the containers, given the fact that the relative mass of water in the vapour phase is negligible, and also there is no systematic dependence of the δ values on the filling level. On the other hand, the artefact becomes more strongly expressed with decreasing vial volume, i.e. with increasing surface to volume ratio. At this stage, the process that causes the artefact is not well constrained – H_2O out-diffusion across the vial walls and/or isotope exchange with the plastic material are the most obvious possibilities. Based on these findings, tests are under way to explore the evolution of δ values as a function of vial type, storage time and temperature. The main project-related conclusions are:

- Both analytical campaigns are affected by currently not well characterised artefacts. These artefacts cannot be properly quantified and corrected. The isotope data based on squeezing are not suited for interpretation, and consequently they are not reported here in Table form.
- Glass vials will be used for future studies, and the interaction of all vial types with water is under investigation.
- If water-isotope analysis cannot be performed within weeks due to *force majeure*, future samples will be sent to an external laboratory for timely analysis.

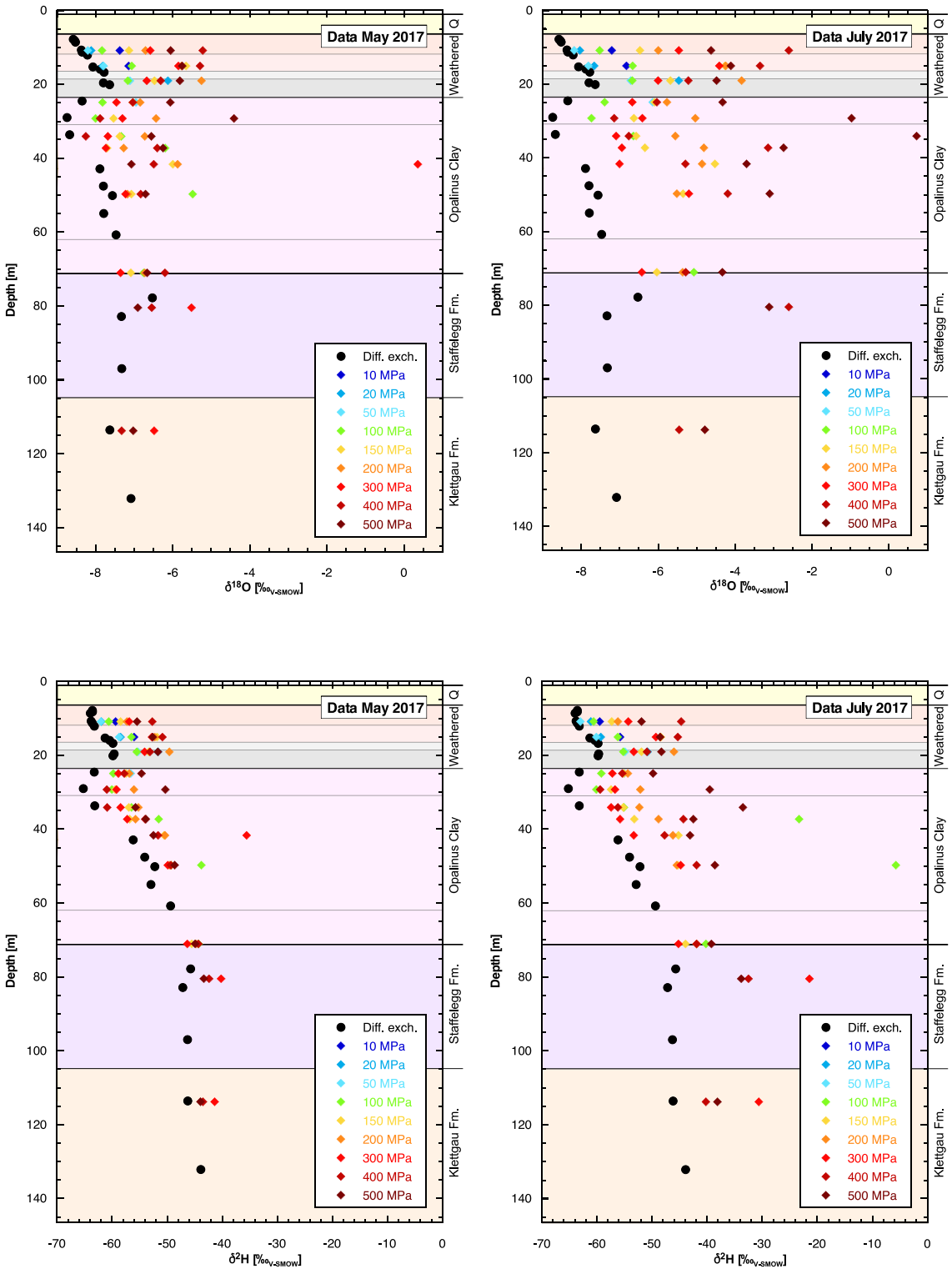

Fig. 4-37: Water-isotope data based on diffusive exchange and on squeezing, with indication of squeezing pressure.

Left: Campaign March 2017; right: Re-analysis July 2017.

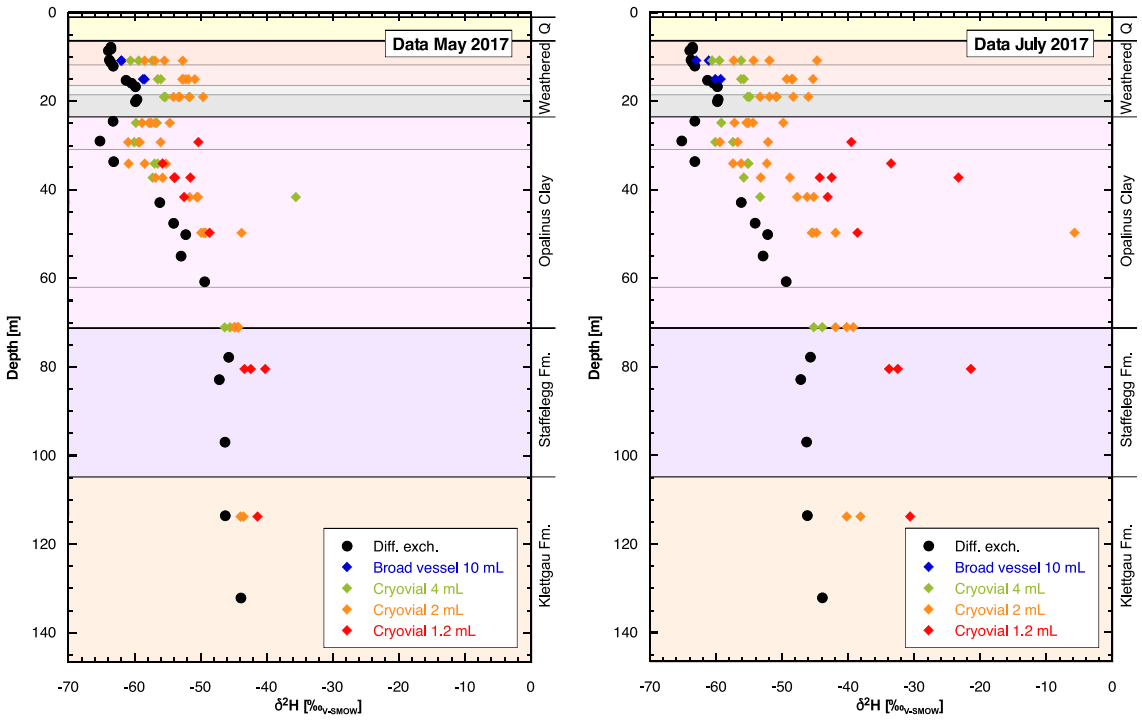

Fig. 4-38: δ^2H based on diffusive exchange and on squeezing, with indication of type of sample container.

Left: Campaign March 2017; right: Re-analysis July 2017.

5 Discussion

5.1 Structural inventory

Brittle structures were logged by Vogt et al. (2016) on the basis of core and borehole-image data. Due to the high degree of fracturing down to 18.4 m, no detailed structural analysis is available from this zone. The spatial distribution of different structure types is shown in Fig. 5-1.

- The frequency of joints is high within the weathered zone and down to about 40 m. Joints are subordinate at deeper levels, suggesting that they may be related to the decompaction of Opalinus Clay. Note that many joints are not broken up in the core, so a possible shear component of deformation cannot be judged in many cases.
- It is remarkable that the depth extension of closely-spaced joints coincides with that of increased porosity (about 40 m, see Fig. 4-27). Decompaction leads to a major volume increase, and the observed joints may be linked to differential movements during this process. The orientation of the joints within and below the weathered zone is not clearly systematic, but moderate dip angles dominate (Fig. 5-2).
- Two small faults and one shear fracture occur in the deeper part of Opalinus Clay. They are bedding-parallel, i.e. horizontal (Fig. 5-2). Faults in the underlying units have the same orientation, indicating that these structures are of tectonic origin, unrelated to decompaction.
- Slickensides are frequent in the lowermost part of Opalinus Clay and in the Klettgau Formation and are likely tectonic features. Their orientation shows a wide scatter, but a systematic difference between orientations in Opalinus Clay and footwall units cannot be identified (Fig. 5-2).

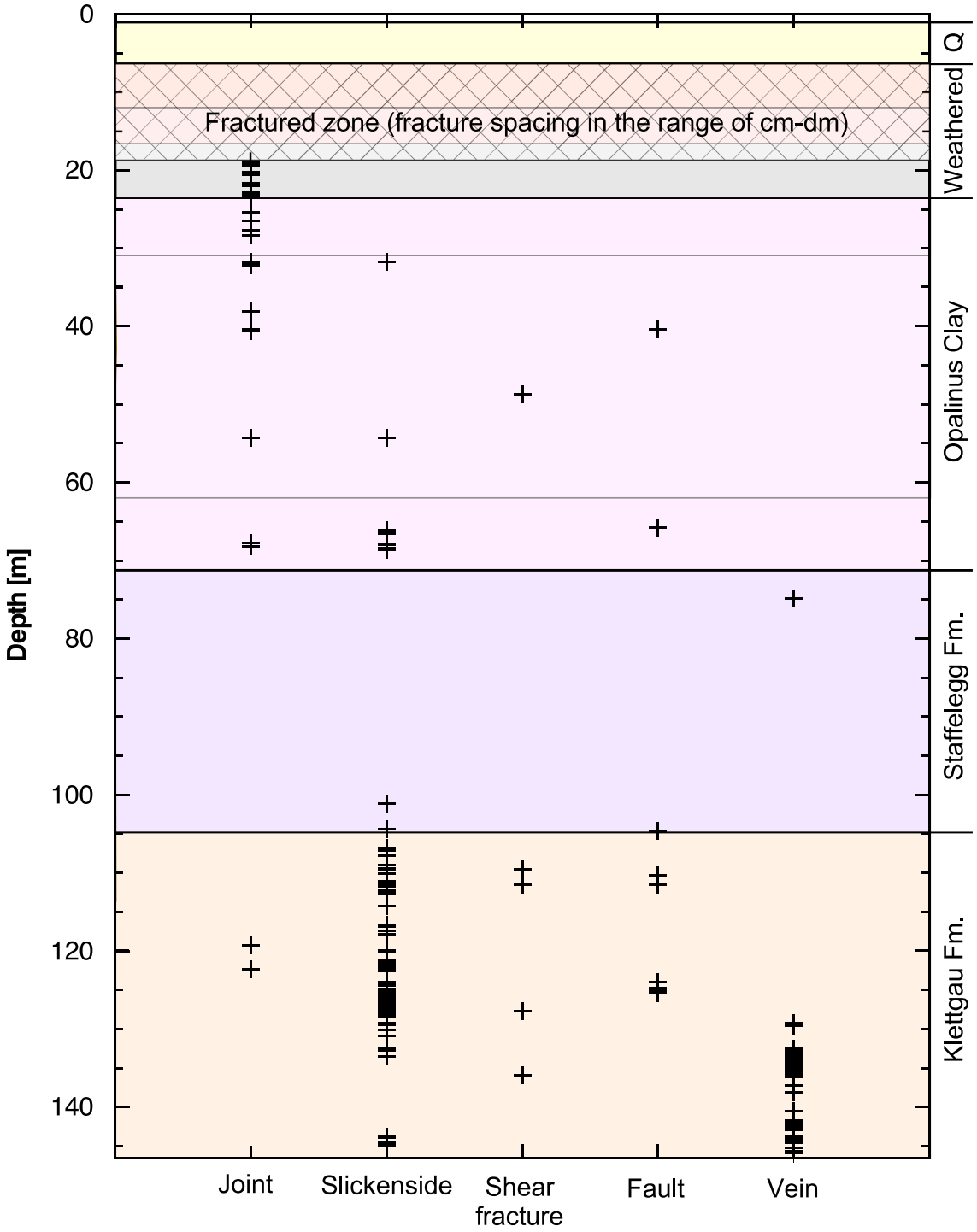

Fig. 5-1: Structural inventory based on data from Vogt et al. (2016).

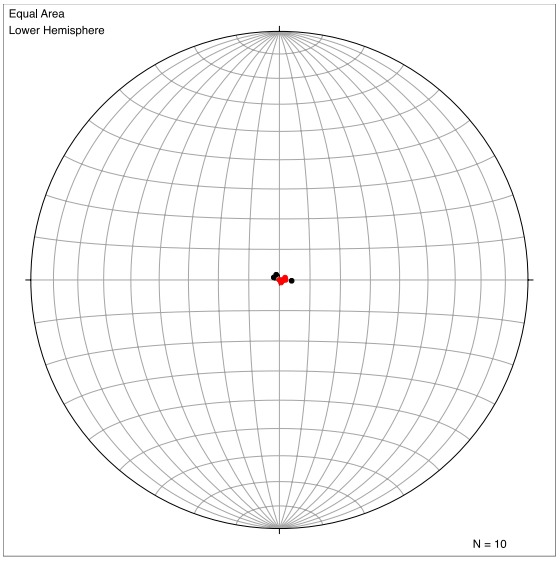

Small faults in Opalinus Clay (black) and footwall units (red)

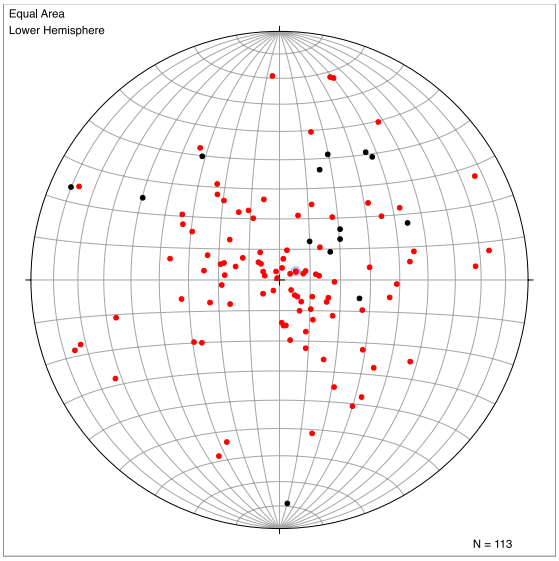

Slickensides in Opalinus Clay (black) and footwall units (red)

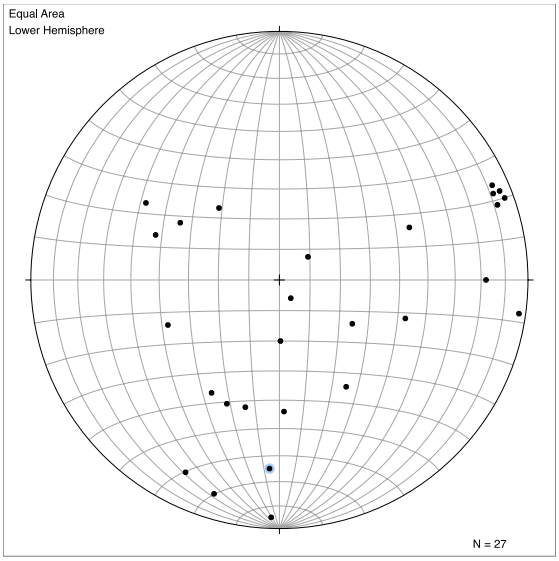

Joints in the weathered zone (18.4 – 23.65 m)

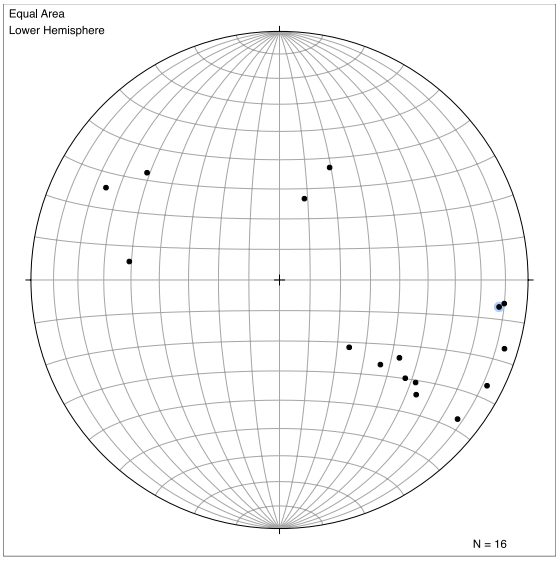

Joints below the weathered zone (23.65 – 40.5 m)

Fig. 5-2: Orientations of brittle structures based on data from Vogt et al. (2016).

5.2 Pore-water chemistry as a function of depth

The depth profile of major-ion compositions on the basis of squeezing data at the lowest pressure can be divided into 3 zones (Fig. 5-3):

- The weathered zone is characterised by low pore-water salinity (0.7 – 1.3 g/L) and ion ratios that differ substantially from those at deeper levels. Note that squeezing data from the weathered zone are uncertain, in particular the probably overestimated Na^+ and Cl^- concentrations obtained at low pressures (Section 4.9). The salinity of sampled ground waters varies in the range 0.2 – 0.6 g/L. Due to the uncertainties, the data from the weathered zone are not discussed here any further.
- In a transition zone (ca. 24 – 40 m), concentrations of all ions increase strongly and reach a salinity of about 11 g/L at the base.
- Below 40 m, salinity remains around 12 – 13 g/L, and concentrations of individual ions show no systematic depth trend (with the possible exception of Br^-).
- Pore waters below 40 m depth appear to be much less affected by surface processes and have the following characteristics:
- Cl^- concentration in free pore water is largely constant at about 3 – 3.5 g/L. This is similar to the range identified in borehole Riniken but lower than in all other boreholes in northern Switzerland (Meier & Mazurek 2011, Wersin et al. 2013), and also lower than at Mont Terri (Pearson et al. 2003, Waber & Rufer 2017).
- The Cl/Br mass ratio in squeezed waters is in the range 700 – 900, which is much higher than the value of modern sea water of 290 that is consistently observed at Mont Terri. In boreholes from northern Switzerland, Cl/Br is mostly higher than the sea-water ratio, except for Schafisheim, which shows ratios in the range 230 – 340 (Meier & Mazurek 2011).
- SO_4^{2-} contents below 40 m are about 4'400 – 5'300 mg/L, which is substantially higher when compared to the lower part of Opalinus Clay at Mont Terri (770 – 1'660 mg/L based on squeezing data from borehole BDB-1, Mazurek et al. 2017) and at Schlattingen (1'000 – 1'500 mg/L, Wersin et al. 2013). While the Cl/SO_4 mass ratio is broadly similar to the value of modern sea water of 7.15 at Mont Terri and at Schlattingen (range 3.6 – 7.5), it is 0.5 – 0.7 at Lausen. In agreement with previous experience (e.g. Mazurek et al. 2012), SO_4^{2-} concentrations based on aqueous extraction, recalculated to pore-water concentrations using the same anion-accessible porosity fraction as for Cl^-, yield values that are more than two times higher compared to the squeezing data.

It is conspicuous that the uppermost 40 m in which pore-water composition is affected by surface processes coincide with the zone of decompaction, given the increased porosity and the presence of densely-spaced joints in this zone. It is likely that the uppermost 40 m contain an interconnected network of moderately dipping fractures with different orientations. However, hydraulic tests (Section 2.3, Fig. 2.3-1) indicate that hydraulic conductivity is extremely low below 27.6 m (possibly at an even shallower level). While joints do occur below this depth, they are sealed and hydraulically insignificant. One exception is the fracture at 31.77 m, which is the likely source of a disturbance of the water-isotope data (see Section 5.3). At shallower levels, fractures probably contribute to the higher hydraulic conductivity as observed in the test interval 18.4 – 27.6 m. Note that the water sample taken from this interval contains abundant ^{14}C, indicative of a young component in the ground water. Fracture flow is directly documented by the presence of oxidation rims and coatings down to a depth of 16.37 m (Fig. 2-2). Note that pore-water salinity starts increasing sharply in sample 24.93, so the basis of the advection-dominated regime is probably close to this depth.

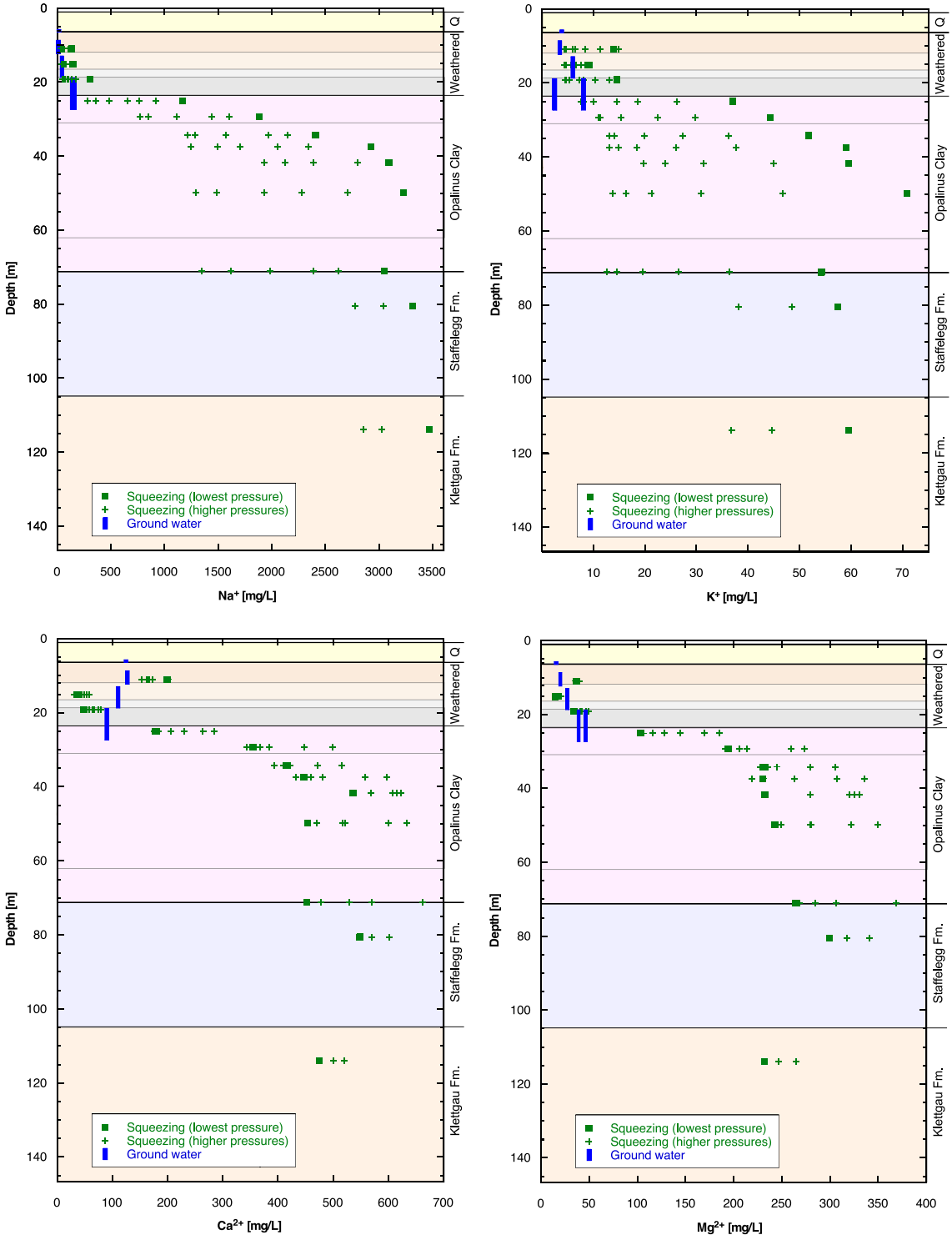

Fig. 5-3: Chemical composition of squeezed waters as a function of depth.

Data for ground waters and Cl^- concentrations obtained from aqueous extraction are also shown.

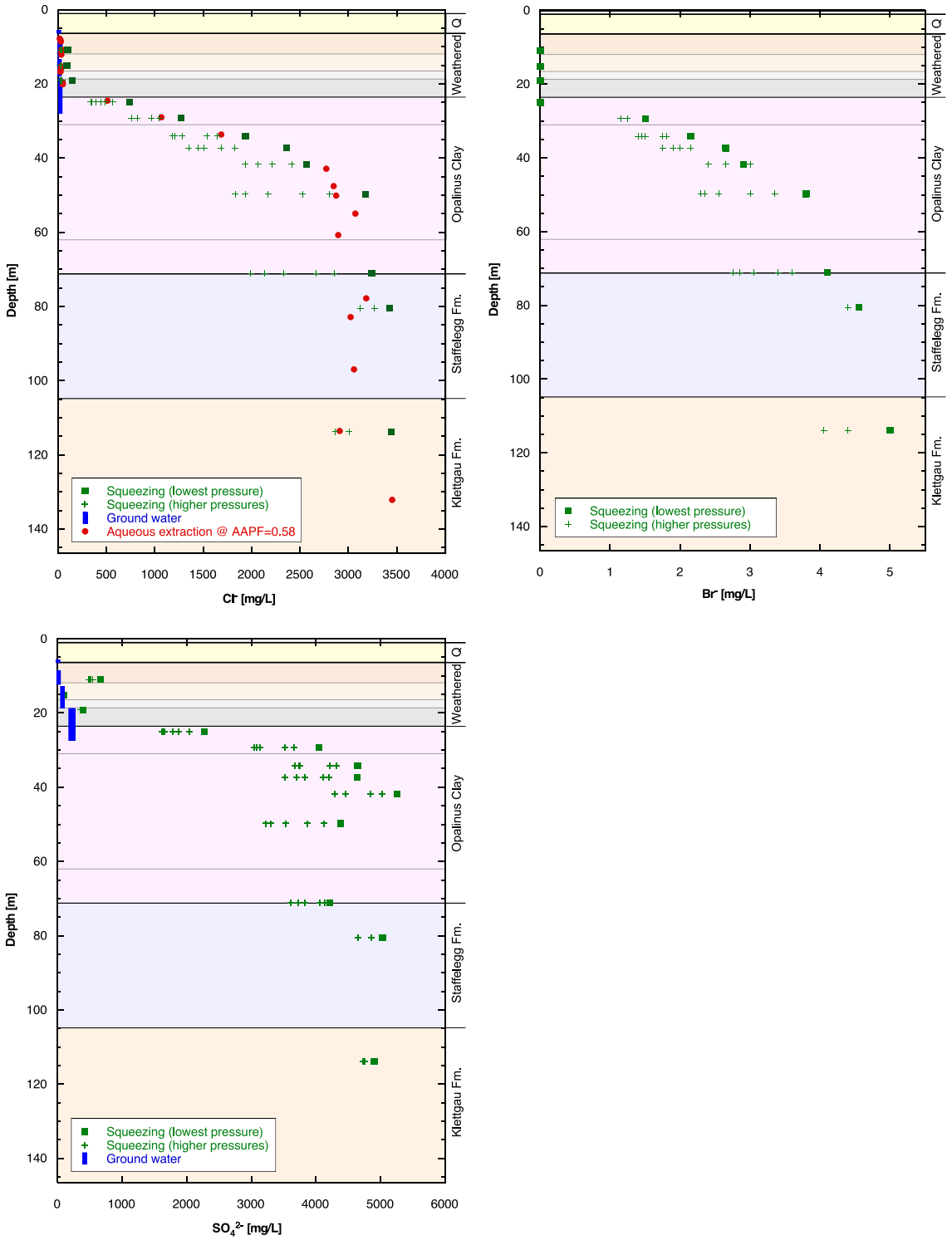
Depth [m]
Cl⁻ [mg/L]
Br⁻ [mg/L]
SO_4^{2-} [mg/L]
Weathered Q
Opalinus Clay
Staffelegg Fm.
Klettgau Fm.
Squeezing (lowest pressure)
Squeezing (higher pressures)
Ground water
Aqueous extraction @ AAPF=0.58

Fig. 5-3: Cont.

5.3 Stable water isotopes in pore water as a function of depth

Within the weathered zone, both $\delta^{18}O$ and $\delta^{2}H$ increase sharply with depth (Fig. 5-4). Between 20 and 40 m, a marked negative excursion of both isotopes is identified. Below 40 m, $\delta^{18}O$ and $\delta^{2}H$ increase again until about 70 m, below which depth no systematic depth trend is observed.

For $\delta^{2}H$, the available data for ground waters are consistent within error with the pore-water data (but the sample in the Quaternary yields a slightly higher $\delta^{2}H$). In contrast, $\delta^{18}O$ of ground-water samples 8.32 – 12.45 m and 13.00 – 18.43 m is distinctly below the pore-water values. The water sample from the Quaternary has higher values for both $\delta^{18}O$ and $\delta^{2}H$ than the drilling fluid, which can be considered to be a good approximation of current local tap water.

All three ground-water samples from the Opalinus Clay contain substantial ^{14}C (44 – 65 pmc). The tritium content of the sample from interval 8.32 – 12.45 m is 11.3 TU, that of sample 13.00 – 18.43 m is 5.1 TU. Sample 18.40 – 27.60 m contains 2.3 TU, even though this is probably due to contamination.

As shown in Fig. 5-5, all ground waters lie close together along the meteoric water line (MWL, whether global [GMWL] or local [CH-MWL]). They are consistent with recent infiltration, and no cold-climate signatures can be resolved. In contrast, pore waters from the weathered zone lie to the right of the MWL, as do the 3 samples from interval 20 – 40 m (negative excursion). The deeper samples lie on the MWL or slightly to the left. The deviation of the water-isotope data in the weathered zone from the MWL is difficult to understand at this stage. Hypothetically, it could be related to oxidative mineral dissolution/precipitation.

The negative excursion identified in the water-isotope data indicates the presence of a geochemical disturbance at a depth of about 30 ± 2 m. Within this interval, there is one single conspicuous fracture at 31.77 m (Vogt et al. 2016, Fig. 5-1) that is also identifiable on the ABI borehole log. Vogt et al. (2016) classified this fracture as a joint or a weakly slickensided shear fracture with an orientation of 118/68 to 121/54, i.e. dipping towards ESE. This fracture, illustrated in Fig. 5-6, lies within hydraulic test i4 (Fig. 2.3-1), with best-estimate T = 1.2E-11 m^2/s and average interval K = 5.2E-13 m/s (Hekel & Brod 2016). Interestingly, while the isotopic disturbance is marked, there are no effects on the major-ion composition of the pore water (Fig. 5-3). It is likely that limited advection along the fracture occurred over extended periods of time and also affected the adjacent rock matrix via diffusion, given the fact that the excursion is about 20 m wide. This could be further explored by transport modelling, but this is beyond the scope of this report. The provenance of the fracture water is enigmatic - infiltrating surface water would be consistent with the isotope data but not with the major-ion data that do not show any depression of concentrations in this depth range.

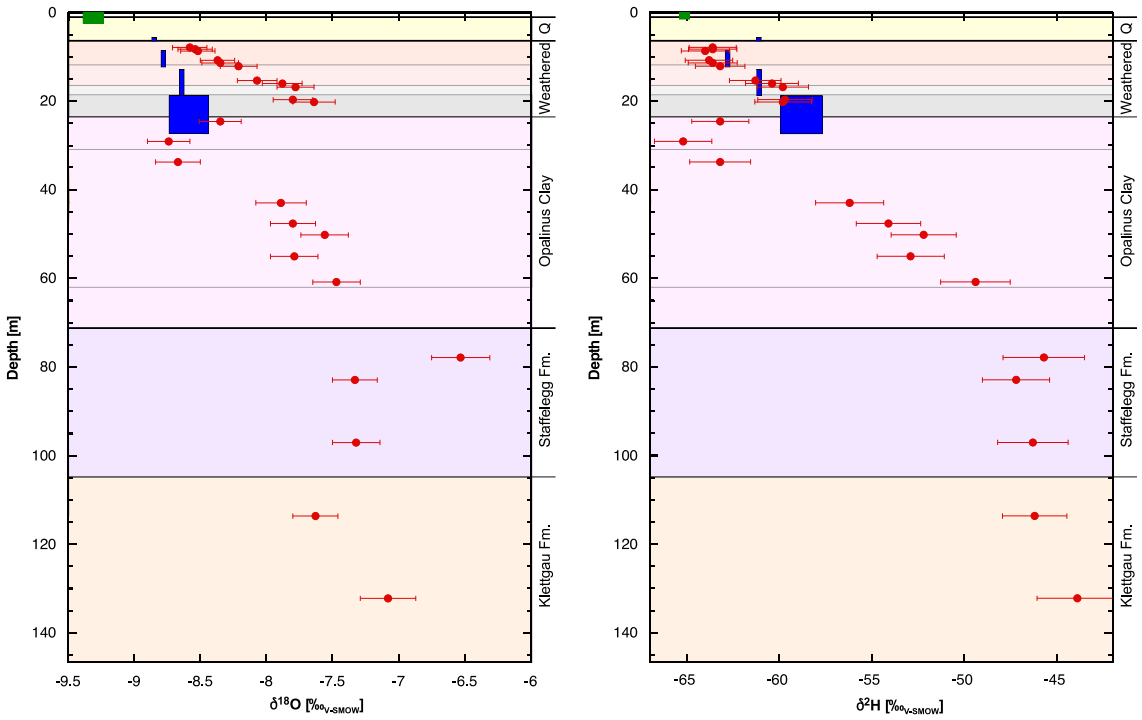

Fig. 5-4: Depth trends of $\delta^{18}O$ and $\delta^{2}H$ of pore water (red symbols, based on diffusive exchange).

Data for ground waters (blue bars) and for drilling fluid used for tests i2 and i3 (green bar) based on Huxol et al. (2017)

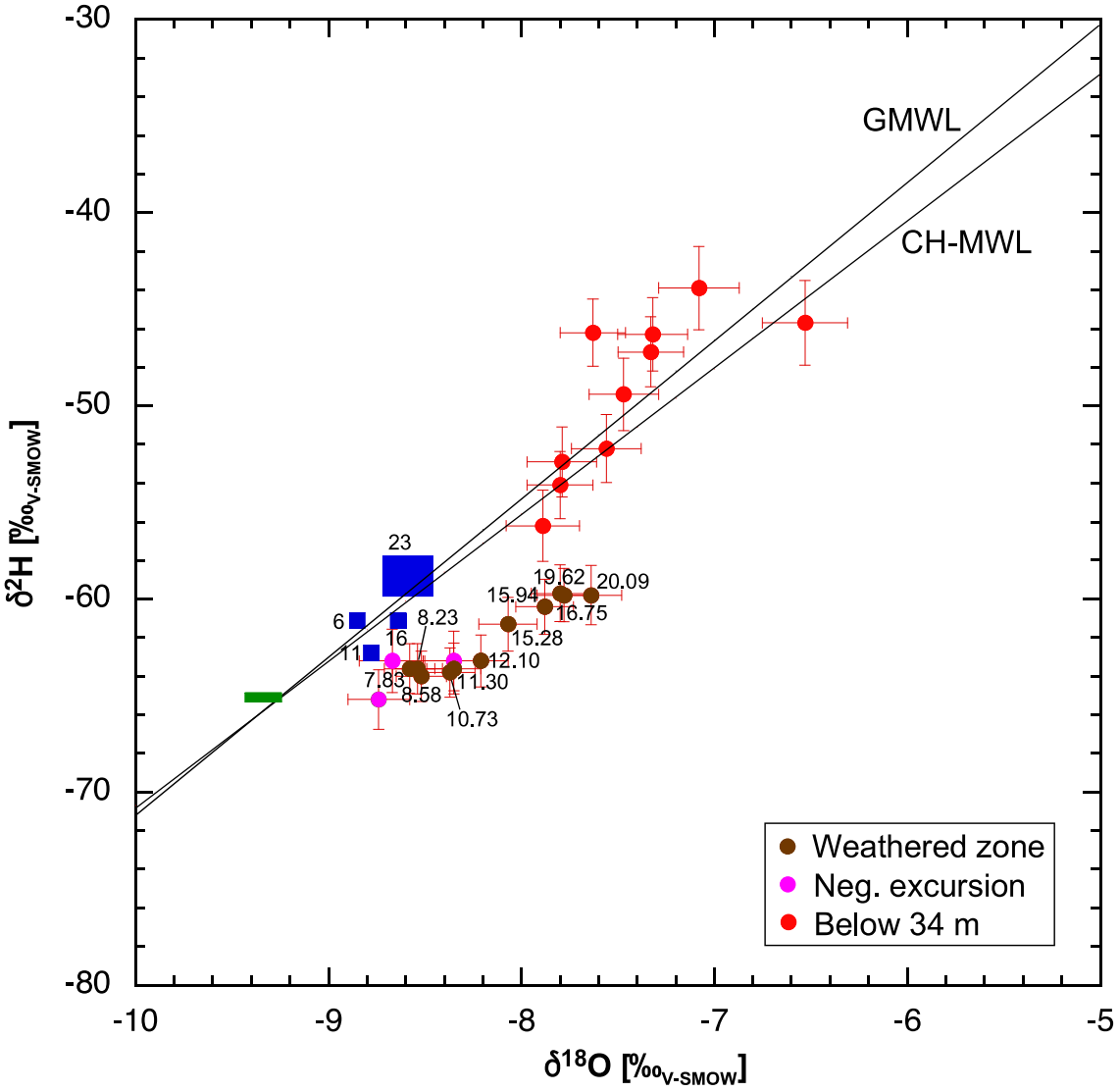

Fig. 5-5: $\delta^{18}O$ vs. $\delta^{2}H$ of pore water (round symbols; based on diffusive exchange).

Data for ground waters (blue bars) and for drilling fluid used for tests i2 and i3 (green bar) from Huxol et al. (2017). Numbers indicate sample depth in m.

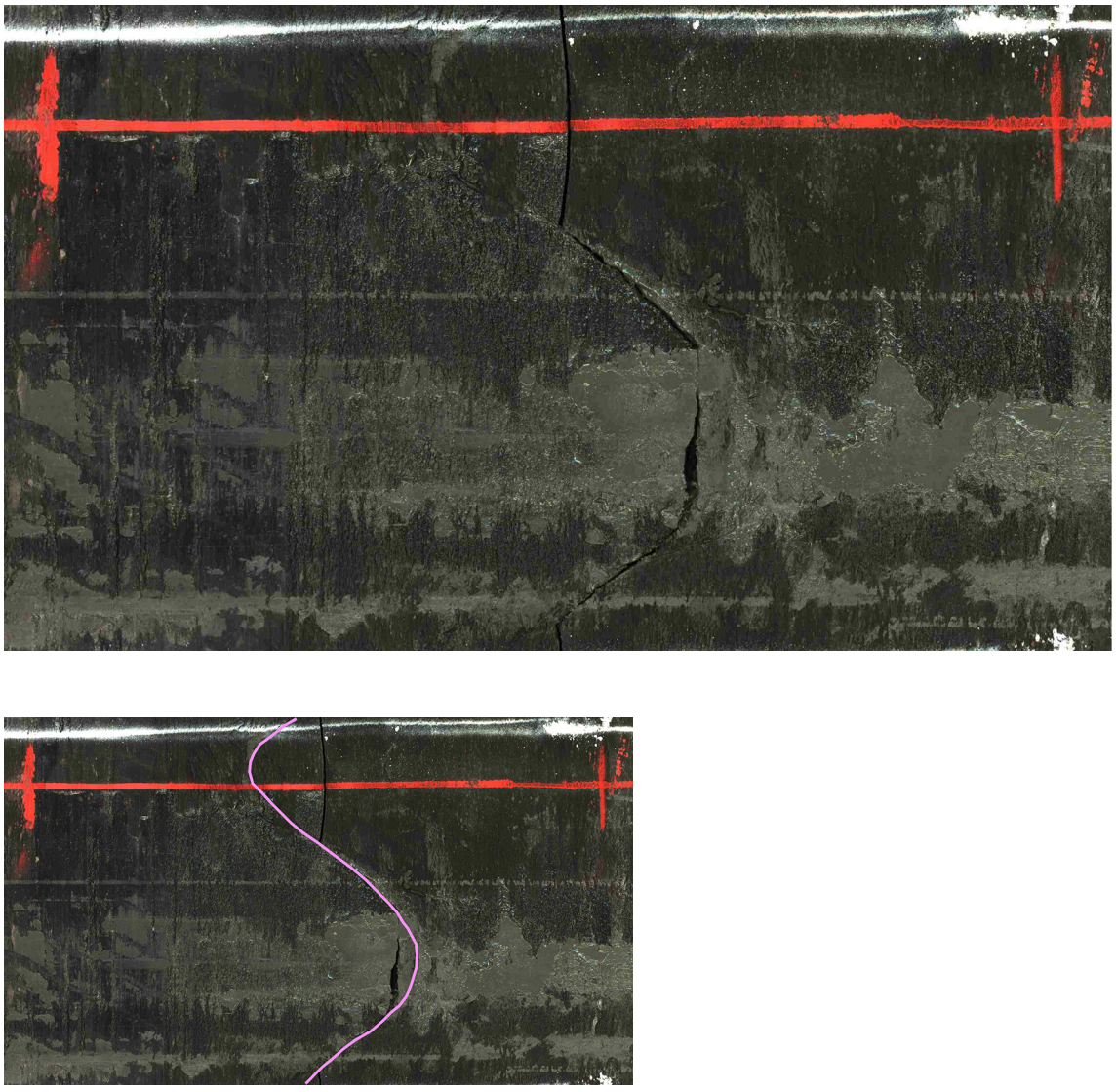

Fig. 5-6: 360° core photograph of the interval 31.5 m (left vertical red line) – 32.0 m (right vertical red line).

Small photograph shows the same interval and highlights the position of the fracture.

5.4 Oxidation processes

Uplift, decompaction and weathering of the Opalinus Clay induced fracturing and penetration of oxygen into the uppermost part of the formation. As a result, oxidation processes occurred both in the clay matrix and in fractures, albeit slightly deeper in the latter case. Redox conditions thus are oxidising down to a depth of 15 m or so, turning reducing below in the clay matrix. In the fractures, circulating oxidising waters have locally created oxidation fronts at greater depths (max. 16.4 m depth).

The impact of oxygen penetration is reflected in the changing iron mineralogy. In the unaffected reduced clay, Fe(II) minerals (i.e. siderite, ankerite, pyrite and structural Fe(II) in clay minerals dominate. These minerals reacted with O_2 forming Fe oxides (mainly goethite), and also led to increase of structural Fe^{3+} in clay minerals. From a thermodynamic viewpoint this can be

explained by the different stability fields of Fe(II) and Fe(III) minerals, as illustrated in a simple pe-pH diagram (Fig. 5-7). Thus, a stable pyrite-siderite phase assemblage in the reduced clay is converted to goethite upon ingress of O_2:

$$FeS_2 + {}^{15}/_4O_2 + {}^5/_2H_2O \rightarrow FeOOH + 2SO_4^{2-} + 4H^+$$

$$FeCO_3 + {}^1/_4O_2 + {}^1/_2H_2O \rightarrow FeOOH + CO_2$$

Furthermore, organic matter may be involved in oxidation reactions, as indicated from its decrease at shallowest levels:

$$CH_2O + O_2 \rightarrow CO_2 + H_2O$$

where CH_2O is used as proxy for organic matter.

The acidity induced by pyrite oxidation may explain dissolution and loss of calcite observed in the upper part of the weathering profile.

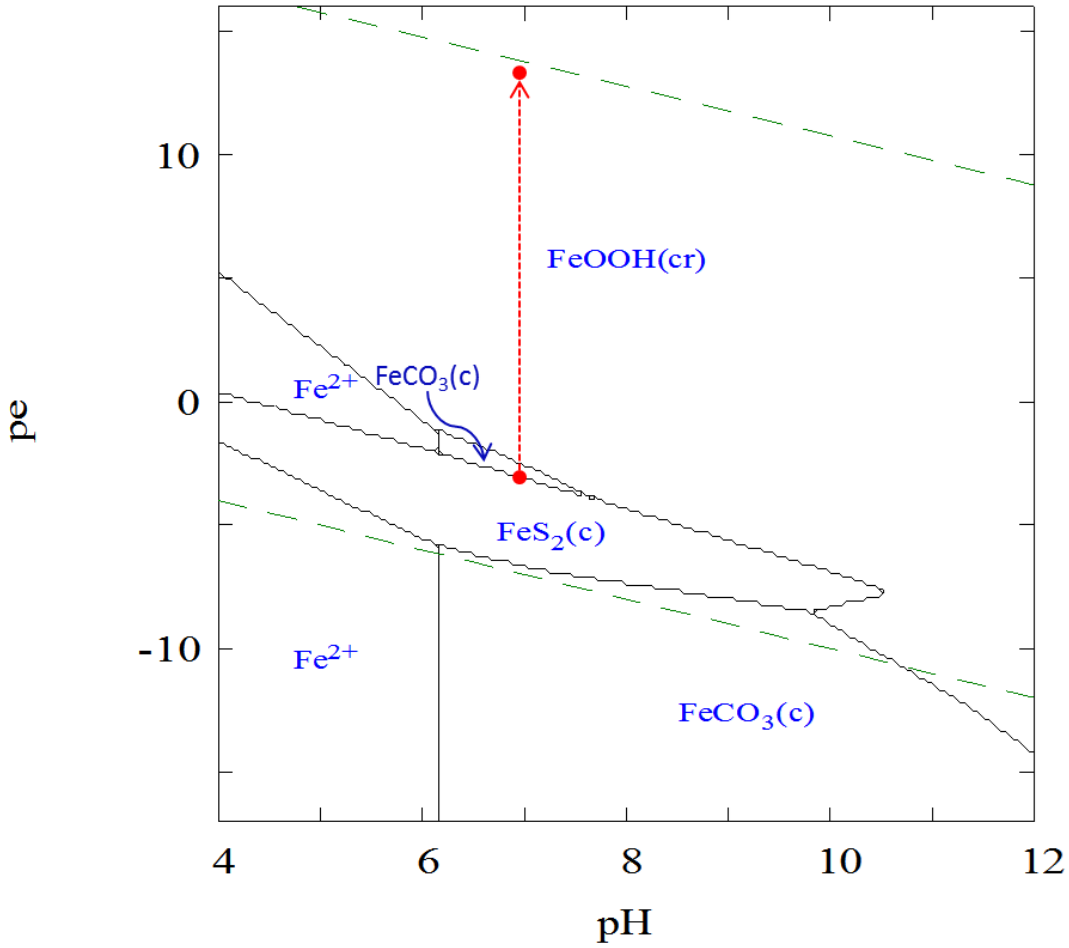

Fig. 5-7: pe-pH diagram of the Fe-S-CO_2-H_2O system at 25 °C. Red arrow shows shift in stability field from reducing to oxidising conditions.

Calculated with MEDUSA (www.kth.se/en/che/medusa) with ionic strength of 0.005 M, [Fe] = 0.01 M, [CO_2] = 0.001 M, [S] = 10^{-6} M. Magnetite and FeS omitted. Dashed lines correspond to equilibrium lines of O_2/H_2O at p_{O2} = 1 bar and H^+/H_2 at p_{H2} = 1 bar

The extent of oxidation encountered at the Lausen site is determined by various geological, structural, geochemical and hydrogeological factors, such as the time scales of erosion and weathering, the stress regime and local ground-water flow. The fracture pattern with larger fractures and higher fracture density down to about 40 m depth has conditioned the oxidation features observed. These are schematicaly illustrated in Fig. 5-8. Thus, at depths below about 16 m the influx of O_2 ceases because of limited fracture flow and rapid consumption by reaction with Fe^{2+} in the rock at shallower levels. Below 16 m, the rock is in the reduced state, containing a large reducing capacity. Further up, the O_2 influx becomes progressively increased. Reduced Fe minerals including pyrite and siderite are depleted down to 9 and 13 m, respectively, but there is still reducing capacity left even in the visibly altered zone (see Fig. 2-2). A fraction of structural reduced Fe in the clay minerals remains even in the shallowest sample.

Note that the ratio NH_4^+/NO_3^- shows a systematic decrease towards the surface within the uppermost 25 – 30 m, likely reflecting oxidation of NH_4^+. Thus the zone of diminished NH_4^+/NO_3^- reaches deeper into the formation than oxidation phenomena identified in the rock. However, these findings need be interpreted with caution, as both chemical reactions and diffusive transport affect the measured NH_4^+/NO_3^- ratios.

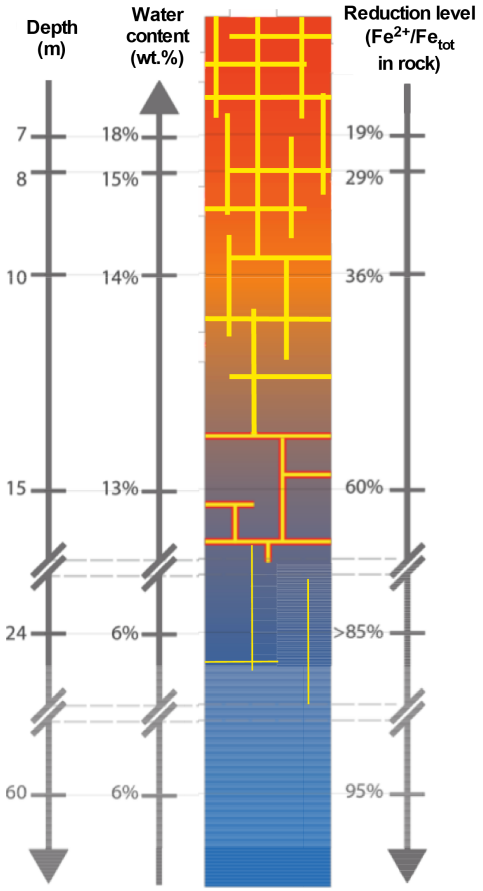

Fig. 5-8: Sketch showing the oxidation process at the Lausen site (see text).

5.5 Comparison with data from the Swabian Alb (Germany)

In a comprehensive study, Hekel (1994) investigated the hydrogeological and geochemical properties of Opalinus Clay cropping out in the Swabian Alb (southern Germany). Five different areas were selected, and a total of 16 boreholes were drilled, each 40 – 60 m deep. The pertinent results and conclusions include:

- Water content (and therefore porosity) is enhanced in the uppermost 3 – 12 m, and values of 20 wt.-% or more are reached in the shallowest samples, comparable to the findings at Lausen. A major difference is the deeper penetration of the water-content anomaly in Lausen, where is extends down to 40 m (Fig. 4-27). It is also interesting to note that within any specific area studied by Hekel (1994), the depth of the anomaly is similar but varies between study areas. This is likely explained by differences in the geomorphological situations, which control uplift and erosion rates and therefore the time over which surface effects can act on a specific rock volume.
- In Hekel's (1994) study, hydraulic conductivity is strongly enhanced in the uppermost 10 – 30 m, reaching values of 1E-6 m/s or higher. The zone of enhanced conductivity always extends to a depth well below the water-content anomaly (typically by a factor of 2). This is taken as an indication for the presence of a connected fracture system, comparable to what was found at Lausen.
- Below about 30 m, hydraulic conductivity at Lausen drops below 1E-12 m/s (Fig. 2.3-1). In Hekel's study, conductivities in the deeper parts of the boreholes remain at higher levels, typically around 1E-10 m/s. Whether these measurements represent true in-situ values or are affected by artefacts remains uncertain at this stage. The experimental setup was in any case not optimised for the quantification of hydraulic conductivity of tight claystone formations.
- Cl^- contents in the deeper parts of the boreholes in the Swabian Alb are similar within each area but vary widely between the areas. Some areas are characterised by low salinity (Cl^- around 0.5 g/L), whereas values of up to 10 g/L are found in others. Note that these concentrations were obtained by aqueous extraction and were re-calculated to the total water content, i.e. anion-exclusion effects were ignored. Considering an anion-accessible porosity fraction of 0.5 would double the values. In any case, the situation at Lausen is within this range (3-3.5 g/L, Fig. 5-3).
- The depth at which Cl^- contents start to drop towards the surface are in the range 20 – 50 m in the Swabian Alb, comparable to what is seen at Lausen (Fig. 5-3). In many of the boreholes, the Cl^- anomaly extends to deeper levels than the zone of enhanced hydraulic conductivity, indicating that diffusion was the likely mechanism of salinity loss.

6 Summary and conclusions: Characteristics of the decompaction zone in Opalinus Clay

The main findings pertinent to the properties of the decompaction zone are shown graphically in Fig. 6-1.

- Decompaction is observed in the uppermost 40 m and is mainly expressed by a substantial increase of porosity as well as by densely-spaced, moderately-dipping fracture systems of variable orientation.
- Hydraulic conductivity is strongly increased to a maximum depth of 28 m, below which depth it remains below 5E-13 m/s. This value is similar to the best-estimate value for Opalinus Clay in the Mont Terri URL. This means that the lower part of the decompaction zone, down to about 40 m, shows no hydraulic effects of the slightly higher porosity and the presence of decompaction fractures. It is concluded that self sealing is functional in this zone.
- The macroscopically visible weathered zone in Opalinus Clay reaches down to about 24 m below surface. Its base is defined by a drop of fracture density below 4 m^{-1}. Down to about 15 m, the rock matrix is brownish due to the presence of goethite, while the underlying part is grey, except for some brownish alteration rims along fractures down to about 16 m.
- The depth until which mineral dissolution triggered by surface effects took place varies:
  - Pyrite and organic carbon are depleted down to about 9 m, i.e. only in the uppermost 3 m of Opalinus Clay.
  - Until about 13 m, siderite is depleted, and chlorite is altered, probably to oxychlorite.
  - Goethite occurs down to about 16 m. Below this depth, the reduction level (i.e. the ratio $Fe^{2+}/[Fe^{2+}+Fe^{3+}]$ in the rock) strongly increases.
- The vertical zonation of Fe minerals (in particular pyrite, siderite, goethite) can be explained by simple thermodynamic relationships assuming a gradual shift from reducing to oxidising conditions towards the surface.
- Pore-water salinity (TDS) is very low down to about 20 m and then increases sharply to about 40 – 45 m. Below this depth, it remains essentially constant at 11.5 – 13 g/L.
- The water type is Na-Cl-SO_4 at depth but changes to Ca-Mg-HCO_3 at the top of Opalinus Clay.
- Cl^- and Na^+ concentrations in the pore water follow the same general trend as TDS. Cl^- concentrations below 45 m are 2.9 – 3.5 g/L, which is in the range observed at Mont Terri and Riniken but lower than at Schafisheim, Weiach, Benken and Schlattingen.
- Stable water isotopes of water show depth trends that are distinctly different from those of major ions:
  - $\delta^{18}O$ and $\delta^{2}H$ increase sharply down to 20 m, while major ions remain low in this interval.
  - A negative excursion is identified in the range 20 – 40 m, probably related to an advective disturbance from a fracture at 31.77 m. Major-ion concentrations increase in this depth range and do not show any excursion.
  - $\delta^{18}O$ and $\delta^{2}H$ values increase slightly down to about 70 m (base of Opalinus Clay) before reaching near-constant values. The surface-related disturbance of water-isotope compositions thus penetrates deeper than the disturbance of major ions (40 – 45 m). This could be explained by the higher diffusion coefficient of water compared to Cl^-.

- $\delta^{18}O$ and $\delta^{2}H$ lie on the right side of the meteoric water line throughout the weathered zone and the negative excursion, whereas deeper pore waters lie close to the line. In contrast, ground waters obtained from the weathered zone lie on the meteoric water line.
- The Ca^{2+}/Na^{+} ratio on exchange sites of clay minerals is high in the weathered zone and progressively decreases with depth. This trend reflects the evolution of the pore-water composition and ionic strength with depth.

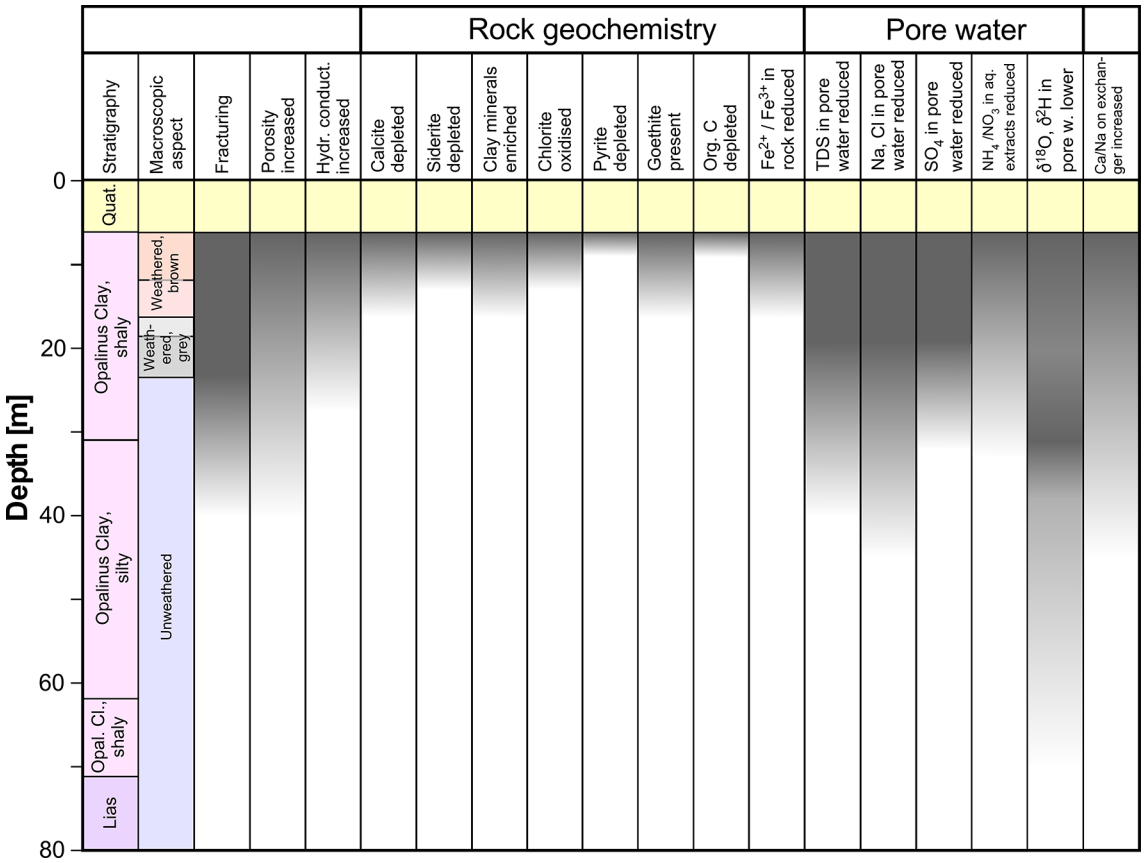

Fig. 6-1: Summary of depth trends of rock and pore-water characteristics.

7 References

Amonette, J.E. & Templeton, J.C. (1998): Improvements to the quantitative assay of non refractory minerals for Fe(II) and total Fe using 1,10-phenanthroline. Clays & Clay Minerals 46, 51 – 62.

Baeyens, B. & Bradbury, M. H. (2004): Cation exchange capacity measurements on illite using the sodium and cesium isotope dilution technique: Effects of the index cation, electrolyte concentration and competition: Modeling. Clays & Clay Minerals 52, 421 – 431.

Borggaard, O. K., Lindgreen, H. B. & Morup, S. (1982): Oxidation and reduction of structural iron in chlorite at 480 °C. Clays & Clay Minerals 30, 353 – 364.

Bradbury, M.H. & Baeyens, B. (1997/1998): Derivation of in situ Opalinus Clay porewater compositions from experimental and geochemical modelling studies. Nagra Technical Report NTB 97-07, with addendum.

Dohrmann, R. & Kaufhold, S. (2009): Three new, quick cec methods for determining the amounts of exchangeable calcium cations in calcareous clays. Clays & Clay Minerals 57, 338 – 352.

Hadi, J., Tournassat, C. & Lerouge, C. (2016): Pitfalls in using the hexaamminecobalt method for cation exchange capacity measurements on clay minerals and clay-rocks: Redox interferences between the cationic dye and the sample. Applied Clay Science 119, 393 – 400.

Hadi, J., Wersin, P., Jenni, A. & Grenèche, J.M. (2017): Redox evolution and Fe-bentonite interaction in the ABM2 experiment, Äspö Hard Rock Laboratory. Nagra Technical Report NTB 17-10.

Hekel, U. & Brod, M. (2016): Kernbohrung Lausen: Messbericht zu den hydraulischen Bohrlochversuchen. Nagra Arbeitsbericht NAB 15-49.

Hekel, U. (1994): Hydrogeologische Erkundung am Beispiel des Opalinustons (Unteres Aalenium). Tübinger geowissenschaftliche Arbeiten C18, Univ. Tübingen.

Hostettler, B., Reisdorf, A.G., Jaeggi, D., Deplazes, G., Bläsi, H. R., Morard, A., Feist-Burkhardt, S., Waltschew, A., Dietze, V. & Menkveld-Gfeller, U. (2017): Litho- and biostratigraphy of the Opalinus Clay and bounding formations in the Mont Terri rock laboratory (Switzerland). Swiss Journal of Geosciences 110, 23 – 37.

Huxol, S., Mair, C., Heidinger, M. & Eichinger, F. (2017): EWS Lausen: Interpretation der hydrochemischen und isotopenhydrologischen Analysen von Wasserproben aus dem Opalinuston einer Kernbohrung für eine Erdwärmesonde in Lausen. Nagra Arbeitsbericht NAB 16-57.

Lerouge, C., Grangeon, S., Claret, F., Gaucher, E., Blanc, P., Guerrot, C., Flehoc, C., Wille, G. & Mazurek, M. (2014): Mineralogical and isotopic record of diagenesis from the Opalinus Clay formation at Benken, Switzerland: Implications for the modeling of pore-water chemistry in a clay formation. Clays & Clay Minerals 62, 286 – 312.

Mäder, U. & Waber, H.N. (2017) in prep: Results of advective displacement/multi-component transport experiments from samples of the Schlattingen borehole. Nagra Arbeitsbericht NAB 17-16.

Martin, R.T. (1954): Reference chlorite characterization for chlorite identification in soil clays. Clays & Clay Minerals 3, 117 – 145.

Mazurek, M., Al, T., Celejewski, M., Clark, I. D., Fernandez, A. M., Kennell-Morrison, L., Matray, J.M., Murseli, S., Oyama, T., Qiu, S., Rufer, D., St-Jean, G., Waber, H.N. & Yu, C. (2017): Mont Terri Project: Comparison of pore-water investigations conducted by several laboratories on materials from the BDB-1 borehole. NWMO Technical Report TR-2017-09, Nuclear Waste Management Organization, Toronto, Canada.

Mazurek, M., Oyama, T., Wersin, P. & Alt-Epping, P. (2015): Pore-water squeezing from indurated shales. Chemical Geology 400, 106 – 121.

Mazurek, M., Waber, H.N., Mäder, U., Gimmi, T., De Haller & Koroleva, M. (2012): Geochemical synthesis for the Effingen Member in boreholes at Oftringen, Gösgen and Küttigen. Nagra Technischer Bericht NTB 12-07.

Meier, D. & Mazurek, M. (2011): Ancillary rock and pore-water studies on drillcores from northern Switzerland. Nagra Arbeitsbericht NAB 10-21.

Meier, L.P. & Kahr, G. (1999): Determination of the cation exchange capacity (CEC) of clay minerals using the complexes of copper(II) ion with triethylenetetramine and tetraethylenepentamine. Clays and Clay Minerals 47, 386 – 388.

Nagra (2014): SGT Etappe 2: Vorschlag weiter zu untersuchender geologischer Standortgebiete mit zugehörigen Standortarealen für die Oberflächenanlage. Geologische Grundlagen – Dossier VI: Barriereneigenschaften der Wirt- und Rahmengesteine. Nagra Technischer Bericht NTB 14-02, VI.

Pearson, F.J., Arcos D., Bath, A., Boisson, J.Y., Fernandez, A.M., Gaebler, H.E., Gaucher, E.C., Gautschi, A., Griffault, L., Hernan, P. & Waber, H.N. (2003): Mont Terri Project - Geochemistry of Water in the Opalinus Clay Formation at the Mont Terri Rock Laboratory. Reports of the Federal Office of Water and Geology (FOWG), Geology Series No. 5.

Rémy, J.C. & Orsini, L. (1976): Utilisation du chlorure de cobaltihéxamine pour la détermination simultanée de la capacité d'échange et des bases échangeables dans les sols. Sciences du Sol 4, 269 – 275.

Stevens, J.G., Khasanov, A.M., Miller, J.W., Pollak, H. & Li, Z. (2005): Mössbauer Mineral Handbook, MEDC.

Stucki, J.W. & Anderson, W.L. (1981a): The quantitative assay of minerals for Fe^{2+} and Fe^{3+} using 1,10-Phenanthroline: I. Sources of variability. Soil Science Society of America Journal 45, 633 – 637.

Stucki, J.W. & Anderson, W.L. (1981b): The quantitative assay of minerals for Fe^{2+} and Fe^{3+} using 1,10-Phenanthroline: II. A photochemical method. Soil Science Society of America Journal 45, 638 – 641.

Vandenberghe, R. & De Grave, E. (2013): Application of Mössbauer spectroscopy in earth sciences. In: Langouche, Y.Y.G. (Ed.), Mössbauer Spectroscopy - Tutorial book. Springer Berlin Heidelberg.

Vogt, T., Ebert, A., Häring, C., Becker, J.K., Traber, D., Deplazes, G., Bläsi, H.R. & Rufer, D. (2016): Kernbohrung Lausen: Geologische, hydrogeologische und bohrlochgeophysikalische Untersuchungen (Rohdatenbericht). Nagra Arbeitsbericht NAB 15-10.

Waber, H.N. & Rufer, D. (2017): Porewater geochemistry, method comparison and Opalinus Clay-Passwang Formation interface study at the Mont Terri URL. NWMO Technical Report TR-2017-10, Nuclear Waste Management Organization, Toronto, Canada.

Wersin, P., Jenni, A. & Mäder, U.K. (2015): Interaction of corroding iron with bentonite in the ABM1 experiment at Äspö, Sweden: A microscopic approach. Clays & Clay Minerals 63, 51 – 68.

Wersin, P., Mazurek, M., Waber, H.N., Mäder, U.K., Gimmi, T., Rufer, D. & De Haller, A. (2013): Rock and porewater characterisation on drillcores from the Schlattingen borehole. Nagra Arbeitsbericht NAB 12-54.